PRE- AND POST- SYNAPTIC REGULATION OF TWO INTERNEURON MICROCIRCUITS IN CEREBELLUM-LIKE STRUCTURES

By

Hsin-Wei Lu

A DISSERTATION

Presented to the Neuroscience Graduate Program
and the Oregon Health & Science University
School of Medicine

in partial fulfillment of the requirements for the degree of

Doctor of Philosophy

June 2016

TABLE OF CONTENTS

ACKNOWLEDGEMENTS

I am indebted to many individuals that have helped me finish this dissertation.

First, I would like thank my advisor, Larry Trussell, for his guidance throughout my PhD career. I am grateful to have him as my mentor, not only because he is knowledgeable and creative in teaching me to become a neurophysiologist, but always being very patient and willing to help during my tough times. I am especially thankful for his efforts reading and editing my English writing. Moreover, whenever I am going to give an oral presentation, he always spends a great amount of time going through all the slides with me. I feel extremely lucky to have such an intelligent and kind scientist as my teacher.

I thank my dissertation committee, Tianyi, Stephen, and John, for their critical and helpful comments on my work. The discussions we have at every committee meeting are always very thought-provocative.

I thank all the Trussell lab members that I have overlapped with for creating an environment that shaped me into an independent scientist. Many thanks to Hai for being my "roommate" in my first five years in the lab, to Jeffrey for his encouragements when I struggled, to Tomo for his relaxing small talks, to Carol for her well-organized management skills, to Pierre for his creative ideas, and to Gabe and Tim for helping me in the UBC project. I would particularly like to thank Dan Yaeger, for his being a great colleague, a workout partner, and a sincere friend.

I thank my family from Taiwan for their encouragements and support across the Pacific Ocean. Every time talking with them on Skype boosts my energy.

Finally, I thank Pei-Yu. Words cannot express my gratitude to her unconditional support, encouragement and love during the last year of my thesis work.

ABSTRACT

Fast chemical synapses mediate rapid communications between neurons. Interestingly, the strength of most synapses is not constant but dynamic, depending on the history of presynaptic activity. In many cases, repetitive activation of presynaptic neurons leads to a rapid decrease in synaptic strength, a phenomenon termed short-term depression. In this study, two synapses that exhibit profound short-term depression were investigated: a glycinergic inhibitory synapse in the auditory brainstem and a glutamatergic excitatory synapse in the cerebellum. The mechanisms underlying short-term depression at these two synapses are strikingly different, and consequently have distinct impacts at cellular or microcircuit level.

In chapter 1, the impact of short-term depression at an inhibitory synapse formed by glycinergic cartwheel interneurons in the dorsal cochlear nucleus was studied. By paired recording of pre- and post-synaptic neurons and computational modeling of short-term depression, I proposed that a high release probability (Pr) and a low Pr pool of synaptic vesicles in the presynaptic cartwheel cells control the degree of synaptic depression. As spontaneous firing rate in cartwheel cells increases, high Pr vesicles are depleted, leading to constant depression. Consequently, it requires more cartwheel cells to effectively inhibit the postsynaptic neuron. However, spontaneous firing can be modulated by neuromodulators, and thus the degree of depression and the number of effective cartwheel inputs are dependent on the presynaptic firing rate. Surprisingly, I found that even at high spontaneous firing rate only a small number (4 -5) of cartwheel cells are sufficient to provide effective inhibition. Computational modeling suggests that this is due to the maintenance of steady-state transmission by low Pr vesicles. Thus, the interplay

between spontaneous spiking, short-term depression, and vesicle recruitment determines the effective size of a convergent neural network.

In chapter 2, a glutamatergic synapse formed between cerebellar mossy fiber and unipolar brush cell was studied. High frequency stimulation of this synapse leads to a pronounced short-term depression of AMPA receptor (AMPAR)-mediated fast excitatory postsynaptic current (EPSC). Interestingly, a slow EPSC lasting several hundreds of milliseconds mediated by the same receptors emerges after the stimulation ends, causing a delayed prolonged excitation. Such delayed slow EPSC has not been observed at other synapses, and it is hypothesized to be due to activation of desensitized AMPARs by glutamate entrapped in its unique giant convoluted synaptic cleft. By using glutamate uncaging, we provide direct evidence showing that AMPARs are desensitized after synaptic depression, and more surprisingly, these desensitized AMPARs mediated the ensuing slow EPSC. By fast application of glutamate to dissociated UBCs, we estimated the glutamate concentration to activate this slow EPSC is ~ 30 μM. We also showed that the AMPAR auxiliary protein stargazin may regulate such slow response. AMPARs desensitize rapidly and usually mediate fast EPSCs in the nervous system. This study showed that they can generate long-lasting excitation if the cleft glutamate decays slowly enough to activate special desensitized states of these receptors.

LIST OF FIGURES

LIST OF TABLES

INTRODUCTION

Neurons communicate via specialized junctions termed synapses. One major form of synaptic transmission is mediated by fast chemical synapses, which convert electrical signals in the presynaptic cell to chemical signals in the form of neurotransmitters released into the synaptic cleft. The transmitters bind to postsynaptic ionotropic receptors, which permeate ions and convert the chemical signal back to an electrical one. There are numerous ways to regulate synaptic transmission at fast chemical synapses, and understanding the mechanisms underlying them is important for studying information processing in neural circuits.

The work presented in this thesis focuses on synaptic transmission in an inhibitory and an excitatory interneuron microcircuit in the mouse dorsal cochlear nucleus (DCN) and cerebellum, respectively (Chapter 1 and 2). Both synapses exhibit profound short-term synaptic depression, a gradual loss of synaptic response upon repetitive stimulation. Interestingly, in the excitatory synapse we see a slow response emerging soon after the synapse is depressed. By using whole-cell patch clamp recordings in the brain slices, I found that a pre- and a post-synaptic mechanism can account for the differences in these two synapses. DCN and cerebellum share the same circuit motifs, and the microcircuits studied in this thesis both reside in the mossy fiber – parallel fiber pathway that is hypothesized to generate predictions about expected sensory inputs (Bell et al., 2008). The studies in this thesis thus provide synaptic basis for understanding the computational function of cerebellum-like structures.

Synaptic depression and vesicle depletion

Short-term synaptic depression was discovered in the 1940s at the neuromuscular junction (Eccles et al., 1941; Feng, 1941), and was later found at other synapses in the peripheral and central nervous system (Zucker and Regehr, 2002). The two synapses studied in this thesis, the glycinergic inhibitory synapse formed by cartwheel interneuron in the DCN (chapter 1) and the glutamatergic excitatory synapse formed by mossy fiber on to unipolar brush cell in the cerebellum (chapter 2) both exhibited profound short-term depression. However, as shown later in the results section of this thesis, the mechanisms causing the depression at these two synapses are quite different: a presynaptic vesicle depletion mechanisms accounts for the depression at cartwheel synapses, and a postsynaptic α-amino-3-hydroxy-5-methyl-4-isoxazolepropionic acid (AMPA) receptor desensitization mechanism dominates at the mossy-fiber unipolar brush cell (UBC) synapse. These two mechanisms in fact reflect two most widespread pre- and post-synaptic processes that are thought to mediate synaptic depression.

Vesicle depletion is probably the most prevalent hypothesis for the generation of synaptic depression. The idea was proposed in the 1950s (Liley and North, 1953), suggesting that elevated presynaptic activity will deplete the transmitter stores available for release, thereby reducing synaptic strength. Its simplest form (Betz, 1970a; Kusano and Landau, 1975; Zucker and Regehr, 2002) states that a synapse contains N_0 readily releasable vesicles, and upon action potential stimulation the synapse will release a fraction of vesicles according to the vesicle release probability P_v. Thus, immediately after the stimulus, there will be $N_0(1-P_v)$ vesicles available for next release. If the stimulus arrives after a certain amount of time Δt, the partially depleted vesicle pool will recover mono-exponentially according to a time constant τ. To generalize, at the i_{th} stimulus, the

number of releasable vesicles N_i will be the number of vesicles immediately available after the last stimulus, plus the fraction recovered during Δt period between current and last stimuli:

$$N_i = N_{i-1} \cdot (1 - P_v) + [N_0 - N_{i-1} \cdot (1 - P_v)] \cdot \left(1 - e^{-\frac{\Delta t}{\tau}}\right), \; i > 1$$

To test whether this model works, several methods have been proposed to find these parameters experimentally. The recovery time constant τ can be determined by the recovery time course from the synaptic depression. However, to determine N_0 and P_v, it is less straightforward. One approach is to deplete the stores of vesicles the terminal, such as applying hypertonic sucrose solution (Rosenmund and Stevens, 1996), uncaging Ca^{2+} at the terminal (Schneggenburger et al., 1999), or depolarize the terminal for a long period of time by direct patch clamping (Neher and Sakaba, 2001). The other approach is to summate postsynaptic responses generated by a high frequency train of action potentials, and then back- or forward-extrapolate the summated responses in order to remove or bypass recovery during train stimulation (Elmqvist and Quastel, 1965; Schneggenburger et al., 1999; Thanawala and Regehr, 2013). With simultaneous recording of the postsynaptic neuron, the responses generated by above-mentioned stimulation approaches are presumed to be the sum of the currents generated by the total number of readily releasable vesicles. Hence, the estimate the readily releasable pool size (N_0) is obtained. Because N_0 obtained this way is in the form of the postsynaptic current, P_v can be calculated as the ratio of the evoked postsynaptic current divided by the pool size.

However, although this simple depletion model can successfully predict the depression evoked by a few stimuli, it is not able to account for steady-state depression at many synapses (Betz, 1970a; Kusano and Landau, 1975; Zucker, 1989; Dittman and

Regehr, 1998). It is therefore suggested that the parameters in this model, such as P_v or τ, may not stay constant during stimulation (Wu and Borst, 1999). Indeed, studies have found that during high frequency stimulation, there is a Ca^{2+} - dependent enhancement of recovery from depression (Dittman and Regehr, 1998; Wang and Kaczmarek, 1998; Weis et al., 1999). Additionally, it has been found that vesicle release rates might not be homogeneous in the same RRP (Neher and Sakaba, 2001; Müller et al., 2010) or different release sites may have distinct P_v (Dobrunz and Stevens, 1997; Murthy et al., 1997; Moulder and Mennerick, 2005). Moreover, there are other presynaptic mechanisms found to cause synaptic depression, such as inactivation of presynaptic Ca^{2+} channels (Forsythe et al., 1998; Xu and Wu, 2005; Catterall and Few, 2008) or action potential propagation failures to the synaptic terminal (Brody and Yue, 2000; Prakriya and Mennerick, 2000; Kawaguchi and Sakaba, 2015). These lines of evidence suggest that the mechanisms underlying presynaptic depression may be more complicated than a simple depletion model. In chapter 1, I addressed these concerns at cartwheel cell synapse and proposed a possible mechanism that can account for its synaptic depression.

Receptor desensitization during synaptic depression

Although presynaptic vesicle depletion is a dominant mechanism contributing to synaptic depression, depression can also be induced postsynaptically. One of the mechanisms is receptor desensitization, which describes a ligand-gated receptor entering a closed state for long periods with agonist still bound (Jones and Westbrook, 1996). Synaptic receptor desensitization was first found in the 1950s, when Thesleff and colleagues applied acetylcholine (Ach) to muscles and found subsequent Ach responses

were depressed (Thesleff, 1955; Castillo and Katz, 1957; Katz and Thesleff, 1957). However, at neuromuscular junctions, synaptic transmission is little affected by desensitization, because the unbinding rate of Ach from nicotinic receptors is faster than desensitization rate (Figure 1) and Ach is cleared from synaptic cleft within hundreds of microseconds (Magleby and Stevens, 1972). Thus, after opened by synaptically released Ach, the nicotinic receptors would be more likely to unbind Ach than to desensitize.

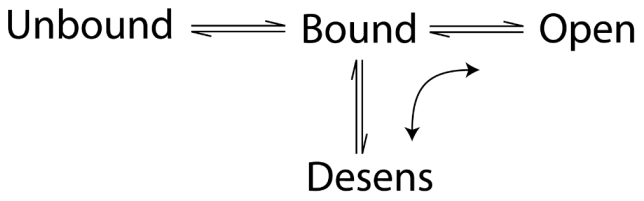

Figure 1: A simple kinetic model for receptor desensitization. Desens: Desensitized state.

Another ligand-gated synaptic receptor that shows significant desensitization are the AMPA receptor (AMPARs), the receptors that mediate fast excitatory transmission at most vertebrate central synapses (Trussell and Fischbach, 1989). Unlike nicotinic receptors, upon binding of glutamate the AMPARs are nearly as likely to open as to desensitize because they have similar high opening and desensitization rates. Moreover, AMPARs can accumulate in the desensitized state readily, as a fraction of AMPARs can desensitize even after brief (~1 ms) exposure of high concentrations of glutamate or after long exposure to low concentrations of glutamate (Trussell and Fischbach, 1989; Colquhoun et al., 1992; Hestrin, 1992; Raman and Trussell, 1995a). This slow recovery suggests the backward rate from desensitized to bound state is slow (figure 1) and suggests that synaptic depression of AMPAR-mediated EPSCs may be caused by postsynaptic receptor desensitization. Indeed, the AMPAR desensitization inhibitor cyclothiazide has been shown to reduce the degree of paired-pulse depression at some

excitatory synapses (Trussell et al., 1993; Rozov et al., 2001; Chen et al., 2002; Xu-Friedman and Regehr, 2003a). In chapter 2, I will show that there is profound AMPAR desensitization at mossy fiber –unipolar brush cell synapse during synaptic depression.

AMPAR desensitization and EPSC time course

AMPAR desensitization may also shape the time course of the excitatory postsynaptic current (EPSC). The decay of AMPAR desensitization in chick auditory brainstem neurons during a long pulse of high concentrations of glutamate is comparable to the decay of synaptic currents, suggesting that the brief synaptic current may be shaped by receptor desensitization (Raman and Trussell, 1992; Trussell et al., 1993). However, at mammalian synapses, the decay of synaptic current is shorter than that of desensitization during long pulse but more similar to the decay of the AMPAR deactivation upon brief exposure (Figure 2) (Colquhoun et al., 1992; Silver et al., 1996). What is the cause of such difference? The glutamate transient at the chick auditory brainstem synapse is likely to decay longer and desensitize AMPARs due to its large size and closely spaced release sites (Trussell et al., 1993), whereas at small conventional mammalian synapse the glutamate transient decays rapidly (1 -2 ms) (Clements et al., 1992). Thus, it is suggested that the glutamate clearance rate at synaptic cleft determines whether the EPSC time course will be affected by desensitization (Trussell et al., 1993; Jonas, 2000). The glutamate clearance rate at mossy fiber – unipolar brush cell synapse studied in chapter 2 is hypothesized to be slow due to its convoluted synaptic structure. This may account for the unique slow AMPAR-mediated current at this synapse, which will be described later in this chapter and in chapter 2 (Rossi et al., 1995; Kinney et al., 1997).

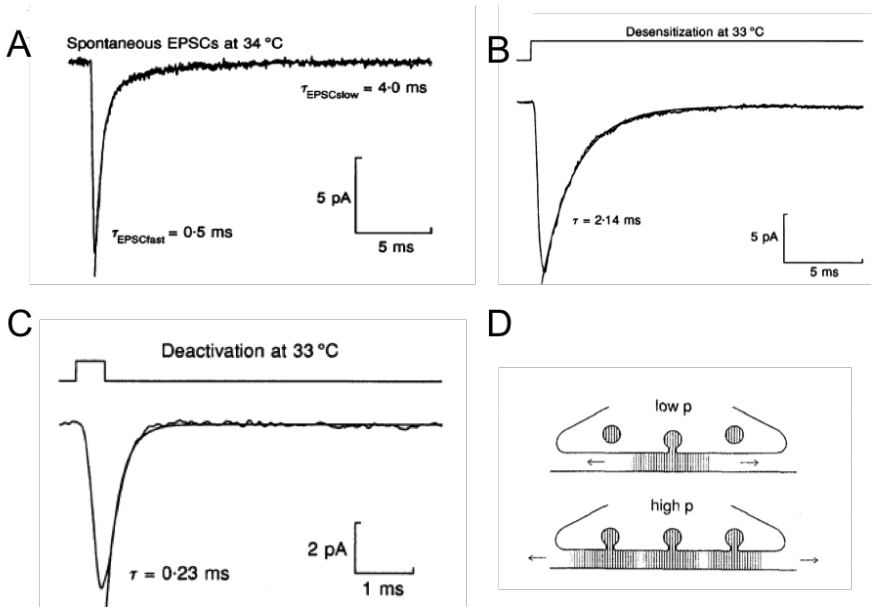

Figure 2. Time course of AMPAR-mediated EPSC. (A-C: taken from Silver et al 1996, D: taken from Trussell et al 1993). (A-C) The decay synaptic EPSC (A) in cerebellar granule cells is more similar to that of deactivation of AMPARs (C) but not to that during desensitization (B). (D) It is suggested that only when clearance of glutamate from synaptic cleft is slow (bottom) can desensitization affects EPSC time course. When clearance is fast (top), EPSC decay is dependent on the deactivation kinetics.

Steady-state AMPAR desensitization

One feature of AMPAR desensitization is that its steady-state response has an non-monotonic, bell shaped dose response relations with glutamate (Figure 3) (Geoffroy et al., 1991; Raman and Trussell, 1992). The steady-state response peaks around at mid-micromolar range and decays to ~ 50-70% when glutamate increases to millimolar range. Interestingly, recent studies have shown that stargazin, the γ2 transmembrane AMPAR regulatory protein (TARP) (Tomita, 2010; Jackson and Nicoll, 2011), is associated with this feature. In expression systems, only AMPARs coexpressed with stargazin exhibited such bell-shaped steady-state dose response curve, whereas AMPARs expressed alone did not (Figure 3) (Morimoto-Tomita et al., 2009; Semenov et al., 2012). It is thus suggested that stargazin can enhance AMPAR responses to mid-micromolar range glutamate. Although this bell-shaped dose response curve has been known for decades, its physiological function remains unclear. The mossy fiber – UBC synapse is hypothesized to utilize this

feature to conduct a slow EPSC (Rossi et al., 1995; Kinney et al., 1997), which will be discussed later in this chapter and in chapter 2.

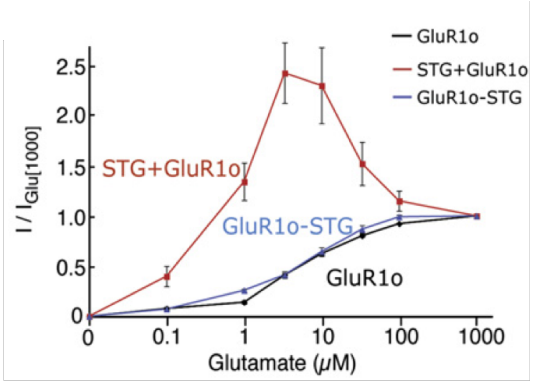

Figure 3. Bell-shaped steady-state dose response curve of AMPARs. (Taken from Morimoto-Tomita et al 2009). Notice that only AMPARs coexpressed with stargazin (STG+GluR1o) has the bell-shaped dose response curve.

Circuitry of DCN and cerebellum: cerebellum-like circuits

The synapses studied in this thesis, the glycinergic inhibitory synapse formed by cartwheel interneuron in the DCN (chapter 1) and the glutamatergic excitatory synapse formed by mossy fiber on to unipolar brush cell in the cerebellum (chapter 2) are located in structures collectively called cerebellum-like circuits, as depicted in figure 4 (Bell et al.,

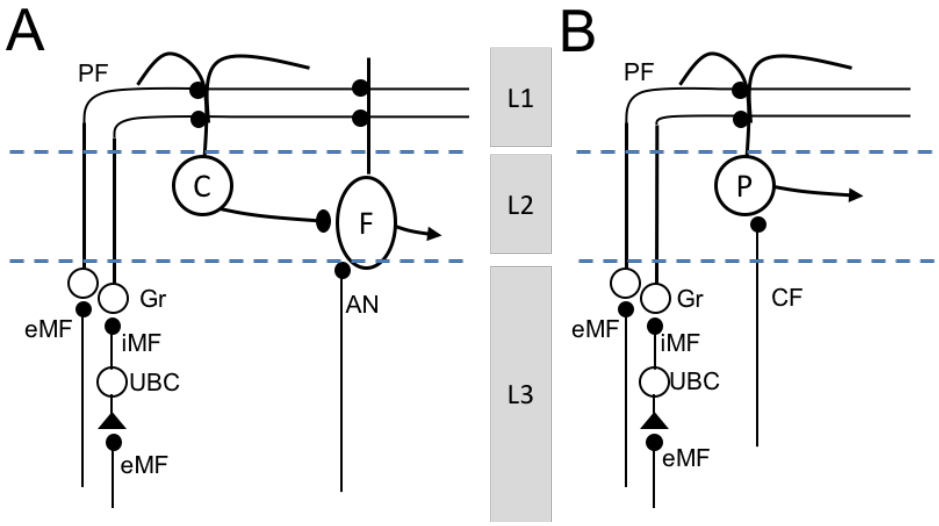

Figure 4. Diagram of cerebellum-like circuits. (A) DCN. (B) Cerebellum. PF: parallel fiber. C: cartwheel cell. F: fusiform cell. eMF: extrinsic mossy fiber. iMF: intrinsic mossy fiber. Gr: granule cell. UBC: unipolar brush cell. P: Purkinje cell. L1: molecular layer. L2: principal cell layer. L3: deep layer (in DCN) or granule cell layer (in cerebellum).

2008). The cerebellum-like circuit contains three layers: molecular (L1), principal cell (L2), and deep (in DCN) or granule cell (in cerebellum) layer (L3). The principal neuron (fusiform cell in DCN and Purkinje cell for cerebellum, respectively) integrates excitatory inputs from L1 (carried by parallel fibers) and L3 (carried by auditory nerve in DCN and by climbing fiber in cerebellum), and sends its output to other nuclei (midbrain inferior colliculus for fusiform cell and deep cerebellar nuclei or vestibular nuclei for Purkinje cell). The synapses studied in this thesis, the cartwheel – fusiform cell synapse and mossy fiber – UBC synapse, are located in two interneuron circuits in L2 and L3, respectively. The detailed anatomy and functions of these two circuits are described below.

Cartwheel-fusiform cell circuit in the DCN: anatomy and function

The DCN is the first station in the ascending auditory pathway that integrates auditory signals with other non-auditory multisensory modalities (Oertel and Young, 2004a). The auditory information is carried by the auditory nerve, which innervates the deep layer and forms excitatory synapses onto basal dendrites of the principal neuron, fusiform cells. The multisensory information, such as vestibular and somatosensory signals (Ryugo et al., 2003; Shore, 2005; Koehler et al., 2011), are first carried by extrinsic mossy fibers (eMF in figure 4) and then relayed by parallel fibers, which form excitatory synapses onto apical dendrites of the fusiform cells. After integrating these signals, fusiform cells send outputs to the midbrain inferior colliculus.

In addition to these excitatory inputs, several local inhibitory inputs also innervate fusiform cell. Cartwheel cells are one of them. They are localized in the multisensory pathway, receiving excitatory inputs from parallel fibers, the axons of the granule cells in

the deep layer, and form gamma-aminobutyric acid (GABA) / glycinergic synapses onto neighboring cartwheel cells or fusiform cell (Golding and Oertel, 1997; Oertel and Young, 2004a; Apostolides and Trussell, 2013). Interestingly, cartwheel cells share many morphological and genetic markers with Purkinje cells in the cerebellum, but they are not considered principal cells in the DCN because their axons project locally (Oertel and Young, 2004a; Bell et al., 2008). However, their inhibition onto fusiform cells are considered to be important in the DCN function.

DCN has been suggested to be involved in localizing the elevation of sound sources, as shown by the spiking output of the principal cells or by lesioning studies in the output axon fibers of the DCN (May, 2000; Oertel and Young, 2004a; Reiss and Young, 2005). Moreover, because of its cerebellum-like circuit, by analogy with the other cerebellum-like structure in weakly electric fish (Bell et al., 2008), the DCN has also been suggested to cancel out self-generated noises (Oertel and Young, 2004a). Either function relies on the multisensory signals provided in the molecular layer pathway, for example, the location of the pinna may provide cues for sound localization (Oertel and Young, 2004a). The cartwheel cells, mediating feedforward inhibition in the multisensory pathway to fusiform cells, can thus temper the excitatory signals relayed by parallel fibers and influence the integration of auditory and non-auditory information in fusiform cells. Hence, it is important to understand how inhibition from cartwheel cells is regulated. One interesting feature of cartwheel cells is that they spontaneously fire and show powerful synaptic depression (Kuo and Trussell, 2011). As a result, their inhibition strength is deeply affected by their spontaneous firing rates. The degree of inhibition is also dependent on how many cartwheel cells are converging onto a fusiform cell. However this is still unknown. In

chapter 1, I will investigate how interplay between spontaneous spiking, synaptic depression, and circuit convergence affects inhibition from cartwheel cells to fusiform cells.

Mossy fiber - UBC synapse in the cerebellum: anatomy and function

Similar to the synapse made by cartwheel cells, the mossy fiber –UBC synapse is also located in the mossy fiber – parallel fiber pathway. Specifically, the UBC functions as an excitatory glutamatergic interneuron that receives single extrinsic mossy fiber inputs and sends its outputs (termed intrinsic mossy fibers) onto granule cells (Diño et al., 2000c). Hence, signals carried by extrinsic mossy fibers are filtered or amplified by this extra synapse before they reach the principal cells.

UBCs are present in both cerebellum and DCN (Mugnaini et al., 2011). Cerebellar UBCs are primarily located in the vestibulocerebellum, i.e. the nodulus (lobe X) and the uvula (lobe IX). They receive extrinsic mossy fiber inputs from either primary vestibular fibers from otolith and canal organs or secondary vestibular inputs from vestibular nuclei (Diño et al., 2000a). Consistent with this finding, in vivo extracellular recordings of UBCs in the mouse vestibulocerebellum responded to vestibular stimulation, with increasing discharge with ipsilateral roll tilt (Barmack and Yakhnitsa, 2008). Thus, they may play an important role in regulating vestibular function. It is worth mentioning that in the electrosensory lobe of weakly electric fish, which is also a cerebellum-like structure, in vivo recordings of UBCs showed that they provide a delayed predictive signal that serves to filter out electrical noises generated by self-motion (Kennedy et al., 2014). Thus, UBCs may provide a temporally precise signal that predicts expected sensory or motor outcome,

which is an important function of cerebellum (Bell et al., 2008). This delayed signal may result from a unique slow AMPAR-mediated EPSC, which is described below.

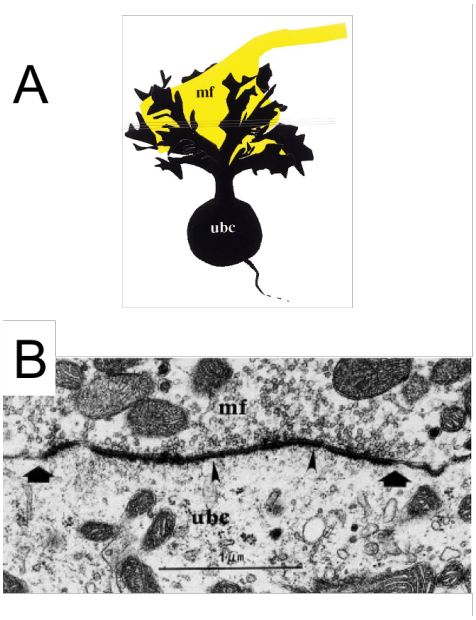

Figure 5. Morphology and synaptic transmission at mossy fiber – UBC synapse. (A) UBC receives single mossy fiber input at its dendritic brush. (Taken from Diño et al 2000b). (B) Transmembrane electron microscopy image of the mossy fiber (mf) – UBC synapse. An unusually wide synaptic cleft (~ several μm) can slow the clearance of glutamate. (C and D) Upon a brief stimulus, a slow EPSC emerges after fast EPSC ends (D), causing prolonged firing (C). (B-D taken from Rossi et al 1995)

Unusually slow AMPAR-mediated EPSC at mossy fiber –UBC synapse

The mossy fiber – UBC synapse has an unusual AMPAR-mediated slow EPSC that lasts at least hundreds of milliseconds, which emerges after typical fast EPSC ends (Rossi et al., 1995; Kinney et al., 1997; Dorp and Zeeuw, 2014; Borges-Merjane and Trussell, 2015) (figure 5). As a result, even upon a brief stimulus, UBC will still respond with prolonged action potential firing (Rossi et al., 1995; Borges-Merjane and Trussell, 2015) (figure 5). The mechanisms underlying such slow EPSC is hypothesized as below (Rossi et al., 1995; Kinney et al., 1997). Because of the extensive contacts between the presynaptic mossy fiber and postsynaptic brush-like dendrites (estimated ~ 12 - 40 μm^2) (Rossi et al., 1995) (figure 5), it is suggested that glutamate clearance from the synaptic cleft is slow. Hence, after glutamate is released from the presynaptic terminal, it will be trapped in the cleft, and due

to the bell-shaped steady-state dose response relations of AMPARs mentioned above (Geoffroy et al., 1991; Raman and Trussell, 1992) (figure 3), as the concentration of glutamate slowly passes across the peak of the curve, a slow inward current will be generated. As mentioned previously in this section, AMPARs desensitize even if they are exposed to low concentrations of glutamate (Trussell and Fischbach, 1989; Colquhoun et al., 1992; Raman and Trussell, 1992). Therefore, if this "glutamate entrapment" hypothesis for mossy fiber – UBC synaptic transmission is true, AMPARs should be desensitized during the course of slow EPSC. Although previous studies have shown that the AMPAR desensiziation inhibitor CTZ blocked the rise of the slow EPSC (Rossi et al., 1995; Kinney et al., 1997), CTZ has known side effects such as slowing down the deactivation kinetics of AMPARs (Patneau et al., 1993; Raman and Trussell, 1995a) and enhancing presynaptic release (Diamond and Jahr, 1995). In chapter 2, I will use glutamate uncaging to directly measure the desensitized states of AMPARs during slow transmission.

CHAPTER 1. SPONTANEOUS ACTIVITY DEFINES EFFECTIVE CONVERGENCE RATIOS IN AN INHIBITORY CIRCUIT

Hsin-Wei Lu[1] and Laurence O Trussell[2]

[1]Neuroscience Graduate Program, Oregon Health and Science University, Portland, Oregon, USA; and [2]Oregon Hearing Research Center and Vollum Institute, Oregon Health and Science University, Portland, Oregon, USA

(Lu and Trussell, 2016)

Abstract

Many neurons fire spontaneously, and the rate of this firing is subject to neuromodulation. How this firing affects functional connectivity of a neural network remains largely unexplored. Here we show that changes in spontaneous firing of cartwheel interneurons in the mouse dorsal cochlear nucleus (DCN) alters the effective convergence ratio of interneurons onto their postsynaptic targets through short-term synaptic plasticity. Spontaneous firing of cartwheel cells led to activity-dependent synaptic depression of individual cartwheel synapses. Depression was rapid and profound at stimulation frequencies between 10 and 200 Hz, suggesting the presence of high release probability (Pr) vesicles at the synapse. Weak, transient synaptic facilitation could be induced after the synapse was pre-depressed, indicating that low-Pr vesicles are also recruited, and may support steady state transmission. A two-pool vesicle depletion model with 10-fold difference in Pr could account for the synaptic depression over a wide range of stimulus conditions. As a result of depression during high spontaneous activity, more cartwheel interneurons were required for effective inhibition. Convergence of 4 interneurons was sufficient to compensate for the effects of depression during physiologically expected rates of activity. By simulating synaptic release during spontaneous firing, we found that recruitment of low-Pr vesicles at the synapse plays a critical role in maintaining effective inhibition with a small population of interneurons. The interplay between spontaneous spiking, short-term synaptic plasticity and vesicle recruitment thus determines the effective size of a convergent neural network.

Significance Statement

We examined the relationship between the structure of a small neural circuit and the properties of its individual synapses. Successful synaptic inhibition of a target cell firing requires a critical inhibitory synaptic strength. Synapses often become depressed during spontaneous presynaptic activity, and this increases the number of presynaptic neurons needed to mediate inhibition. We show that depression is limited by the presence of a pool of vesicles that resist depletion. Thus the size of this vesicle pool determines the size of the circuit needed to mediate inhibition during different patterns of activity.

Introduction

Many neurons fire spontaneous action potentials even without afferent stimuli (Do and Bean, 2003; Häusser et al., 2004; Hermann et al., 2007; Person and Raman, 2012a). At synapses with relatively high vesicular release probability (Pr), such ongoing activity would deplete the available pool of vesicles, leading to sustained synaptic depression (Zucker and Regehr, 2002; Hermann et al., 2007; Yang and Xu-Friedman, 2015). Consequently, spontaneously active neurons may fail to relay the information from afferent stimuli. Indeed, studies have shown that synaptic depression induced by spontaneous spiking in presynaptic cells significantly reduces stimulus-driven responses in the postsynaptic cell (Hermann et al., 2007; Groh et al., 2008). Importantly, spontaneous spiking rate can be modified, for example by neuromodulators, thus regulating synaptic depression and the efficacy of afferent signals (Kuo and Trussell, 2011; Owen et al., 2013).

However, neural circuits do not only relay afferent signals but also integrate multiple sources of information carried by different sets of afferent inputs. Accordingly,

depressed synapses, which individually may not drive a postsynaptic cell to spike, may be effective when different inputs are active simultaneously. Such coincident detection of afferent stimuli can be important for sensory integration in the nervous system (Kuba et al., 2002; Cook et al., 2003; Groh et al., 2008). Hence, at synapses with activity-dependent depression, presynaptic spontaneous spiking can not only reduce the strength of individual afferents but also determine the needs for integration from multiple afferents converging onto the postsynaptic cell. Thus we distinguish between an anatomical convergence ratio onto a postsynaptic neuron and an effective convergence ratio that accounts for dynamic changes in synaptic strength at individual synapses.

The interplay between spontaneous spiking, synaptic depression, and integration of multiple afferent inputs to define the effective convergence ratio is studied here in a circuit formed by cartwheel inhibitory interneurons onto fusiform principal cells in the mouse dorsal cochlear nucleus (DCN). The DCN is an initial station in the ascending auditory pathway that integrates multisensory modalities with auditory information (Oertel and Young, 2004b). Multisensory inputs are relayed by excitatory parallel fibers and influence sound-evoked responses in the fusiform cells (Koehler et al., 2011) (Fig 1A). This modulation involves not only direct excitation from parallel fibers but also feedforward inhibition from cartwheel interneurons (Roberts and Trussell, 2010; Kuo and Trussell, 2011). In fact, in vivo stimulation of parallel fiber/multisensory pathway often cause a long-lasting inhibition of fusiform cell firing, highlighting the potency of cartwheel cell activity (Young et al., 1995; Davis et al., 1996a; Shore, 2005; Kanold et al., 2011). However, cartwheel cells fire spontaneously in vivo (Davis and Young, 1997; Portfors and Roberts, 2007; Ma and Brenowitz, 2012), leading to sustained synaptic depression and weaker feedforward

inhibition driven by parallel fibers (Kuo and Trussell, 2011). This phenomenon raises the question of how chronically depressed cartwheel synapses can provide effective inhibition under physiological conditions.

We hypothesize that the number of presynaptic neurons required for inhibition, i.e., the effective convergence ratio, is a function of the state of depression of individual synapses. Thus the spontaneous firing rate of neurons and the microphysiology of their synapses together may impact the ratio. To quantify the depression level of synaptic transmission at different spontaneous firing frequencies, we made recordings between connected cartwheel-fusiform cell pairs and analyzed the kinetics of synaptic depression under diverse stimulus paradigms. We described the process of depression quantitatively using a model featuring two pools of vesicles with distinct Pr. The depletion of these two populations of vesicles at different proportions leads to rate-dependent depression at cartwheel synapse. Despite prominent synaptic depression, the effective cartwheel-fusiform convergence ratio at high spontaneous spiking rates was surprisingly small (< 4). The synaptic depression model suggests that low-Pr vesicles sustain the release during high frequency spiking and thus ensure effective inhibition performed in a small circuit. Hence, the properties of synaptic vesicles that control the degree of synaptic depression provide a foundation for defining effective circuit convergence as spike rates of neurons are varied by neuromodulators. This work may be generalized to other brain regions that utilize convergent circuits and depressing synapses.

Methods

Animals

Wildtype C57/Bl6 mice (P16 – P27) were used for paired recording experiments. For photostimulation experiments, GlyT2-Cre;Ai32 transgenic mice were used, generated by crossing male ChR2(H134R)-EYFP reporter line (Ai32) with a female GlyT2-Cre line. Use and handling of animals in this study were approved by Oregon Health and Science University Institutional Animal Care and Use Committee.

Brain slice preparation

Animals were anesthetized by isofluorane and then decapitated. After removing the skull, a coronal cut at the midbrain was made to dissect out the brainstem. The front side of the brainstem was then glued on a stage. The lateral side of the brainstem was turned to face the vibratome (Leica VT1200S) blade and tilted downwards at an angle of ~10˚. Coronal brainstem slices containing DCN (220 μm thick) were collected in warm (34˚C) artificial cerebrospinal fluid (ACSF) solutions containing (in mM): 130 NaCl, 2.1 KCl, 1.2 KH_2PO_4, 3 Na-HEPES, 11 glucose, 20 $NaHCO_3$, 1 $MgSO_4$, and 1.7 $CaCl_2$, saturated with 5% CO_2-95% O_2, ~305 mOsm. After cutting, the slices were stored in ACSF at 34˚C for ~30 minutes for recovery and then kept at room temperature (~22˚C) until use.

Electrophysiology

During recording, slices were transferred to a recording chamber constantly perfused with warm ACSF (~34˚C) controlled by a peristaltic tubing pump (Ismatec CP78016-30). Cells were visualized with a 40X magnification objective on the stage of an upright microscope (Olympus BX51WI) equipped with an infrared Dodt contrast mask and fluorescence optics. Typically, round cells with diameter ~15μm in the DCN molecular layer were usually

cartwheel cells and were confirmed by complex spiking in response to a current step. Elliptoid cells with transverse diameter ~ 20 μm in the DCN fusiform cell layer were usually fusiform cells and were confirmed by their large membrane capacitance (>35 pF) and their regular spiking pattern. Recording electrodes (4-7 MΩ) were pulled from borosilicate glass (WPI 1B150F-4) by a vertical puller (Narishige P-10). Series resistances were usually < 12 MΩ, compensated by 80%, and monitored throughout the course of the recording. Data were discarded if the series resistance changed by more than 25%. In paired recording experiments, we used a pipette solution containing (in mM): 113 K-Gluconate, 1.75 $MgCl_2$, 2.75 $MgSO_4$, 9 HEPES, 0.1 EGTA, 14 $Tris_2$-phosphocreatine, 0.3 Tris-GTP, and 4 Na_2-ATP, with pH adjusted to ~7.3 with KOH and osmolarity adjusted to ~295 mOsm with sucrose. The calculated chloride reversal potential (E_{Cl}) using this solution was ~ - 97 mV. To establish paired recordings from synaptically connected cartwheel-cartwheel or cartwheel-fusiform cells, whole-cell voltage-clamp recordings from both cells were performed; each cell received a burst of voltage pulses (from -60 mV to +20 mV, 0.2 ms/pulse, 3 pulses at 200 Hz) to test if that cell could evoke inhibitory postsynaptic currents (IPSCs) in the other cell. The latency for the unitary IPSC after the presynaptic escaping spike was usually less than 0.5 ms (Roberts et al., 2008). Cartwheel-to-fusiform cell IPSCs have sub-ms rise times (Roberts and Trussell 2010) suggesting somatic and proximal dendritic sites of contact, consistent with morphological analyses (Rubio and Juiz 2004). In each paired recording, the membrane potential of the presynaptic cell was held at -60 mV while the postsynaptic cell was held between -50 mV and -60 mV. For current clamp recordings, the pipette solution contained 2.75 $MgCl_2$, 1.75 $MgSO_4$ instead of 1.75 $MgCl_2$ and 2.75 $MgSO_4$ to mimic the E_{Cl} of fusiform cell measured by perforated-patch

recording (- 84 mV) (Kim and Trussell, 2009). The membrane potential of fusiform cells was kept ~ -60 mV by bias current injection (from -100 to -250 pA). Corrections to holding potential were only made to estimate synaptic conductance, based on a 13 mV junction potential (Fig. 6). In some experiments the chloride reversal was shifted to -44 mV (V_{hold} = -70 mV) using a pipette fill containing (in mM) 105 K-Gluconate , 15.5 KCl , 4.8 $MgCl_2$, 10 HEPES, 0.1 EGTA, 14 Tris2-phosphocreatine, 0.5 Tris-GTP, 4 Na_2-ATP, in order to achieve inward IPSCs.

Data acquisition

Electrophysiological data were acquired with a Multiclamp 700B amplifier and pClamp 10.3 software.

Photostimulation

To activate ChR2 in the brain slices, we used a 470nm LED (Sutter Instruments TLEDPLUS-Y) coupled through the epi-illumination port of the microscope. Pulses of blue light (0.5 ms/pulse) were delivered through pClamp control and cells were illuminated at the focal plane under the 40X 0.8NA objective. The illumination area at the focal plane had a diameter ~ 1mm. The maximum power of the incident light provided by the LED under the objective was ~3.4 mW (Newport 1815-C power meter with 818-ST sensor), corresponding to an irradiance of ~ 4.3 mW/mm^2. The irradiance used during photostimulation experiments was usually much weaker, and ranged from 3.8 μW/mm^2 to 1.8 mW/mm^2 (see Fig. 7).

Data analysis

Electrophysiology data were analyzed in IGOR Pro 6.34 (Lake Oswego, OR) using Neuromatic package (http://www.neuromatic.thinkrandom.com/) and custom-written procedures. Peak IPSC amplitudes from each cell were measured from traces averaged from at least 15 trials. Statistical comparisons were done in IGOR or R (http://www.R-project.org/). Averages are represented as mean ± SEM. Group comparison was done by t-test if the data were distributed normally (data normality was tested using Shapiro-Wilk test in R), otherwise a Wilcoxon signed-rank test was used. Optimal number of ChR2-evoked synaptic inputs to each cell was determined using K-means cluster analysis and elbow method (Ferragamo et al., 1998; Cao and Oertel, 2010; Chabrol et al., 2015a) with custom-written scripts in R.

Modeling synaptic depression

A computational model for synaptic depression was devised in IGOR using custom written procedures. Single- and two- pool vesicle depletion model for synaptic depression were adopted from a release site model as described in previous studies (Weis et al., 1999; Brenowitz and Trussell, 2001; Trommershäuser et al., 2003). For the single-pool model, the synapse had n_{ini} available release sites at rest and each site released a vesicle with probability p in response to stimulation. Hence, upon stimulation, there were on average N vesicles released, where

$$N = n_{ini} \cdot p$$

After stimulation, the number of emptied sites recovered (so that they can be releasable again) following a rate constant ($1/\tau$). The number of available release sites n_i just before the i_{th} stimulus is given by:

$$n_i = n_{i-1} \cdot (1-p) + [n_{ini} - n_{i-1} \cdot (1-p)] \cdot \left(1 - e^{-\frac{\Delta t}{\tau}}\right), \qquad i > 1$$

Δt = interval between i_{th} and $(i\text{-}1)_{th}$ stimulation

Assuming that p does not change during stimulation, the i_{th} stimulus causes N_i vesicles to be released:

$$N_i = n_i \cdot p$$

For the two-pool model, the number of total release sites at rest n_{ini} was divided among each pool according to fractions *r1* and *r2* ($r1 + r2 = 1$) so that pool 1 contained ($n_{ini} \cdot r1$) release sites and pool 2 contained ($n_{ini} \cdot r2$) release sites. Upon stimulation, each pool depletes and replenishes vesicles independently according to its own p and τ. The total number of vesicles released at the i_{th} stimulation during train stimulation (N_i) is the sum of release from each pool. The evoked responses can therefore be presented as the total number of released vesicles multiplied by quantal size. We assumed that the quantal size is the same for each pool and does not change during stimulation because glycine receptors do not desensitize quickly (Harty and Manis, 1998). Therefore, the normalized IPSC predicted by the model is exactly the normalized number of vesicles released during train stimulation. The normalized release were then compared with experimental data using a curve fitting procedure GenCurvefit (Copyright (C) 2006 Andrew Nelson and Australian Nuclear Science and Technology Organisation) to obtain best-fit parameters for the two-pool model.

Immunostaining for ChR2-(H134R)-EYFP

One GlyT2-Cre; Ai32 mouse was transcardially perfused with 4% paraformaldehyde and the brainstem part containing DCN was dissected out for post-fixation. After post-fixation, the tissue was sectioned at 30 μm thickness, washed in phosphate buffer saline (PBS) for several times, blocked in bovine serine albumin (BSA), and incubated in a rabbit polyclonal anti-GFP Alexa Fluor 488 Conjugate (1:200; A21311, Life Technologies) overnight. The sections were then examined under a confocal microscope (Olympus Fluoview1000).

Reagents and chemicals

All reagents stated, except for SR-95531 (Tocris), were purchased from Sigma.

Results

Rapid short-term depression at cartwheel cell synapse

Synaptic depression at cartwheel cell glycinergic terminals has been previously reported (Mancilla and Manis, 2009; Kuo and Trussell, 2011), however a detailed description of its kinetics is still lacking. We therefore measured short-term plasticity in paired recordings from synaptically coupled cartwheel cells (n = 10, amplitude of $IPSC_1$: from 124.1 to 532.1 pA, median 261.6 pA, mean ± sd: 301.6 ± 151.8 pA) or coupled cartwheel and fusiform cells (n = 5, amplitude of $IPSC_1$: from 264.0 pA to 2883.0 pA, median: 480.2 pA, mean ± sd: 958.8 ± 1099.7 pA) (Fig 1A and B). There was one particularly strong cartwheel-fusiform connection in our dataset (2883.0 pA), while the others ranged from 124.1 to 850.0 pA. Apart from this outlier, the range is consistent with

previous studies (Roberts and Trussell 2010). The range of strengths may reflect the variable distances between cells and the effects of tissue slicing. Statistical analysis showed no differences in the kinetics of synaptic depression between the types of connections (cartwheel-cartwheel vs cartwheel-fusiform) and therefore these data were pooled together (Fig 1B; t-test). Cartwheel cells fire bursts of high-frequency complex spikes (3-5 spikes at > 200Hz) and regular simple spikes (~0.1 - 20Hz) spontaneously or in response to current injection (Kim and Trussell, 2007; Bender et al., 2012). In order to measure synaptic responses to a fixed number of presynaptic action potentials in the absence of background firing, we voltage-clamped presynaptic cartwheel cells at – 60 mV and induced escaping simple spikes by delivering a train of 0.2 ms, 80 mV voltage steps (Fig 1B) (Roberts et al., 2008). We found that the synapse exhibited a fast and pronounced synaptic depression in response to 10-Hz-train stimulation, reaching steady state (~ 20 % of the initial response) rapidly after roughly 5-6 stimuli (Fig 1D, decay constant: 1.70 ± 0.04 stimuli when fit to a single exponential function).

We next tested if high-frequency stimulation of the synapse could also lead to such strong synaptic depression, since high-frequency activity can in principle lead to calcium accumulation at terminals and trigger facilitation (Zucker and Regehr, 2002). However, cartwheel synaptic responses to a 20-pulse, 200-Hz train still showed strong synaptic depression (Fig 1C). The profile of this decay could be fit with a double exponential function with 1.39 ± 0.18 stimuli and 4.58 ± 1.05 stimuli for fast and slow decay time constants (fast component 59 ± 11% of fit), respectively. Together with the 10-Hz responses, these results suggested that cartwheel synapses always exhibit synaptic depression when activated from a quiescent state.

It has been suggested that release probability is low in vivo due to low $[Ca^{2+}]_e$ in the cerebrospinal fluid, resulting a reduction in the degree of short-term synaptic depression compared to in vitro conditions (Borst, 2010). However, at cartwheel synapse we still observed a ~70% decrease in peak IPSC amplitude during a 20-pulse 10-Hz stimulation when we reduced $[Ca^{2+}]_e$ to 1.2 mM ($IPSC_{16-20}$ / $IPSC_1$: 0.28 ± 0.07; data not shown). This suggests that in vivo, continuous low-frequency activity would still depress cartwheel synapse by a large degree.

Single-pool vesicle depletion model is unable to explain synaptic depression

We next explored the mechanism of such fast and pronounced short-term depression. We excluded postsynaptic receptor desensitization, because cartwheel cell synapses are mostly glycinergic (Apostolides and Trussell, 2013) and glycine receptors desensitize slowly (Harty and Manis, 1998). Moreover, desensitization as a causative factor in depression is inconsistent with the observation that the depression decay rate, in terms of stimulus number, for 10 Hz was similar to the fast decay rate at 200 Hz (1.7 vs 1.37 respectively). Depression is also unlikely to be caused by receptor saturation, because depression occurs even at low frequency (10 Hz) and glycine should unbind the receptor completely during the 100-ms interstimulus interval. We also repeated the experiments using high $[Cl^-]$ internal (E_{Cl}: - 44 mV) and found that there was no significant difference in steady-state response (mean ± SD of $IPSC_{16}$ – $IPSC_{20}$: low $[Cl^-]_i$: 0.20 ± 0.03, n = 15; high $[Cl^-]_i$: 0.19 ± 0.04, n = 6; p = 0.67, unpaired t-test), excluding the possibility that $[Cl^-]_i$ accumulation during repetitive stimulation would lead to a decrease in chloride driving force and cause synaptic depression (Thompson and Gahwiler, 1989). Therefore

depression is most likely to have a presynaptic mechanism. Indeed, as predicted from a vesicle depletion model, the paired-pulse ratio of the second versus the first IPSC peak amplitude during 10 Hz stimulation tends to be smaller when the first IPSC was larger (Fig 1E; 581 points, pooled data from 15 cells, > 20 trials per cell, linear regression fit, $R^2 = 0.14$ $p < 0.001$) (Debanne et al., 1996; Regehr, 2012)

To explore the hypothesis of vesicle depletion quantitatively, we began with its simplest form, which assumes that every release site in the pool has the same vesicle Pr and replenishment rate, with replenishment rate proportional to the number of emptied release sites (Brenowitz and Trussell, 2001; Thanawala and Regehr, 2013). To estimate the Pr, we first calculated the size of the readily-releasable pool. Two methods were used: (1) by back-extrapolating from the last 5 points of cumulative normalized IPSC amplitude during 200-Hz stimulation to the y-axis (Schneggenburger et al., 1999); and (2) by extrapolating the first 4 points of the normalized IPSC amplitude versus cumulative normalized IPSC amplitude plot to the x axis (Elmqvist and Quastel, 1965; Lu and Trussell, 2000). Although each method emphasizes different features of the data, they gave similar estimates of the relative size of readily releasable pool compared to the first release in the 200-Hz train (2.86 from method 1 and 2.89 from method 2; Fig 1F). Hence, we obtained a rather high Pr of ~ 0.35 by calculating the released fraction in the first response (1/2.86 = 0.349, method 1; 1/2.89 = 0.346, method 2). Combined with the previously measured recovery time constant (5.5 seconds) from synaptic depression (Kuo and Trussell, 2011), a single-pool depletion model for the cartwheel synapse was built. However, although the model predicted well the rate of decay of the first four responses to the 10-Hz or 200-Hz train stimulation, it greatly overestimated the degree of depression at steady state, similar

to an observation in a previous study (Weis et al., 1999) (Fig 1G). Because the pool size and Pr estimation methods mentioned above are only valid when the vesicle population is homogeneous (e.g. vesicles have the same Pr and recovery time constant) (Neher, 2015), this result suggests that there might be different distributions in the vesicle properties at cartwheel synapse. The overestimation of the degree of depression suggested that the depletion rate of vesicle pool was slower during steady-state depression, and this could be explained by recruitment of low-Pr vesicles (Sakaba and Neher, 2001a; Trommershäuser et al., 2003).

Two-pool vesicle depletion model accounts for synaptic depression

If low-Pr vesicles are recruited during synaptic stimulation, one would expect to see short-term synaptic facilitation after depression is complete, since low-Pr vesicles are often subject to facilitation (Müller et al., 2010). Indeed, when high-frequency stimulation was applied after the synapse was pre-depressed by low-frequency stimulation, we observed a modest (~20 % compared with the first response to high-frequency stimulation) synaptic facilitation in the second and third responses (Fig 2A and B, asterisk in 2B). Further high-frequency stimuli continued to depress the synapse. Interestingly, the decay rate of the responses to this high-frequency stimulation is similar to the slow component of the decay seen upon high-frequency stimulation evoked from a non-depressed state (5.87 ± 0.583 stimuli vs 4.57 ± 1.05 stimuli), and no fast phase was present. This result suggests that the initial 10-Hz train fully depleted a population of high-Pr vesicles, and that sustained transmission was mediated by a population of low-Pr vesicles which are subject to

facilitation and followed by further depression when the stimulation rate is sharply increased.

To model this two-vesicle-pool hypothesis, we assumed that the properties of each pool (i.e. Pr and recovery time constant) are independent of one other and both pools are activated simultaneously upon stimulation. We set the recovery time constant of one pool to 5.5 sec to accord with the measured recovery time constant from depression (Kuo and Trussell, 2011) but let all other parameters be optimized during the fitting procedure. The model was then fit to the averaged population data shown in Fig 2D, which contains responses to a 10 Hz → 200 Hz → 200 Hz train stimuli, with a 15 sec gap between the first 200 Hz and the second 200 Hz train. Two pools of vesicles with a ten-fold difference in release probabilities gave the best fit (high Pr: 0.44, low Pr: 0.04), and accounted for initial and steady state depression well throughout the complex pattern of stimulus trains. It should be noted that the two 200-Hz trains used here are expected to probe distinct presynaptic conditions, as the first occurs during steady state depression and should deplete only the low-Pr pool, while the second occurs at quiescent state and should deplete two pools differentially. We found the best-fit parameters from this sequence describes the data better (with smaller sum of square error of the residuals) than fitting the model to two frequencies only (i.e. a 10 Hz → 200 Hz sequence with or without 15 sec gap in between), although the latter also give similar estimates (a small high-Pr pool with Pr ~0.46 and recovery time constant 5.5 s, and a large low-Pr pool with Pr < 0.10 and recovery time constant around several hundred milliseconds, data not shown). Thus, our fitting result suggests that the synapse utilizes vesicles with two distinct release probabilities.

The two-pool model also predicts that, as the number of stimuli increases, vesicles from the low-Pr pool contributed more to the total release (Fig 2D). How do the properties of each pool account for such a trend during repetitive stimulation? From the best-fit parameters (Fig 2C), the size of the low-Pr pool was twice that of the high-Pr pool, but its Pr was only 10% of the high-Pr pool (0.04 vs 0.44). The release at the beginning of the train was therefore dominated by the high-Pr pool (Fig 2D, bottom panel). However, the high-Pr pool was depleted rapidly due to its slow recovery time constant (5.5 sec) and the ensuing release was mostly contributed by the low-Pr pool (Fig 2D bottom panel). The fast recovery rate of the low-Pr pool (recovery time constant ~130 ms) sustains the release during steady state depression at 10 Hz and only gets depleted upon stimulating at 200 Hz. Due to lack of activity-dependent increase in Pr in the parameters, this depletion model cannot predict the small facilitation during high frequency stimulation after the synapse is depressed. However this phase was a minor part of the synaptic response, and the model still described well the majority of short-term depression at the cartwheel synapse.

Ca^{2+}-dependent recovery does not mediate transmission during depression

The other possible mechanism that slows pool depletion rate during repetitive stimulation, and could potentially explain our results, is activity-dependent enhancement of vesicle replenishment rate (Dittman and Regehr, 1998; Wang and Kaczmarek, 1998; Weis et al., 1999). While models incorporating such activity-dependent recovery mechanisms were also effective (modeling not shown), we sought experimental evidence to confirm whether they were justified at this synapse. Accelerated vesicle recovery is often Ca^{2+}-dependent (Dittman and Regehr, 1998; Wang and Kaczmarek, 1998; Sakaba and

Neher, 2001b). Indeed, at cartwheel synapses, there is accelerated recovery from synaptic depression after long 200-Hz trains (Fig 3A). Such speeding of recovery was not observed when the Ca^{2+} chelator EGTA (1 mM) was included in the presynaptic recording pipette, showing that recovery was Ca^{2+}-dependent (Fig 3A and B, recovery fraction in control: 0.36 ± 0.05, n = 5; in 1 mM EGTA: 0.13 ± 0.01, n = 6; p = 0.003, unpaired t-test). However, only long (20-pulse) but not short (3-pulse) high-frequency stimulation could induce such acceleration of recovery (Fig 3A and B, recovery fraction after 3-pulse 200 Hz stimulation: 0.18 ± 0.02, n = 5; p = 0.01 when compared to 20-pulse stimulation in control, paired t-test). Importantly, neither the rate nor the extent of depression changed in the presence of 1 mM EGTA at either 10 Hz or 200 Hz (Fig 3C, $p > 0.05$, unpaired t-test for every stimulus number). Similar results were obtained with cartwheel cells loaded with 10 mM EGTA, while 5 mM BAPTA sharply decreased release (not shown). We therefore conclude that although there is Ca^{2+}-dependent acceleration of pool replenishment at the cartwheel synapse, it requires massive Ca^{2+} influx and may not play a role in sustaining the release during steady-state depression. However, it may nevertheless be that some untested patterns of activity could still reveal a contribution of Ca-dependent recovery in sustaining transmission, requiring further investigation.

Low-Pr pool dominates release during spontaneous activity

We next tested if the two-pool depletion model would predict responses to spontaneous spiking, which contains much more irregular patterns of inter-stimulus intervals. Spontaneous spiking frequency of cartwheel cells ranges from 0-30 Hz *in vivo* (Parham and Kim, 1995; Ma and Brenowitz, 2012). To mimic cartwheel cell spontaneous

spiking pattern, we constructed a stimulation paradigm consisting of Poisson spike train with mean frequencies centered at 5 Hz, 10 Hz, and 20 Hz. We then applied these spike trains to the presynaptic cell in paired cartwheel-fusiform cell recordings. Of the 5 pairs tested, we found that the two-pool model was able to predict synaptic responses well, with fractional error of 6.5 ± 3.7 % (Fig. 4 A-D). In fact, the model showed that there is a frequency-dependent depression of the steady-state response during spontaneous firing, which corresponded well with the experimental data observed in the current and a previous study (Kuo and Trussell, 2011) (Fig 4E).

How does the contribution of each pool varies as the spontaneous spike frequency changes? To explore this question, we estimated the relative proportions of vesicles released from high- and low- Pr pools during steady-state depression at different spiking frequencies. As shown in Fig 4F, when spontaneous spiking frequency goes above 2.5 Hz, the low-Pr pool is expected to dominate the release compared to the high Pr pool. This shift is due to the slow recovery rate of the high Pr pool and the large size of the low Pr pool, which can be observed in the time course of change of the pool size during 20 Hz stimulation in Fig 4D. In conclusion, high Pr and low Pr vesicles contribute differentially to release under low vs high frequency spontaneous spike conditions.

Small convergence ratio in the cartwheel-fusiform circuit

Our results suggest that inhibition from single cartwheel cells is reduced to ~ 20% of its original strength once the cells' average spontaneous firing rate increases from 0 to >5 Hz. Therefore, as the spontaneous firing rate of cartwheel cells increases, the size of the cartwheel cell population needed to provide effective inhibition onto a fusiform cell must

increase. Connected cartwheel-fusiform cell pairs share common spontaneous IPSCs, indicating that there are at least two cartwheel cells converging onto the same fusiform cell (Roberts and Trussell, 2010). Is the size of convergent circuit large enough to provide effective inhibition during high-frequency spontaneous firing, despite synaptic depression? We explored this possibility by using optogenetics to selectively activate cartwheel cells. Cartwheel cells express glycine transporter 2 (GlyT2) (Apostolides and Trussell, 2013), allowing us to use a GlyT2-Cre;Ai32 mouse line to drive channelrhodopsin expression in cartwheel cells (see Materials and Methods).

We first tested whether the expression of ChR2(H134R)-EYFP driven by GlyT2-Cre is sufficient to activate cartwheel cells. Immunostaining for EYFP showed that ChR2 was most densely expressed on DCN molecular layer spiny neurons, which exhibit the morphological characteristics of cartwheel cells (Wouterlood and Mugnaini, 1984) (Fig 5A). In agreement with this observation, cell-attached recordings of cartwheel cells showed that brief, pulses of blue light (0.5 ms duration) could evoke spiking (Fig 5B). On some occasions, they would fire more than one spike, consistent with their tendency to generate spike bursts (Bender et al., 2012) (Fig 5B). Moreover, firing probability increased with light intensity, indicating that more cartwheel cells were recruited with stronger light pulses (Fig 5C).

We next examined the specificity of ChR2(H134R)-EYFP expression in the DCN because two other types of fusiform-cell-targeting interneurons, vertical cells and stellate cells, may also express ChR2 driven by GlyT2-Cre. Because stellate cell synapses are predominantly GABAergic (Apostolides and Trussell, 2014) while cartwheel synapses are mainly glycinergic, for ChR2 experiments we included $GABA_A$ receptor blocker SR-95531 (5

μM) in the bath to prevent contributions from stellate cells. There were dim GFP signals in the DCN deep layer, suggestive of ChR2 expression in glycinergic vertical cells (Fig 4A). Indeed, cell-attached recordings revealed that vertical cells could be activated by sustained blue light stimulation (duration: 100 ms, intensity: ~ 1 mW; data not shown). However, only 3 out of 13 vertical cells tested fired spikes in response to brief (0.5 ms) light pulse stimulation and they required higher light intensity compared with cartwheel cells (Fig 5B and C, vertical cells: > 1.4 mW). Since the unitary conductance of a vertical-fusiform synapse is 10% that of a cartwheel-fusiform synapse (Kuo et al., 2012), we reasoned that optically-evoked IPSCs (oIPSCs) in fusiform cells are mostly from cartwheel cells.

We used two approaches to estimate the convergence ratio, i.e., the number of cartwheel cells contacting a fusiform cell. The first was to divide the maximum light-evoked conductance over average unitary conductance of the cartwheel synapse measured with paired recordings (Person and Raman, 2012b). Due to light scattering, cells in the deeper layers of the slice are presumably exposed to weaker light stimulation as compared to cells on the surface. We thus decided to use strong light stimulation (3.5 mW) to recruit potentially all cartwheel cell inputs to the recorded fusiform cells despite the risk that it might activate some vertical cell inputs. We noticed that the responses in fusiform cells by 10-Hz light pulse stimulation only exhibited moderate synaptic depression (10^{th} IPSC/ 1^{st} IPSC = 0.5 ± 0.1, Fig 5A; compared to 0.2 in paired-recordings, Fig 1D) so it is likely that some cartwheel synapses were already depressed by spontaneous spiking. The maximal evoked synaptic conductance measured under this condition would be therefore underestimated. To silence the spontaneous activity and relieve synaptic depression, we applied 10 μM noradrenaline to the bath (Kuo and Trussell, 2011). Consistent with

previous finding, the peak of the 1st oIPSC increased to ~2.5 times of its initial size and the train stimulation evoked more robust synaptic depression after noradrenaline application (Figure 6A-C). Indeed the depression triggered by light pulses in noradrenaline was similar in magnitude to that seen with paired recordings (Fig. 6B), indicating that exocytosis triggered by channelrhodopsin and electrical stimulation are similar. Moreover, IPSCs triggered by channelrhodopsin were completely blocked by TTX (0.5 μM, data not shown). Such similarity in depression kinetics also suggests that the contributions from other GlyT2-expressing neurons to oIPSCs (e.g. vertical cells) are minor. The maximum evoked conductance measured in the presence of noradrenaline ranged from 57.4 to 327.1 nS in the 11 fusiform cells tested (average: 138.5 ± 28.3 nS, Fig 6D). Dividing those over the population average of the unitary conductance from connected cartwheel-fusiform pairs (40.0 ± 17.3 nS, n = 6,), we obtained a ratio from 1.4 to 8.2, giving an average of 3.5 ± 0.7 cartwheel cells converging onto a fusiform cell (Fig 6G). To address the concern that the neurons' projections are cut during brain slicing, we performed these measurements in slices of two different thicknesses (260 μm vs 360 μm) and did not see a significant difference (260 μm: 2.9 ± 0.3, n=5; 360 μm: 3.9 ± 1.3, n = 6; p = 0.66, Mann-Whitney test). Therefore the data were pooled together (Fig 6G).

Given the wide range of unitary conductance of cartwheel-fusiform cell connections, the number of inputs estimated above might be biased because this approach assumes that each individual unitary conductance should be close to the population average. We therefore took another approach by examining how many increments are revealed in the peak optically-evoked IPSC amplitudes as we gradually increased the light stimulation intensity, which presumably would recruit increasing numbers of cartwheel cells (Fig 6 E

and F). Each step resolved by this method should represent one cartwheel cell's input. To reduce quantal fluctuation upon repeated trials, 4 mM Ca^{2+} was included in the bath. During the course of recording, it is possible that cartwheel synapses were depressed during some but not all trials due to the irregular pattern of spontaneous firing. This would mislead the interpretation of each 'step' as individual cartwheel inputs. We therefore applied a train of 10 light stimuli before each test light pulse to pre-depress inputs. The number of increments of evoked currents were then determined by K-means cluster analysis (see Materials and Methods) (Fig 6 E and F) (Ferragamo et al., 1998; Cao and Oertel, 2010). The number obtained by this method is consistent with that obtained from the maximum conductance over unitary conductance described above: there were on average 3.3 ± 0.2 inputs to the 12 fusiform cells recorded (Fig 6G, $p = 0.60$ compared with maximum-over-unitary conductance method, t-test; $p = 0.34$, Mann-Whitney test). Taken together, our results indicate that the convergence ratio of cartwheel cells is small, consisting of about 3-4 cartwheel cells targeting a single fusiform cell.

Size of effective convergence increases with spontaneous spiking rate

The rather small size of the convergent circuit formed by cartwheel cells raises the question of whether a given cartwheel cell can provide effective inhibition during high spontaneous spiking rate, i.e. when the synapses are depressed. To answer this, we induced wide-field ChR2 stimulation in order to elevate firing frequency of the entire cartwheel cell population.

We first tested whether the number of cartwheel cells required to inhibit a postsynaptic fusiform cell, i.e. the effective convergence ratio, increases with spontaneous

firing frequency. Action potentials were evoked in a fusiform cell by injecting an EPSC-like waveform while simultaneously varying blue light pulse intensity to recruit inhibition from different numbers of cartwheel cells. The amplitude of the EPSC-like current (400 - 500 pA) was sufficient to trigger spikes in all trials, and was consistent with previous estimates for securely suprathreshold parallel-fiber-evoked EPSCs (Roberts and Trussell, 2010). The inhibition induced in this way would increase with light intensity as cartwheel cells are recruited and fully prevent fusiform cell from firing when the light reaches a critical level (Fig 7A). After repeating this protocol for 10-15 trials, a 'light-inhibition' curve for the fusiform spike probability against different light intensities was constructed and an 'IC_{50}' value for the amount of light that inhibits 50% of the spike generation was obtained from a sigmoidal fit to the data (Fig 7B). The same protocol was then applied to the cell again, except this time a train of 5 light pulses was delivered 250 ms before current injection to increase cartwheel cell population spiking rate and cause depression. The amount of light just sufficient to inhibit fusiform cell spiking under control condition no longer inhibited spiking, indicating that the light train depressed cartwheel synapses. However, with stronger light intensity the recruited inhibition could once again effectively prevent spiking in the fusiform cell (Fig 7A). This was reflected in a rightward shift in the curve and an increase in IC_{50} in the spike probability-light intensity plot (Fig 7B). This rightward shift was observed in all 7 fusiform cells tested (Fig 7C) (control IC_{50}: 0.55 ± 0.05 mW vs depression IC_{50}: 1.15 ± 0.11 mW; $p = 0.001$, paired t-test). Therefore, despite the powerful synaptic depression induced by spontaneous spiking, recruitment of multiple inputs enabled effective inhibition to the postsynaptic principal cell.

Low-Pr pool is critical for effective inhibition in a small convergent circuit

The fact that such a small convergent circuit can provide effective inhibition despite strong synaptic depression was rather surprising. Because our synaptic depression model suggests that low-Pr vesicles dominate the release during high-frequency spontaneous spiking (Fig 4), it seems that they are critical to setting the limiting number of cartwheel cells required for inhibition. We therefore used the model to quantify the effect of different pools of vesicles on functional convergence during various spontaneous spiking frequencies (Fig 8 A , B). We assume an 'inhibition threshold' such that any IPSC larger than the threshold would inhibit fusiform cell spiking. We posited 50% depression as the maximum depression tolerable for effective inhibition by a single cartwheel cell, given that an undepressed cartwheel cell is capable of inhibiting fusiform cell firing (Roberts and Trussell, 2010). The number of effective inputs can thus be estimated by dividing the threshold over the inhibition strength at different depression levels (Fig. 8A, B). The effective number of cartwheel inputs estimated using this method roughly matched the experimentally estimated convergence (~3 cartwheel cells), supporting the idea that cartwheel-fusiform circuit can provide effective inhibition in a small convergent diagram. In addition, the number of effective inputs was much larger if the synapse only utilized the high-Pr pool (30 cells vs 3 cells) (Fig 8B). This was due to a much more profound frequency-dependent depression when the synapses lacked low-Pr vesicles (Fig 8A). Hence, the functional size of a convergent neural circuit is defined by the properties of its synaptic vesicles.

Discussion

Although short-term synaptic depression and modulation of neuronal spontaneous firing have been described in numerous brain regions, it remains unclear how their interaction impacts functional neural circuit connectivity. We characterized a dynamic relationship between spontaneous firing rate, synaptic depression, and the effective convergence of an interneuron circuit. Due to activity-dependent synaptic depression, synaptic strength from cartwheel interneurons is weakened by increased spontaneous firing. Thus, the number of cartwheel cells needed to effectively inhibit fusiform cells increases with its spontaneous firing rate. Interestingly, analysis of the synaptic depression kinetics suggests that the type of vesicles utilized by the synapse is critical for the effective size of the circuit. Because low-Pr vesicles with fast recovery rate prevent cartwheel synapse from complete depression at high spontaneous firing rate, effective inhibition can be performed in a relatively small circuit. Only three-to-four cartwheel cells are estimated to converge onto a single fusiform cell, and these are sufficient to provide effective inhibition when synapses are depressed by spontaneous firing. The interplay between spontaneous firing rate, synaptic depression, and vesicle recruitment therefore determines the size of the convergent circuit that can effectively influence postsynaptic spiking.

Vesicle pool dynamics and synaptic depression

In this study, we suggest that vesicle depletion mediates synaptic depression at the cartwheel cell synapse. In addition to vesicle depletion, several other mechanisms have been proposed to contribute to short-term synaptic depression, including reduced Ca^{2+}-influx at the presynaptic nerve terminal (Xu and Wu, 2005; Catterall and Few, 2008),

postsynaptic receptor desensitization (Trussell et al., 1993; Brenowitz and Trussell, 2001) or saturation. The former seems unlikely since peak amplitudes of action-potential-induced Ca^{2+} transients at cartwheel cell boutons summate linearly in response to a train of high-frequency action potentials (Roberts et al., 2008; Bender and Trussell, 2009). Regarding receptor desensitization, because synaptic responses evoked by cartwheel cells are mainly glycinergic (Golding and Oertel, 1997; Roberts et al., 2008; Apostolides and Trussell, 2013) and glycine receptors show slow desensitization kinetics (~30% decline in response to 1 sec, 1 mM glycine application; (Harty and Manis, 1998)), receptor desensitization should contribute little to such fast synaptic depression. Furthermore, we found a negative correlation between paired-pulse ratio and the peak amplitude of the first IPSC, indicating a presynaptic mechanism that mediates short-term plasticity (Debanne et al., 1996; Regehr, 2012) (Fig 1E). Thus, we conclude that vesicle depletion is likely to be the major mechanism contributing to the depression.

We propose that the synaptic depression at cartwheel synapse is contributed by depletion of two pools of vesicles: a high-Pr, slow recovery pool that contributes mainly to the IPSCs in the initial phase of the depression, and a low-Pr, fast recovery pool that sustains release during steady state activity. Here, our definition of 'pool' refers to the 'readily-releasable pool' (RRP), vesicles immediately available upon neural stimulation (Rizzoli and Betz, 2005). While we were not able to directly clamp or measure capacitance from inhibitory boutons, and thus directly measure vesicle pool dynamics, such measurements has been possible at large nerve terminals, particularly the calyx of Held. Interestingly, although the calyx and the cartwheel bouton differ greatly in size and transmitter content, our two-pool depletion model for cartwheel synapse shares many

similarities with that proposed for the calyx of Held. First, vesicle depletion also leads to synaptic depression at the calyx of Held , and deconvolution analysis of vesicle depletion kinetics in response to prolonged voltage steps in the calyx revealed that the RRP consists of a fast- and slow-releasing component, which corresponds to a high-Pr and low-Pr pool in response to short-pulse stimulation (Sakaba and Neher, 2001a). Second, the recovery rate of the fast-releasing pool at the calyx of Held synapse is much slower than that of the slow-releasing pool (Sakaba and Neher, 2001b). Third, although the calyx exhibits Ca^{2+}-dependent acceleration of recovery (Wang and Kaczmarek, 1998), introducing Ca^{2+}-chelator did not change the steady state level of depression (Weis et al., 1999) and a two-pool vesicle model with distinct release probabilities predicts frequency-dependent depression better than a single pool model with Ca^{2+}-dependent recovery (Trommershäuser et al., 2003). Finally, synaptic facilitation at the calyx can be revealed by high-frequency stimulation after the synapse is pre-depressed, suggesting low-Pr vesicles mediating the release at depressed state (Müller et al., 2010). In addition to the calyx, studies at other synapses also propose that the vesicular Pr decreases as the number of stimuli increases, thereby sustaining the release during steady-state depression (Betz, 1970b; Saviane and Silver, 2006; McElvain et al., 2015). Thus, our two-pool depletion model for transmission at the cartwheel cell glycinergic synapse may be generalizable to other synapses. A recent study proposes that depression and steady state release involves distinct release sites for the two phases of the response, based on statistical arguments (Wen et al., 2015). We cannot however distinguish between models in which the two pools represent distinct populations acting in parallel or a single population in different states of priming (Neher, 2015).

Small effective size of a convergent circuit

In this study, we estimated that 3-4 cartwheel cells converge onto a single fusiform cell, using two different physiological approaches. This value should in principle be an underestimate since some inputs might be lost during our slicing procedure. However, our results corroborates a recent anatomical study using serial EM reconstruction in hamster DCN, which suggested a low convergence ratio (3-4) based on numbers of somatic boutons on fusiform cells joined by a common axon (Salloum et al., 2014). Moreover, our estimate is similar to an anatomically determined convergence ratio (4.07) in rat DCN based on cell counts in EM (Wouterlood and Mugnaini, 1984). Despite such a small degree of convergence, synchronous activation of these inputs was sufficient to inhibit fusiform cell spiking even when synapses were maximally depressed by high-frequency of spontaneous firing. Combined with the previous finding that a single cartwheel cell at rest (i.e. without spontaneous spiking) can effectively inhibit fusiform cell spiking (Roberts and Trussell, 2010), inhibition of fusiform cells is maintained across the full range of spontaneous spike rates using one to four inhibitory cells. Such small effective size of convergent circuits has been observed in other brain regions. Cerebellar Purkinje cells, which share genetic, morphological, biochemical and biophysical similarities with cartwheel cells (Berrebi and Mugnaini, 1991; Oertel and Young, 2004b), also converge onto target cerebellar nuclear cells (Person and Raman, 2012a). Interestingly, although the estimated Purkinje-to-nuclear convergence ratio is an order of magnitude larger than that of the cartwheel-fusiform cell circuit (~30-40 vs 3-4), synchronous activation of only 2 Purkinje cells is able to entrain spike timing in the target nuclear cell (Person and Raman, 2012b). In the ventral cochlear

nucleus, as few as 2 suprathreshold auditory nerve fibers can reduce spike jitter by 40% in the target bushy cells (Xu-Friedman and Regehr, 2005). Similar to cartwheel cell synapses, the examples mentioned above also display spontaneous activity and frequency-dependent synaptic depression (Telgkamp and Raman, 2002; Xu-Friedman and Regehr, 2005), and so the effective convergence in those circuits might also vary with their background spontaneous firing rates. Nevertheless, these findings suggest that small effective size convergent circuits is probably common in the brain.

Implications for sensory processing in DCN

This study provides a possible mechanism for cartwheel interneurons to regulate multisensory integration in DCN via functional connectivity reconfiguration. When the spontaneous firing rate in cartwheel cells is slow, activation of single cartwheel cells is sufficient to inhibit fusiform cell spiking. Conversely, when cartwheel cell spontaneous firing rate is high, only synchronous activation of multiple cartwheel cells will effectively inhibit a fusiform cell. Because cartwheel cells converging onto the same fusiform cell likely do not share the same sets of parallel fiber inputs (Roberts and Trussell, 2010), recruitment of different numbers of cartwheel cells may require activation of distinct sets of parallel fibers, and potentially distinct sets of sensory signals. Spontaneous spiking in cartwheel cells can be regulated by a variety of neuromodulators (Bender et al., 2010; Kuo and Trussell, 2011), presumably released during different behavioral states of the animal (Lee and Dan, 2012). One scenario is that specific sets of parallel fibers can effectively inhibit fusiform cell spiking only under certain behavioral states – in this way the neuromodulators can enhance the salience of a specific sensory signal carried by parallel

fibers. For example, sparse parallel fiber activation might effectively inhibit fusiform cells only when noradrenaline is released in vigilant states, during which cartwheel cells are relieved from depression (Berridge and Waterhouse, 2003; Kuo and Trussell, 2011). An alternative view is that the shift of inhibition from multiple to single convergent cartwheel cells through neuromodulation increases the impact of the multisensory pathway vs the auditory (cartwheel cell independent) pathway in shaping fusiform cell firing. In either scenario neuromodulator-dependent shifts in the significance of a given interneuron's activity shows that the convergence ratio in neural circuits can, from a functional standpoint, be a 'tunable' parameter, and that the balance of different vesicle pools at individual nerve terminals provides the link between patterns of spikes activity and the effective level of synaptic convergence.

Acknowledgements

This study is funded by National Institutes of Health (N.I.H.) Grants NS028901 and DC004450 (to L.O.T.); N.L. Tartar Trust Fellowship (to H.-W.L). We thank members from the Trussell lab for helpful discussions. We thank Drs. Erwin Neher, Sam Young, Dan Yaeger, and Tomohiko Irie for critical comments on the manuscript. We thank Dr. Carol Borges-Merjane for help with immunostaining experiments. We are grateful for Michael Bateschell and Ruby Larisch for help with mouse colony management. Floxed-ChR2(H134R)-EYFP breeder mice were kindly provided by the Westbrook lab at the Vollum Institute. The authors declare no competing financial interests.

Figure 1.1

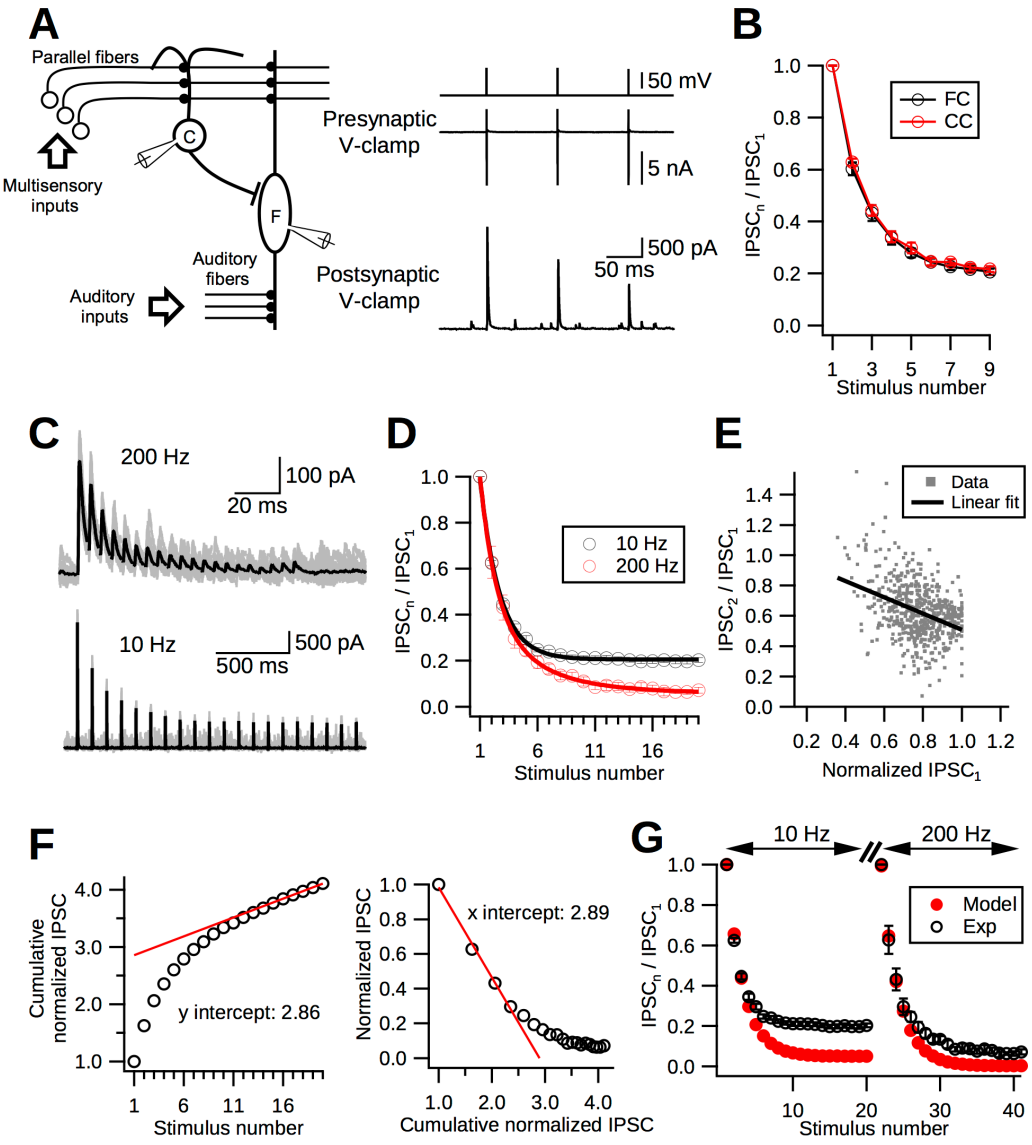

Figure 1.1 Short-term depression at cartwheel cell synapses

(A) Left, simplified DCN circuit and paired recording diagram. Right, example traces from a connected pair. Presynaptic cartwheel cell (C) was voltage clamped at -60mV and escaping spikes evoked by 0.2 ms voltage pulses (80 mV). Corresponding IPSCs were recorded in the postsynaptic cell, in this case a fusiform cell (F).

(B) Kinetics of short-term synaptic depression in cartwheel-cartwheel connections (CC, red) and cartwheel-fusiform cell connection (FC, black) are not significantly different ($p>0.05$, t-test). Data collected from these two connections were therefore pooled (n = 10, CC; n = 5, FC).

(C) Example traces showing synaptic depression occurs at low and high frequencies. Top, IPSCs evoked by 20 pulses of 200-Hz stimulation. Bottom, IPSCs evoked by 20 pulses at 10 Hz. Black traces are the averages of at least 15 individual sweeps (gray).

(D) Summary of short-term depression at low and high frequencies. Black, synaptic depression kinetics at 10 Hz. N= 15 connections. A single exponential function can be fit with a decay constant of 1.70 ± 0.04 stimuli. Red, synaptic depression at 200 Hz. N = 6 connections. A double exponential function can be fit with 1.37 ± 0.18 stimuli and 4.57 ± 1.05 stimuli for fast and slow decay constants, respectively. Fast component is 59 ± 11 % of fit.

(E) Negative correlation between the paired-pulse ratio (IPSC2/IPSC1) and peak amplitudes of IPSC1. N = 15 connections. Each gray dot represents the paired-pulse ratio with its corresponding IPSC1 amplitude in a single trial during 10 Hz stimulation. At least 20 trials were repeated for each connection. The peak IPSC1 amplitudes in each connection were normalized to the biggest IPSC1 amplitude in the same connection. Black line represents a linear regression fit to all the dots. $P < 0.001$, $R^2 = 0.14$, 581 points.

(F) Two approaches to estimating the size of the readily-releasable pool and initial vesicular Pr (Pr). Left, plot cumulative normalized IPSCs against the stimulation number (open circles). The relative size of the pool is the y-intercept (2.86) of a linear regression line (red) back-extrapolated from the last five points. Right, plot normalized IPSC amplitude against the cumulative normalized IPSC amplitude. The relative size of the pool is the x-intercept

(2.89) of the linear regression line (red) extrapolated from the first four points. Both approaches give similar estimates for the Pr (Left, 1/2.86 = 0.349; right, 1/2.89 = 0.346)

(G) Single-pool depletion model (Pr = 0.35, recovery time constant: 5.5 sec) cannot account for cartwheel synaptic depression. Black, experimental data. Red, model predictions. The model matches the first four data points during depression but greatly overestimates the degree of depression in both 10 Hz and 200 Hz –evoked responses.

Figure 1.2

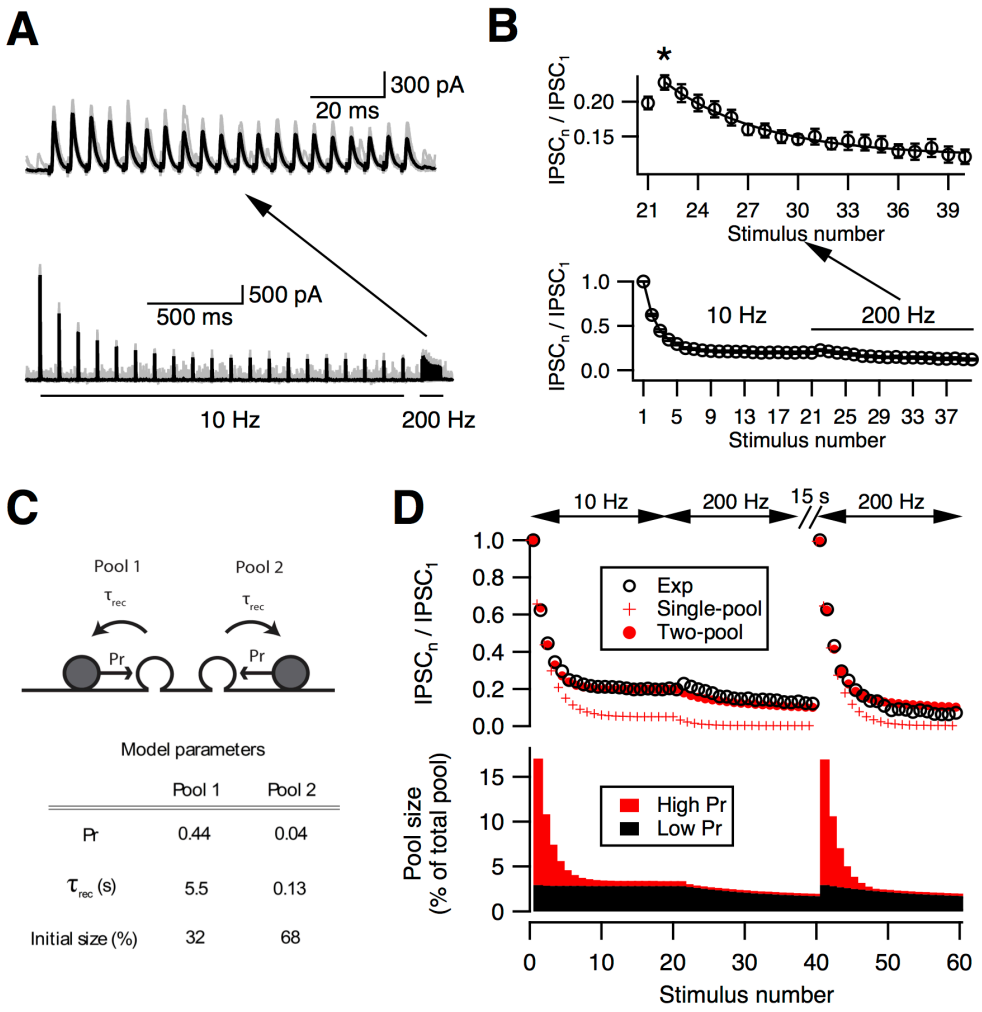

Figure 1.2. Two-pool depletion model accounts for synaptic depression at cartwheel synapses.

(A) Example traces showing that short-term facilitation was revealed by high frequency (200Hz) stimulation after the synapse is pre-depressed by low frequency (10 Hz) stimulation. Top is the zoom-in of the traces evoked by 200-Hz stimulation shown below. Black, average trace from 20 individual traces (gray).

(B) Summary of synaptic facilitation kinetics from 15 connections. Top panel is the zoom-in of the 200-Hz evoked responses shown below. The decay of the 200-Hz responses can be fit by a single exponential with a decay constant of 4.57 ± 1.05 stimuli, which is similar to the slow decay time constant (5.87 ± 0.58 stimuli) of the 200 Hz responses evoked from a resting state. This indicates the depletion of a slow-releasing pool can only be revealed by high-frequency stimulation. N = 15 connections.

(C) Top, diagram of a two-pool depletion model. Each pool has independent vesicular Pr (Pr) and recovery time constant (τ_{rec}). Bottom, parameters from the best fit. Notice that the low Pr pool (Pool 2) has a faster recovery time constant and a larger initial size.

(D) Top, comparison between the experimental data (Exp, open circle) and predictions from single-pool (Single-pool, red cross) versus two-pool (Two-pool, red solid circles) depletion model. Bottom, the relative releases from each pool predicted by the two-pool depletion model during repetitive stimulation. Red, high-Pr pool. Black, low-Pr pool. Notice that the high-Pr pool contributes most of the release during fast depression and the low-Pr pool contributes most of the release during steady state or slow depression.

Figure 1.3

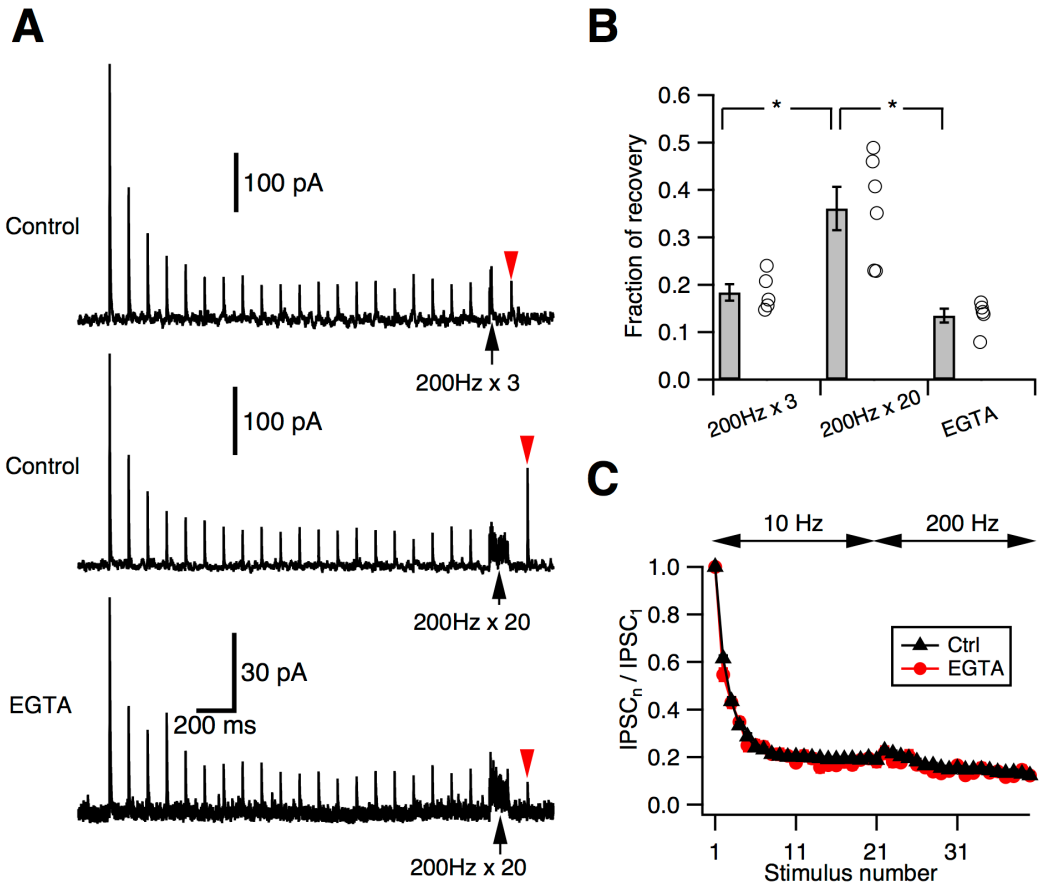

Figure 1.3. Ca^{2+}-dependent recovery does not contribute to steady-state transmission. (A) Example traces illustrating Ca^{2+}-dependent recovery at cartwheel synapses. Top, a train of 3-pulse stimuli at 200 Hz (black arrow) did not enhance recovery (red arrowhead) from synaptic depression. Middle, a train of 20-pulse stimuli at 200 Hz (black arrow) did enhance recovery (red arrowhead) from synaptic depression. Bottom, when 1 mM EGTA was included in the presynaptic recording pipette, the 20-pulse stimuli at 200 Hz (black arrow) could no longer enhance the recovery (red arrowhead) from depression. Traces are averaged from at least 15 trials. Top and middle are from the same cell. Recovery was tested 100 ms after the end of train stimulation.

(B) Summary of the recovery from depression under the three conditions shown in (A). Recovery was measured as the fraction of the peak amplitude of the IPSC1. Recovery from 200 Hz x 3 stimuli: 0.18 ± 0.02, n = 5; recovery from 200 Hz x 20 stimuli: 0.36 ± 0.05, n = 5; recovery from 200 Hz x 20 stimuli in 1 mM EGTA: 0.13 ± 0.01, n = 6. Recovery from 200 Hz x 20 is significantly larger than that from 200 Hz x 3 ($p = 0.01$, paired t-test) or that in 1 mM EGTA ($p = 0.003$, unpaired t-test).

(C) Kinetics of synaptic depression in response to a 10 Hz → 200 Hz stimulation when 1 mM EGTA was included in the presynaptic pipette (red, n = 5) is not significantly different from control (black, n = 15). $p > 0.05$ for every stimulus number, unpaired t-test.)

Figure 1.4

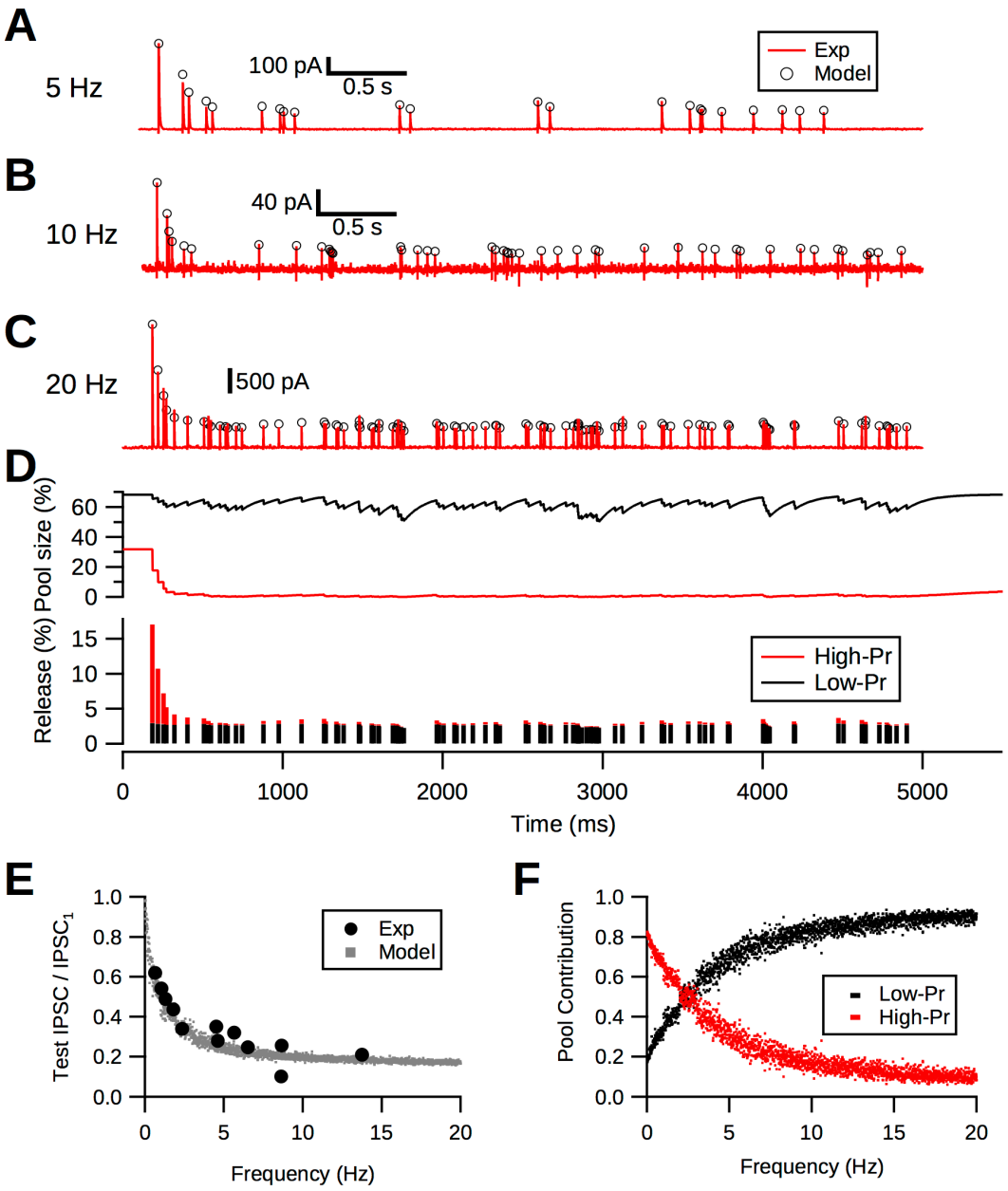

Figure 1.4 Two-pool depletion model predicts frequency-dependent synaptic depression.

(A)-(C) Random (Poisson) evoked responses (red) centered at 5, 10 and 20Hz are predicted by the two-pool depletion model (open circles). Each trace is from different connection.

(C) Middle, time course of the change in pool size during Poisson stimulation at 20 Hz. Note that the low-Pr pool (black) has a faster recovery rate compared to the high-Pr pool (red) and therefore the depression is caused by the depletion of the high-Pr pool.

(D) Relative number of vesicles released from each pool during each stimuli. Low-Pr pool sustains the release after the synapse is depressed.

(E) Two-pool depletion model predicts the frequency-dependent depression evoked by spontaneous spiking. Solid circles, data from Kuo and Trussell (2011). Gray dots, predictions of the steady state response of Poisson stimulation-evoked responses at various frequencies by the two-pool model.

(F) Two-pool depletion model shows that the low-Pr pool contributes most of the release during steady state depression when the average firing frequency is > 3Hz.

Figure 1.5

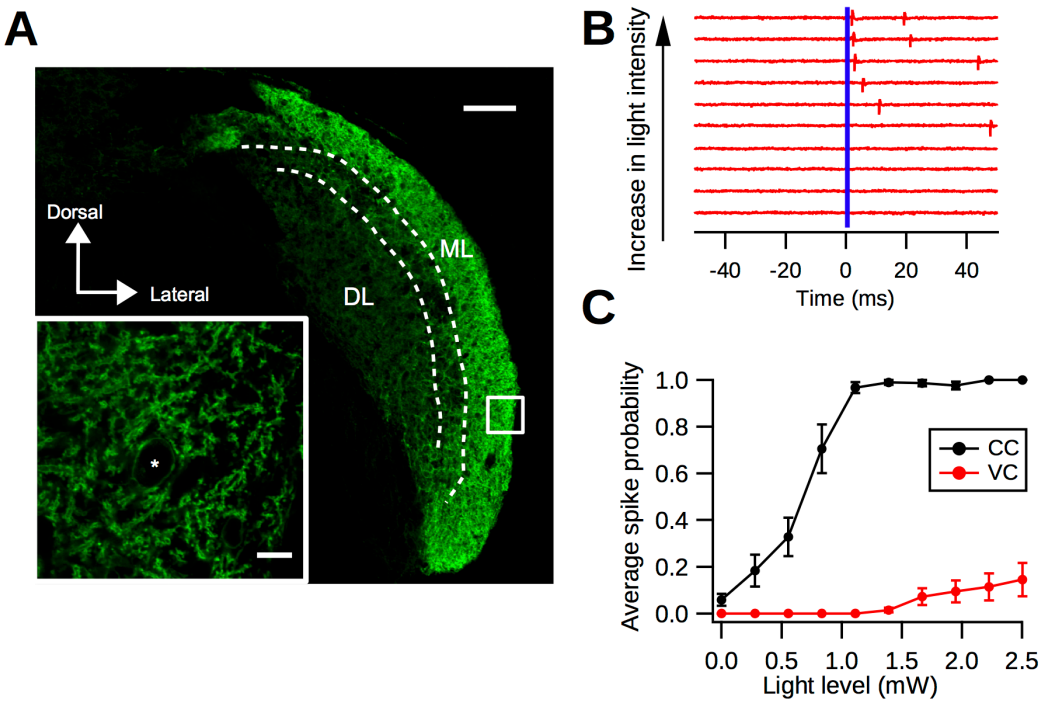

Figure 1.5. Optogenetic activation of cartwheel cells.

(A) Immunolabeling of ChR2-EYFP in a coronal section of DCN from a GlyT2-Cre;Ai32 animal. Strong expression of ChR2-EYFP is seen in the DCN molecular layer (ML), where cartwheel cells are located. The deep layer (DL) shows less dense expression of ChR2-EYFP. Scale bar: 100 µm. Inset, a single focal plane image of the white selection. Note strong labeling of ChR2-EYFP in spiny dendrites characteristic of cartwheel cells. Star represents a possible cartwheel cell soma. Scale bar: 10 µm.

(B) Cartwheel cell spikes with blue light flash. Example traces of a cell-attached recording from a cartwheel cell in response to blue light of different intensities. The blue bar indicates the onset of the light stimulation (duration: 0.5 ms). Each red vertical stroke represents an action potential. The spike probability and response latency decreases with increasing light intensity.

(C) Population averages of spike probability (the chance of generating a spike within 10 ms after the light stimulation) from cartwheel cells (CC, black, n = 9) and vertical cells (VC, red, n = 13). Only 3 out of 13 vertical cells respond to light stimulation stronger than 1.5 mW and even with 2.5 mW blue light stimulation, the spike probability is low (0.15 ± 0.07) .

Figure 1.6

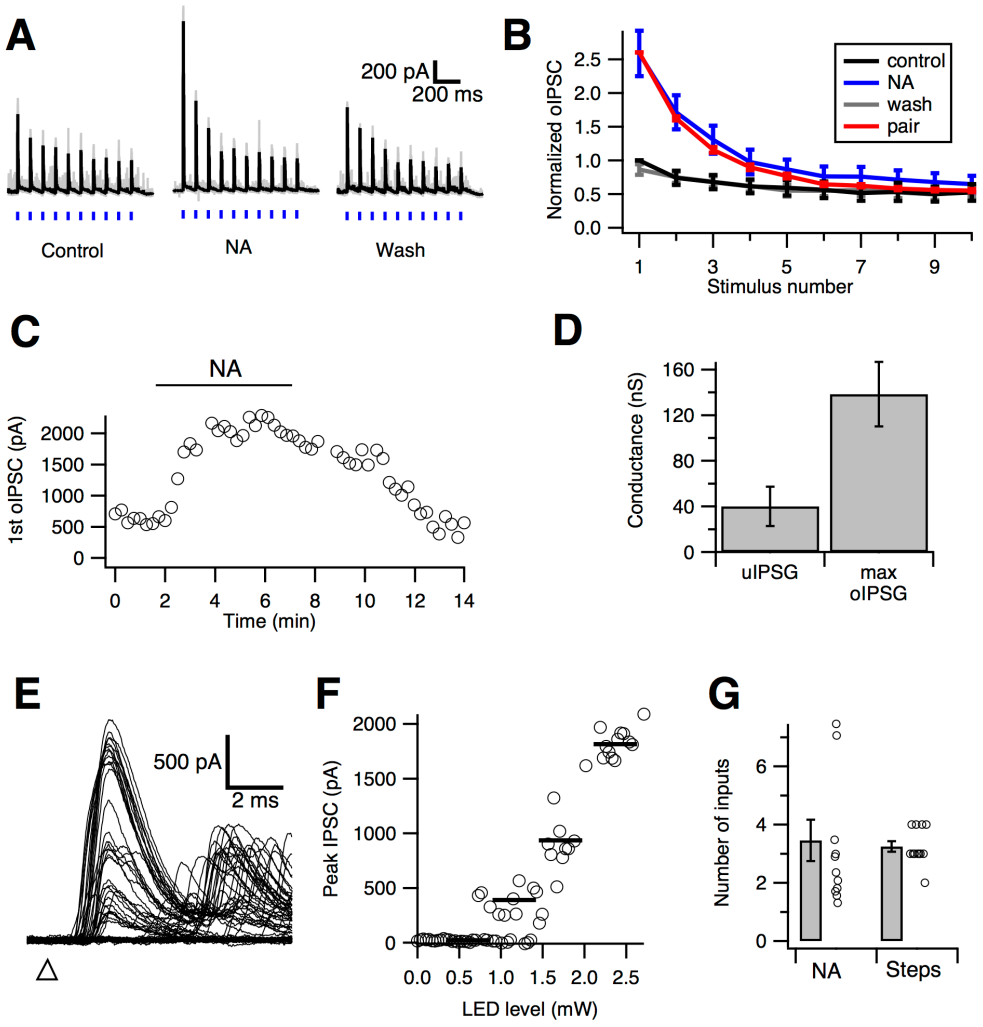

Figure 1.6 Low convergence ratio in the cartwheel-fusiform circuit.

(A) Optically-evoked IPSCs (oIPSCs) in fusiform cells during 3.5 mW blue light stimulation (blue vertical bars). The amplitude of oIPSC and its degree of depression is enhanced by 10 μM noradrenaline (NA) (Kuo and Trussell 2011), as NA relieves sustained cartwheel cell synaptic depression by blocking spontaneous spiking. Black, average traces from 10 individual traces (gray).

(B) Summary of peak oIPSCs during repetitive light stimulation. Peaks are normalized to the first oIPSC in control. NA not only increased peak oIPSC amplitudes, but also revealed a

stronger degree of synaptic depression. Also shown is data from paired-recordings in Figure 1B (red, scaled to the first response in NA), showing that depression of oIPSCs or electrically evoked IPSCs is similar.

(C) Time course of change in peak amplitude change in the first oIPSC of a train during application of NA.

(D) Comparison between the unitary conductance of cartwheel-fusiform synapse from paired recordings (uIPSG, 40.0 ± 17.3 nS, n = 6) and the maximum optically evoked synaptic conductance in the presence of NA (Max oIPSG, 138.5 ± 23.3 nS, n = 11).

(E). Example traces of oIPSCs in a fusiform cell evoked by increasing light intensities (triangle: start time of flash).

(F). Plot of the peak oIPSC amplitudes of the traces shown in (E) against LED stimulation intensity (gray circles). Black bars indicates the steps resolved by K-means cluster analysis. Three jumps are evident, indicating 3 cartwheel cells converged onto this fusiform cell.

(G) Summary of the number of cartwheel cell inputs converging onto a fusiform cell estimated by the two methods (A-D vs E-F). Number estimated by the maximum conductance method (NA) is 3.7 ± 0.9 (n=11), and the number estimated by the steps method (step) is 3.3 ± 0.2 (n = 12). No significant difference is observed between the two methods (p = 0.34, Mann-Whitney test).

Figure 1.7

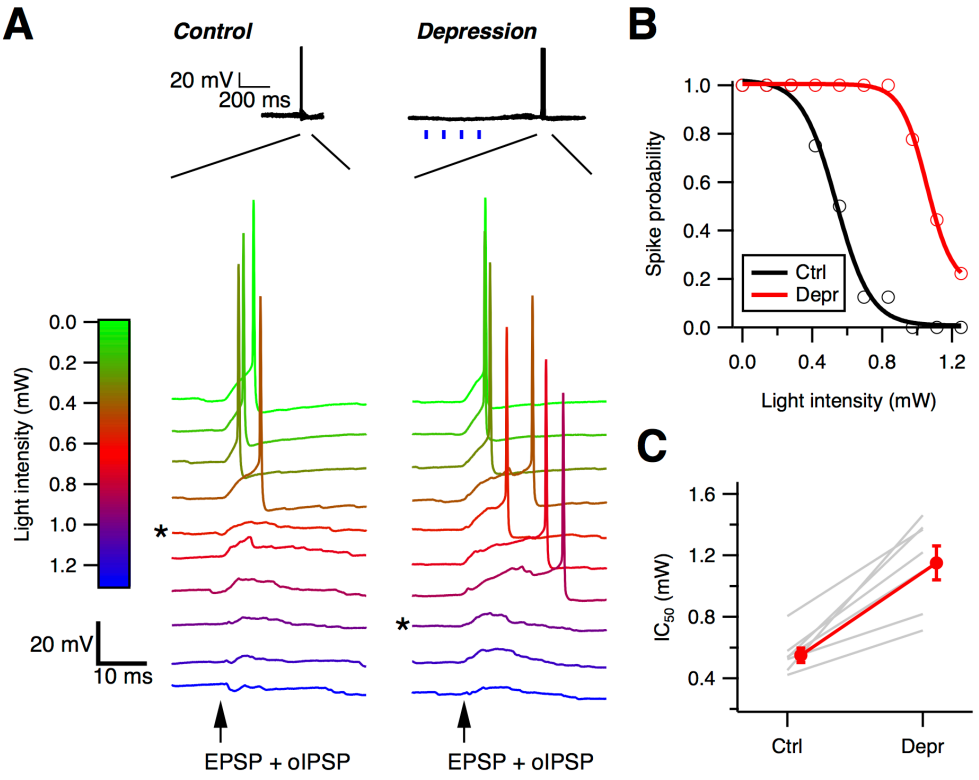

Figure 1.7 Effective size of cartwheel-fusiform circuit increases with spontaneous spiking in cartwheel cells.

(A) Example traces of action potentials in a fusiform cell evoked by current injection of an EPSC waveform plus optically-evoked IPSPs (oIPSPs) by different intensities of blue light under control (Ctrl, left) and enhanced-synaptic depression (Depr, right) conditions. Top, under enhanced-depression conditions four repetitive light-stimulation pulses (blue vertical bars) were applied before action potential generation to increase spiking and synaptic depression in the entire cartwheel cell population.

(B) A plot of fusiform cell spike probability against the light intensities that evokes oIPSPs can be made after repeating the protocol in (A) for 10-20 times. A sigmoidal fit to the points yields a light-inhibition curve and an IC_{50} of the light intensity that inhibits 50% of spike generation for each condition.

(C) Summary of IC_{50} changes in 7 fusiform cells recorded. In every cell, the IC_{50} shifts towards more positive under the enhance depression state, indicating the number of cartwheel cells required to effectively inhibit fusiform cell firing increases as their spontaneous spiking rate increases. IC_{50} for Ctrl: 0.55 ± 0.05 mW, Depr: 1.15 ± 0.11 mW. p = 0.001, paired t-test.

Figure 1.8

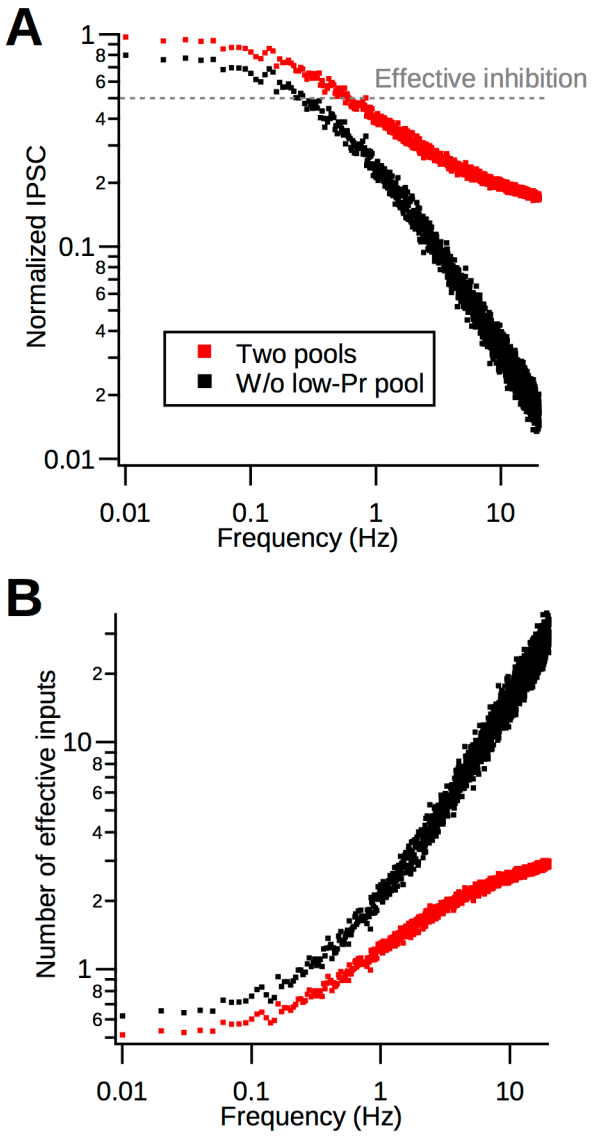

Figure 1.8 Vesicular release probabilities define effective convergence

(A) Normalized peak IPSC amplitude decreases as the spontaneous spiking frequency increases in single cartwheel cells. The red dots are generated by two-pool depletion model, the black dots are generated by the same model but lacking the low-Pr pool. The gray dotted line is the assumed effective inhibition strength needed to inhibit a fusiform cell from spiking (50% of maximum IPSC).

(B) Number of effective inputs predicted by the model when two pools are utilized (red dots) or only when the model lacks the low-Pr pool (black dots). The effective number is derived by dividing the effective inhibition strength (0.5) by each dot in (A). When the synapse lacks the low-Pr pool, it requires a much larger number of inputs in order to effectively inhibit fusiform cell spiking compared to when both pools are present. For example, when cartwheel cells spontaneously fire at 10 Hz, it only requires 2-3 cells to provide effective inhibition when the two pools are present at the synapse. The effective convergence ratio increases to ~30 cartwheel cells when the synapse lacks the low-Pr pool.

CHAPTER 2: SLOW SYNAPTIC TRANSMISSION MEDIATED BY DESENSITIZED AMPA RECEPTORS.

Hsin-Wei Lu[1], Gabriel E Romero[2,], Timothy S Balmer[3], and Laurence O Trussell[3]

[1]Neuroscience Graduate Program, [2]Department of Physiology and Pharmacology, and [3]Oregon Hearing Research Center and Vollum Institute, Oregon Health and Science University, Portland, Oregon, USA

Forward

This is a multiple-author project in which I am the principal investigator. I conducted and analyzed uncaging and most electrophysiology experiments in slices, Tim Balmer conducted experiments mentioned in Fig 2.1 B and F, Gabe Romero conducted the dissociated cell experiments mentioned in Fig 2.3. Larry Trussell constructed the kinetic model in Fig 2.4 and 2.7. All the authors contributed to the analysis and design of experiments.

Abstract

AMPARs mediate the briefest synaptic currents in the brain by virtue of their rapid gating kinetics. However, at the mossy fiber-to-unipolar brush cell (UBC) synapse in the cerebellum, AMPAR-mediated EPSCs last for hundreds of milliseconds. We show that the slow EPSC results from restricted clearance of transmitter combined with a mechanism of receptor gating dependent on transmembrane AMPAR regulatory proteins (TARPs) that enhances the response to low levels of transmitter. Glutamate uncaging on the synapse revealed that synaptically-released transmitter desensitized AMPARs by >90%. The remaining current gradually increases after exocytosis stops, and its eventual decay was slowed by reducing glutamate's diffusion coefficient. Dose-response analysis showed that wildtype UBC AMPARs respond non-monotonically to glutamate, while recordings from mice lacking γ2 TARP had monotonic dose-response curves and reduced slow currents. The biophysical features of the UBC synapse and its receptors thus provide a unique means for transformation of cerebellar mossy input.

Introduction

AMPA receptors (AMPARs) are the major ionotropic glutamate receptors mediating brief excitatory postsynaptic currents (EPSCs) at synapses (Jonas, 2000). One factor that leads to a milliseconds-long time course is the short lifetime of synaptically released glutamate in the synaptic cleft, estimated to be about 1 ms (Clements et al., 1992). Hence, AMPARs quickly deactivate as cleft [glutamate] decays, abbreviating the EPSC. Another key factor contributing to fast AMPAR-mediated EPSCs is the receptor's rapid desensitization, which decreases response amplitudes by >90% within ~10-15 ms upon prolonged exposure to glutamate (Colquhoun et al., 1992; Hestrin, 1993; Raman and Trussell, 1992; Silver et al., 1996; Trussell and Fischbach, 1989). Thus, even when cleft glutamate clearance is slow, desensitization still forces AMPAR-mediated EPSCs to decay quickly (Trussell et al., 1993).

In stark contrast to this picture of the typical AMPAR synapse is the large mossy fiber-unipolar brush cell (UBC) synapse in the granular layer of cerebellar cortex and cochlear nucleus (Floris et al., 1994; Rossi et al., 1995). Stimulation of this synapse not only evokes typical fast EPSCs, but also a slow, AMPAR-mediated EPSC lasting hundreds of milliseconds (Borges-Merjane and Trussell, 2015; Kinney et al., 1997; Rossi et al., 1995). Kinney et al. (1997) proposed that the slow current is the combined result of the synapse's unique ultrastructure and the biophysical properties of AMPARs. The morphology of the rat mossy fiber–UBC synapse has an extensive, convoluted synaptic cleft between the presynaptic terminal and postsynaptic brush-like dendrite (Rossi et al., 1995). It was hypothesized that this morphology slows the clearance of glutamate as compared to conventional synapses. Upon such prolonged glutamate activation, synaptic AMPARs will

enter steady-state desensitization and periodically reopen, generating the slow ionic current (Kinney et al., 1997). However, direct evidence for this "glutamate entrapment" hypothesis (Rossi et al., 1995) has been hindered by lack of information about the kinetic state of receptors during synaptic transmission and the molecular underpinnings of this unusual synaptic response.

We have reexamined this hypothesis in mouse UBCs of the vestibular cerebellum using fast UV uncaging of glutamate at different time points after synaptic stimuli, finding that at onset of the slow synaptic response, >90% of AMPAR are desensitized (i.e., unresponsive to glutamate test pulses), leaving a residual current generated by receptors cycling between open and desensitized states. After exocytosis halts, receptors recover from desensitization concurrent with a gradual increase in the slow EPSC amplitude. Dose-response relations confirm that AMPARs produce smaller equilibrium responses to mM levels of glutamate than to micromolar levels, suggesting that cleft glutamate lingers in the micromolar range for extended periods. This decrease in equilibrium responses to high [glutamate] was absent in UBCs from γ2 transmembrane AMPAR regulatory protein (TARP)-mutant stargazer (*stg*) mice, which also had reduced slow EPSCs. Thus, a 'giant' synapse is used by the UBC not to generate large, fast responses, but to retain transmitter in order to take advantage of the biophysical properties of an AMPAR-accessory protein complex, thus facilitating integration of sensory signals.

Methods

Animals

Three mouse lines were used in this study. Wildtype C57BL/6J or transgenic C57BL/6J-TgN(grm2-IL2RA/GFP)1kyo (referred to as mGluR2-GFP) mouse line were used as control animals. In the latter mouse line, GFP is tagged to human interleukin-2 receptor α subunit with expression driven by the metabotropic glutamate receptor 2 (mGluR2) promoter (Watanabe et al., 1998). Since UBCs express mGluR2 (Borges-Merjane and Trussell, 2015; Jaarsma et al., 1998; Nunzi et al., 2002, 2001), this mouse line was used for identifying UBCs in the brain slice or dissociated cell preparations. For simplicity, these two lines were referred to as "wildtype" (wt) in this study. A third mouse line, stargazer (*stg*) (Hashimoto et al., 1999; Noebels et al., 1990), was used for experiments to measure the effect of TARPγ2 (stargazin) mutant. This mouse line has a retroviral-like, early transposon insertion in the second intron of stargazin gene, resulting in a significant reduction of protein expression (Letts, 2005; Letts et al., 1998). *Stg* pups were produced by crossing heterozygous males with either heterozygous or homozygous females. The pups were genotyped according to the protocol described on Jackson Lab website (https://www.jax.org/strain/001756). *Stg* pups also expressed ataxic phenotype as described in previous studies (Hashimoto et al., 1999; Qiao et al., 1996). Breeding of all three mouse lines were maintained in the animal facility managed by the Department of Comparative Medicine and all procedures were approved by the Oregon Health and Science University's Institutional Animal Care and Use Committee. Pups from both sexes were used. Because synapse formation between mossy fiber and UBC is mature in animals older than postnatal day 21 (P21) (Morin et al., 2001) , we only used pups older than this age (P21 – P39) for experiments.

Brain Slice preparation

Animals were anesthetized with isoflurane, decapitated, and the cerebellum was dissected from the skull under ice-cold high-sucrose artificial cerebral spinal fluid solution (ACSF) containing (in mM): 87 NaCl, 75 sucrose, 25 $NaHCO_3$, 25 glucose, 2.5 KCl, 1.25 NaH_2PO_4, 0.5 $CaCl_2$, 7 $MgCl_2$, bubbled with 5% CO_2 / 95% O_2 (Bischofberger et al., 2006). Sagittal cerebellum sections containing lobe X were cut at 300 μm with a vibratome (VT1200S, Leica) in ice-cold high-sucrose ACSF. After cutting, slices were allowed to recover at 35°C for 30 minutes in ACSF containing (in mM): 130 NaCl, 2.1 KCl, 1.2 KH_2PO_4, 3 Na-HEPES, 10 glucose, 20 $NaHCO_3$, 2 Na-pyruvate, 2 $CaCl_2$, 1 $MgSO_4$, and 3 myo-inositol, bubbled with 5% CO_2 / 95% O_2 (Borges-Merjane and Trussell, 2015). After recovery, slices were kept at room temperature (~ 22°C) in ACSF until use.

Electrophysiology

For whole-cell recording in brain slices, slices containing cerebellar lobe X were transferred to a recording chamber perfused with warm ACSF (~ 34°C) controlled by a peristaltic pump (Ismatec CP78016-30). Cells were visualized with a 40X magnification objective on the stage of an upright microscope (Olympus BX52WI) equipped with an infrared Dodt contrast mask and a blue LED for fluorescence optics. In slices from mGluR2-GFP mouse line, UBCs were identified as GFP-positive neurons with brushy dendritic structure. In brain slices from wildtype or stargazer mouse line, UBCs were first identified as round cells with soma diameter ~ 10 μm in the cerebellar granular layer. Only data from UBCs in the lobe X were used for analysis in this study. All cells recorded were filled with 10 μM Alexa Fluor 488 hydrazide sodium salt (Molecular Probes) via the recording pipette

in order to visualize the dendritic morphology. Only cells with a brushy dendrite and rebound burst firing were identified as UBCs (Borges-Merjane and Trussell, 2015). Recording electrodes (6 – 8 MΩ) were pulled from borosilicate glass (WPI 1B150F-4) by a horizontal puller (Sutter Instrument P97). Series resistances were usually < 30 MΩ and were compensated by 50 – 60 %. For data acquisition we used a Multiclamp 700B amplifier and pClamp 10 (Molecular Device) or Ephus software (Suter et al., 2010) (http://www.ephus.org) running in MATLAB 2007b (Mathworks). Signals were sampled at 40 KHz, low-pass filtered and digitized at 10 KHz using a Digidata (1440A, Molecular Devices) analog-digital converter board (for pClamp) or a NI-6229 board (National Instruments). The recording pipette solution contained (in mM): 113 K-gluconate, 9 HEPES, 4.5 $MgCl_2$, 0.1 EGTA, 14 Tris-phosphocreatine, 4 Na_2-ATP, 0.3 Tris-GFP, with osmolality adjusted to 290 – 300 mOsm with sucrose and pH adjusted to pH 7.3 with KOH. In some cases, 5 mM QX-314 was added to prevent escaping spikes during electrical stimulation. To isolate AMPAR-mediated currents, NMDAR blocker MK-801 (3 – 15 μM), inhibitory synaptic blockers picrotoxin (100 μM) and strychnine (0.5 μM) were added to the bath solution. Recent studies in the dorsal cochlear nucleus and cerebellum showed that, depending on its response to glutamate, UBCs can be categorized into two groups: an ON cell type which shows an slow inward current mediated by mGluR1 receptors, and an OFF cell type which shows an outward current mediated by mGluR2 receptors (Borges-Merjane and Trussell, 2015; Rousseau et al., 2012). Because both types of UBCs have an AMPAR-mediated slow EPSC and both types of mGluRs may contribute to the synaptic response, we always applied mGluR1 and mGluR2 antagonists to the bath solution (1 μM JNJ-16259685 and 1 μM LY-341495, respectively) to isolate AMPAR-mediated responses.

Data collected in this study therefore were presumably from both populations of UBCs. In brain slice recordings, cells were voltage-clamped at -70 mV without junction potential correction. Extracellular stimulation of mossy fibers was achieved by applying voltage pulses (10 – 50 V, 100 μs) using a stimulus isolation unit (Iso Flex, A.M.P.I.) via an ACSF-filled monopolar glass electrode (same as the recording electrode) placed near the brush. In some cases a concentric electrode placing in the white matter was used. For dissociated cell recording, the same internal solution was used, however the recording bath solution was oxygenated Tyrode's solution (see below) instead of ACSF. Recordings were made at room temperature and the cells were voltage-clamped at -60 mV without junction potential correction (-4 mV).

MNI-glutamate uncaging

The UV-laser uncaging setup was modified from the Laser Scanning Photostimulation System (LSPS) described in Shepherd (2012) and was controlled by Ephus software (Suter et al., 2010). Voltage-controlled mirror galvanometers (Model 6210; Cambridge Technology) was used to target a 355 nm UV laser beam (3500-SMPS, DPSS Lasers) at the dendritic brush of the recorded UBC, which was filled with Alexa-488 and could be visualized under the fluorescence microscope through a CCD camera (Ret 2000R, QImaging). Laser power was controlled by Ephus via a Pockels cell (Conoptics) and a neutral density filter wheel (Edmund Optics). The online laser power was measured by a UV-sensitive photodiode (Edmund Optics) detecting a deflected beam in the light path and calibrated for the power measured offline under the objective (40X, NA 0.8, Olympus) by a UV-sensor (PM3Q, Coherent) and power meter (FieldMate, Coherent). Unless otherwise

stated, the UV-uncaging power was estimated to be 5 mW under the objective. The duration of uncaging pulse was controlled by Ephus via a mechanical shutter (VMM-D1, Uniblitz). The duration of uncaging pulse was 2 ms. MNI-Glutamate (1 mM; Tocris) was used as caged glutamate compound and bath applied in the recirculating recording ACSF (total volume ~30 mL).

We confirmed that uncaged glutamate activates the same set of receptors as those reached by synaptic stimulation by testing the spatial resolution of uncaging. Indeed, a fast-then-slow uncaging-evoked EPSC (uEPSC) was evoked by the flash only when the UV uncaging beam targeted the brush but not the soma or dendrite of the recorded neuron or an area adjacent to the brush (Fig 2.5, n =3), indicating that AMPARs are largely restricted to the brush. Second, we tested whether uncaging restricted to the brush activates the same AMPARs as those activated by synaptic stimulation. We applied synaptic stimulation immediately after uncaging, and found that the uncaging pulse markedly desensitized subsequent fast synaptic EPSCs (not shown). The peak of the fast EPSC decreased to 3.9±3.9 % (n = 2) or 32.6±9.6 % (n=5) of its original size 15 ms and 200 ms after uncaging, respectively. The particularly profound desensitization 15 ms after uncaging suggests that uncaging activates the same AMPARs as those evoked by synaptic stimulation. These data confirm that MNI-glutamate uncaging can selectively activate synaptic AMPARs when targeted to the brush.

Dissociated Cell preparation

Acute cerebellar slices were collected and then placed into a 31˚C oxygenated (100% O_2) chamber containing Eagle's minimal essential medium, 10 mM HEPES (pH 7.4),

40 U of papain (Worthington), 0.5 mM EDTA and 1 mM cysteine (Raman and Trussell, 1992). Slices were incubated in this solution for 20 minutes, and then washed twice with oxygenated (100% O_2) Eagle's minimal essential medium containing 10 mM HEPES (pH 7.4), 1 mM EDTA, 2 mM cysteine, 1 mg/ml bovine serum albumin, and 1 mg/ml trypsin inhibitor. Lobes IX and X of the cerebellum were dissected using black-enameled insect pins, then washed with oxygenated (100% O_2) Tyrode's solution (150 mM NaCl, 4 mM KCl, 2 mM $CaCl_2$, 2 mM $MgCl_2$,10 mM HEPES, 10 mM glucose, pH 7.4), and cut into smaller chunks by eye (~300 μm^3). The cerebellar tissue was transferred to poly-D-lysine-coated glass-coverslips and triturated 10-15 times with fine-tipped 8"-long Pasteur pipettes. The dissociated neurons were allowed to settle undisturbed for 1 hour.

Fast application of glutamate

The recording chamber consisted of two-compartments: one for the dissociated cells and a second for rapid application of glutamate. Once a whole-cell patch was achieved both chambers were flooded with Tyrode's solution and the cell was transported to the application-chamber. Glutamate was rapidly applied through a Perfusion Fast-Step System (SF-77B, Warner Instruments) with a glass three square-barrel piping system. Multiple solutions were feed into each square-barrel (700 μm width and height), totaling 10 solutions: one control solution (oxygenated Tyrode's solution containing synaptic blockers) per barrel and seven concentrations of glutamate (control solution with 0.1 to 1000 μM glutamate). Each solution was gated by a two-way valve, and the control solution was used to wash each barrel between differing glutamate concentrations. During experiments, the dissociated cell was placed about 100-200 μm from the barrel interface and centered in

front of a barrel primed with control solution. Flow for all three barrels was started, and the barrel adjacent to the control barrel was switched to a glutamate concentration. Exchange of solution was accomplished by rapid movement of the barrels. The flow from each barrel was approximately 450 µl/min, and solutions were exchanged within 50 ms over the surface of the cell.

Pharmacology

All drugs unless otherwise noted were purchased from Sigma. All drugs in the slice experiments were bath applied. Receptor antagonists used this study contained: GYKI-53655 (AMPAR; Tocris), LY-341495 (group II mGluR; Tocris), MK-801 (NMDAR; Sigma), picrotoxin ($GABA_AR$; Sigma), strychnine (GlyR; Sigma). MNI-glutamate was purchased from Tocris. Dextran (MW 35000 – 45000) was purchased from Sigma (D1662) .

Data analysis and statistics

All recordings were analyzed in IgorPro (WaveMetrics) or MATLAB. Graphs were made with IgorPro. Unless otherwise stated, all data are displayed as mean ± sem. Statistics were done in IgorPro or Excel (Microsoft).

Kinetic modeling

The kinetic model was developed using AxographX software. Parameters (Table 2.1) were adjusted to account for steady state dose response curve, rate of decay of the fast initial EPSC in a train, the rate of decline of the amplitude of fast EPSCs during the train, the relative amplitude of the peak fast EPSC vs the peak slow current after the train, and the

rise and decay time of the slow current. As noted in the main text, the key feature yielding a non-monotonic dose response relation was the differences in the rates governing entry and exit of D1-2 vs D3-4. Alterations in rates of opening and closing of the different open states could also generate a fall-off in current at high agonist concentrations, but also distorted fast deactivation to an unacceptable degree. Transmitter timecourse was approximated with exponentially decaying agonist pulses. Transmitter decay profiles from individual release events were added linearly to generate the trains. No presynaptic depression was assumed. Varying the magnitude and duration of the slow phase of clearance affected the amplitude, rise and decay times of the slow EPSC (not shown), but the essential features of the current, i.e., the fall-off in amplitude of fast EPSCs and the delayed rise of the slow EPSC, were robust.

Results

Slow EPSC is mediated by synaptic AMPA receptors

We examined whether the slow EPSC requires restricted glutamate clearance from the synaptic cleft. A 100-Hz, 10-stimulus train evoked a characteristic fast-then-slow EPSC sequence in UBCs in mouse cerebellar brain slices (Fig 2.1A) (Borges-Merjane and Trussell, 2015; Rossi et al., 1995; van Dorp and de Zeeuw, 2014), and a complete block by GYKI 53655 (75 μM) confirmed the currents were AMPAR-mediated (Fig 2.1B). In 17 cells tested, the amplitudes of the fast EPSCs depressed rapidly and nearly completely during train stimulation (fit to decay of peak amplitudes: fast decay τ: 9.7±7.7 ms, slow decay τ: 18.5±2.0 ms, fast component 55% of total; average of $EPSC_{5\text{-}10}/EPSC_1$: 4.3±0.5%, Fig 2.1C-D). Despite such strong synaptic depression, a slow EPSC emerged, reaching a peak of

13.6±1.5 pA (19.1±5.0% of $EPSC_1$) 130.1±9.0 ms after the train stimulation, and decaying with a τ 453.5±53.5 ms back to baseline (Fig 2.1C, E). This slow EPSC generated a charge transfer 7 times the size of that produced by all prior fast EPSCs, including the tonic current between each fast EPSC (charge transferred during fast EPSCs: 1.1±0.1 pC, slow EPSC: 7.6±1.1 pC, n = 17). This caused prolonged spiking that outlasted the synaptic stimulation (Fig 2.1B). Thus, the slow EPSC was the was the dominant synaptic signal.

The slow EPSC may reflect a spillover current mediated by extrasynaptic receptors (Nielsen et al., 2004). If that were true, one would expect the slow EPSC to begin during a long stimulus train as accumulated glutamate spilled out to distant receptors. However, when we varied stimulus number, the slow EPSC began and reached its peak only after the termination of stimulation (Fig 2.1E). Furthermore, the current's rise time after stimuli were halted was constant, regardless of the number of stimuli (range 5-100 stimuli; p=0.24, R^2=0.06, linear regression fit; Fig 2.1F). This result argues against the hypothesis that the delayed current is mediated by diffusion to extrasynaptic receptors, as such diffusion should not depend on the cessation of transmitter release. Rather, the results indicate that synaptic AMPARs are partially inhibited by glutamate accumulated in the synaptic cleft, and this inhibition is relieved as transmitter levels gradually decline (Kinney et al., 1997).

If indeed there is a slow decline in transmitter, the EPSC time course should be prolonged by restricting the diffusion time of glutamate. We thus applied 5% dextran in the bath solution, to increases the viscosity of extracellular space and retard transmitter diffusion (Ford et al., 2010; Min et al., 1998; Rusakov and Kullmann, 1998). After 15 minutes in dextran, the time-to-peak and decay time constant of the slow EPSC were significantly prolonged (time-to-peak: from 135±12 to 214.3±38.5 ms, p=0.03, n=8; decay

time constant: from 464.5±74.2 to 688.9±125.7 ms, p=0.007, n=8; paired t-test), confirming that the mossy fiber-UBC cleft severely limits the clearance of transmitter (Fig 2.1G,H).

Slow EPSC is mediated by desensitized AMPARs

If glutamate persists in the cleft then AMPAR must desensitize, and thus the slow EPSC would represent an equilibrium state of receptors moving between closed, desensitized and open states. Although this idea was explored using the desensitization blocker cyclothiazide (Kinney et al., 1997; Rossi et al., 1995), the drug has confounding effects, slowing AMPAR gating (Patneau et al., 1993; Raman and Trussell, 1995) and distorting presynaptic release rate (Diamond and Jahr, 1995).

To directly probe the kinetic state of receptors during synaptic transmission, we used glutamate uncaging. MNI-glutamate (1 mM) was bath applied, and a 2-ms UV flash was delivered over the UBC brush to locally uncage glutamate; this method was combined with synaptic stimulation at varying intervals. As the flash area contains the compact region of the brush, we expect it to activate all synaptic receptors. Control experiments confirmed that AMPARs were largely restricted to the brush region and that uncaged glutamate accessed synaptic receptors (Fig 2.5). We found that the peak of the uncaging response (uEPSC) was greatly reduced when evoked closer to the end of train stimulation (Fig 2.2B-C), with maximal decrease of ~ 90% 15 ms after the final stimulus. Furthermore, the reduction in sensitivity gradually recovered as the synaptic-uncaging stimulus intervals increased, with a τ of 267.1±24.4 ms (Fig 2.2C; n=6). A similar phenomenon was also observed using a paired-uncaging pulse protocol, in which the peak uEPSC evoked by the second uncaging pulse recovered with a τ of 413.9±68.1 ms (Fig 2.2D,E; n=8). Assuming the

amount of uncaged [glutamate] is similar in each trial, the reduction in peak uEPSC can only be explained by desensitization of AMPARs. As uncaging activates the same set of receptors utilized by synaptic transmission, we conclude that slow EPSCs are mediated by desensitized AMPARs.

Since recovery from desensitization requires removal of free agonist, the initial rise in the slow EPSC must be generated by a decrease in [glutamate]. This interpretation explains two additional observations. First, we observed an 'undershoot' of current right after uncaging, most obvious near the peak of the slow EPSC (arrows in Fig 2.2A, D. This undershoot during the uncaging response always reached a level similar to the current level just after the last synaptic stimulus, and was followed by its own rise and fall in slow current (Fig 2.2A, D). Thus, cleft [glutamate] increases upon uncaging, further desensitizes the receptors, and then evokes a slow EPSC as [glutamate] declines again. Moreover, when uncaging pulses were applied either at the beginning of the rise of the slow EPSC or at a later point in the EPSC when current had fallen back to the same level as at the beginning, the uncaging responses were distinctly different (Fig 2.6 A,C). Plotting baseline EPSC just before an uncaging pulse against the fractional recovery of the uncaging response from desensitization revealed a bell-shaped relation among the population of cells studied, with a maximum at about 40% recovery (Fig 2.6 B, D). Since the slow EPSC reaches the peak when ~60% AMPARs are desensitized, this result suggests that an intermediate glutamate level is still in the synaptic cleft, and it is this concentration that evokes the largest equilibrium response of AMPARs.

Glutamate sensitivity of AMPAR and role of TARPs.

TARP coexpression is associated with reduced desensitization and enhanced steady-state AMPAR currents (Jackson and Nicoll, 2011; Tomita, 2010). To test for a role of TARPs in the UBC synapse we recorded EPSCs in UBCs from stargazer (*stg*) mice, which lack γ2 TARP (Letts et al., 1998). In 12 of 13 cells tested, EPSCs in *stg* UBCs feature both fast and slow components upon train stimulation, as in wildtype (wt) UBCs (Fig 2.3A, B). Nevertheless, the absolute peak amplitudes of slow EPSCs in *stg* UBCs were ~60% smaller compared with wt (Fig 2.3B; *stg* vs wt: 5.2±0.4 vs 13.5±1.5 pA, n = 13 vs 17, respectively, $p<0.001$, unpaired t-test). In contrast, the peak amplitudes of the initial fast EPSC in both genotypes were similar (Fig 2.3B; *stg* vs wt: 79.3±20.4 vs 108.2±18.0 pA, n=13 vs 17, $p=0.30$, unpaired t-test). Hence, these results suggest that the total number of AMPARs in *stg* UBCs is comparable to that in wt, yet *stg* receptors are more desensitized by transmitter, thus generating a smaller slow EPSC.

A striking effect of heterologous TARP expression is the induction of a bell-shaped glutamate dose-response relation, termed 'auto-inactivation' (Morimoto-Tomita et al., 2009; Semenov et al., 2012), a feature described in some native AMPARs (Geoffroy et al., 1991; Raman and Trussell, 1992). Given that the slow EPSC rises as cleft glutamate decays, and that TARPs support this slow current, we expected that wt but not *stg* UBCs should feature a non-monotonic sensitivity to glutamate. UBCs enzymatically isolated with intact brush dendrites were used for constructing dose-response relations (Fig 2.3C), as glutamate transporters in slices may limit the access of exogenous glutamate to receptors. As shown in Fig 2.3D-F, when 1 μM glutamate was applied to the cell, a steady current was generated without apparent desensitization. A fast transient current could be observed at higher [glutamate] (32–1000 μM), which quickly desensitized and reached steady state.

This steady-state response is presumed to be the current through bound AMPARs at an equilibrium between microscopic open, closed and desensitized states. The steady-state response was plotted against [glutamate] as absolute or normalized amplitudes (Fig 2.3E-F). The steady-state response increased with [glutamate] up to ~32 μM (105.6±6.0 % of the 100 μM response, n = 9); at higher concentrations the steady-state current was smaller, such that at 1 mM the response was only 69.8±6.0 % of the 100 μM response (n = 11). Mean absolute values for currents at 32 μM and 1 mM were significantly different (32 μM vs 1mM: 11.1±1.8 vs 6.8±0.6 pA, n= 9 vs 11, p=0.022, unpaired t-test).

These experiments were then repeated on *stg* UBCs, and revealed clear differences with wt AMPARs. Maximal steady-state current was about half that of wt (at 32 μM, wt: 11.1±1.8 pA, n=9; *stg*: 6.1±1.2 pA, n=7, p = 0.048, unpaired t-test). These values were comparable to the peak amplitude of the slow EPSC within the same genotype (wt: P=0.34; stg: P=0.39, unpaired t-tests). Notably, the shape of the *stg* dose-response relation was monotonic (Fig 2.3E, F), with responses at 32 μM not significantly different from those at 1 mM (p=0.78, unpaired t-test). Thus, the γ2 TARP endows the AMPAR of UBCs with reduced desensitization, particularly in the range of 10-100 μM, and this concentration range mediates a slow EPSC.

AMPAR gating and glutamate diffusion

A kinetic model of the AMPA receptor was developed to explore the roles of gating kinetics and transmitter clearance in shaping the EPSC at the UBC synapse. A sequential model with 4 binding sites was used, with each closed, bound state linked to an open and a desensitized state (Fig 2.4A; Table 2.1). The biphasic nature of the curve was closely

mimicked by increasing the residence time in desensitized states when 3 or 4 glutamates were bound, relative to the 1 or 2 bound desensitized states (Fig 2.4B). The effect of this change was to favor access to open states having fewer glutamates bound, and could account for the shape of the curve from wt dissociated cells almost exactly (Fig 2.4B). From this model we predicted that a gradual fall in glutamate would reduce the level of overall desensitization and transiently increase the slow current.

This prediction was tested by driving the model with different glutamate transients. The basic glutamate transient rose within 20 μs to 2 mM, decaying with a 0.5 ms τ in order to approximate rapid diffusion from a release site (Barbour and Häusser, 1997). This generated a rapid EPSC in the model with an exponential decay time of 2.3 ms (Fig 2.4Ci). A train of ten such transients delivered at 100 Hz (Fig 2.4Ciii) generated a train of fast EPSCs that decayed by 50%, similar to mossy fiber-granule cell synaptic currents (DiGregorio et al., 2007). To mimic delayed clearance from the cleft, we added to the fast decay phase a second decay phase with an amplitude of 40 μM and a decay τ of 80 ms (Fig 2.4Cii). Including a slow phase resulted in a two-part current decay (Fig 2.4Cii). When 10 pulses were applied, the fast EPSCs desensitized almost completely, followed by a slow EPSC similar to wt UBCs (Fig 2.4Civ). The cleft [glutamate] at the peak of this slow EPSC was 50 μM, as expected from the shape of the dose-response curves. Of note was that modeling currents that resembled the small EPSCs recorded in UBCs required a surprisingly small number (100) of receptors, suggesting that the synapse functions more by reactivating a few receptors than by brief, synchronous activation of a large receptor pool, as at other giant synapses.

We then explored what could account for the kinetic features of the *stg* EPSC. By giving all four desensitized states the same kinetics (Table 2.1), a monotonic dose-response relation was obtained whose peak current was equivalent to the response to the highest dose for the wt model (Fig 2.7A, red trace). Modeled wt and 'TARP-less' dose-response relations bore striking similarity to published curves for AMPAR expressed with and without stargazin protein (Morimoto-Tomita et al., 2009, their Fig 2.4C-D). However, the TARP-less dose-response relation was right-shifted as compared to our *stg* experimental data (Fig 2.7A, blue circles). It is possible that UBCs in *stg* mice may still express another TARP, possibly γ7 (Yamazaki et al., 2010). Indeed, a model containing a mix of 50 wt /50 TARP-less receptors gave a monotonic dose response relation nearly identical to that found in *stg* UBCs (Fig 2.7A, blue line). Driving these three kinetic models (wt, TARP-less, and mixed) with a modeled UBC glutamate transient gave currents with varying shapes and amplitudes of slow EPSC (Fig 2.7B), with the smallest slow EPSC from TARP-less receptors. These simulations suggest that variation in slow EPSCs between cells (van Dorp and de Zeeuw, 2014) might arise not only from differences in synaptic morphology but also in the distribution of TARPs among a small number of receptors.

Discussion

This study demonstrates that the slow EPSC of UBCs depends upon restricted glutamate clearance from a broad synaptic cleft, and unusual kinetic properties of its receptors. Since the synapse can generate fast EPSCs, the gating kinetics of AMPARs and the initial decline of glutamate levels after exocytosis must both be rapid. Therefore, a second, slow phase of glutamate clearance is required to generate a slow AMPAR EPSC; the further

slowing of the EPSC with dextran highlights that glutamate must be retained at low levels in the cleft for hundreds of milliseconds. This glutamate "entrapment", first proposed by Rossi et al. (1995), is quite distinct from mossy fiber synapses onto granule cells (Rothman et al. 2008) or highly fenestrated mature calyceal synapses (Ford et al., 2009), and allows the synapse to transmit in a tonic mode despite sensing phasic exocytosis.

Desensitized AMPARs during synaptic transmission

The remarkable speed of AMPAR desensitization (Kiskin et al., 1986; Tang et al., 1989; Trussell et al., 1988) raised the possibility that desensitization kinetics could determine the decay time course of the EPSC (Trussell and Fischbach, 1989; Trussell et al. 1993), or impact the amplitude of EPSCs during repetitive activity (Digregorio et al., 2007), depending upon ease of clearance of glutamate and the rate of recovery from desensitized states. This study demonstrates a very different role for desensitization. Rather than determining the fast EPSC decay time or amplitude, the key contribution of desensitization in UBCs is to allow TARP-containing receptors to enter equilibrium states that give stable currents during slowing changing levels of transmitter. In this way, the UBC synapse can more effectively integrate presynaptic activity over longer periods of time than would be obtained with fast EPSCs.

Role of stargazin in synaptic transmission

The 60% reduction of slow EPSC in *stg* UBCs in this study suggests that the γ2 TARP stargazin is present in wt UBCs and regulates glutamate sensitivity of AMPARs. Interestingly, granule cells, another major target of cerebellar mossy fibers, also express

stargazin (Hashimoto et al., 1999; Yamazaki et al., 2010) and *stg* granule cells lack functional AMPARs at mossy fiber synapses because of impaired AMPAR trafficking (Chen et al., 2000; Hashimoto et al., 1999). Stargazin also regulates AMPAR gating, slowing down deactivation and desensitization rates (Priel et al., 2005; Tomita et al., 2005; Turetsky et al., 2005), and indeed miniature EPSCs in cultured hippocampal neurons were slower when stargazin was intact (Tomita et al., 2005). These studies suggest that the role of stargazin is to affect the size and shape of fast EPSCs. Stargazin also enhanced the equilibrium-state AMPAR current and generated non-monotonic dose-response curves (Morimoto-Tomita et al., 2009; Semenov et al., 2012). However, since such currents would not be produced at typical fast glutamatergic synapses, the physiological significance of these later results remained obscure. Our observations at UBC synapse thus provide the first evidence for stargazin to regulate synaptic transmission by enhancing the ability of the synapse to respond to steady low levels of glutamate.

AMPARs as mediators of transmission over multiple time scales

Previous studies identified two types of UBC based on immunohistochemical markers and response to mossy fiber stimulation (Borges-Merjane and Trussell, 2015; Nunzi et al., 2002). ON UBCs express an mGluR1-gated slow inward current. Nevertheless, AMPARs mediate the majority of transmission, although it is possible mGluR1 might be recruited during extended periods of activity (Borges-Merjane and Trussell, 2015). Why use AMPARs instead of an mGluR? By fine tuning a fast-gating receptor to respond to slow glutamate transients, the UBC has the capacity to respond quickly to the onset of synaptic activity yet supply maintained responses for longer lasting signals. Interestingly,

transmission in OFF UBCs is dominated by an mGluR2-gated outward current that inhibits spiking by activation of GIRK channels (Borges-Merjane and Trussell, 2015). Here, the IPSC builds up slowly, and lasts about as long as the EPSC of ON cells, presumably because of slow glutamate clearance and slow deactivation of the GIRK channels. Therefore, unlike mGluR-mediated currents, AMPAR-mediated excitation can be both fast and prolonged when desensitized TARP-containing AMPARs experience prolonged synaptic glutamate.

Acknowledgements

This study is funded by National Institutes of Health (N.I.H.) Grants NS028901 and DC004450 (to L.O.T.); N.L. Tartar Trust Fellowship (to H.-W.L); DC014878 to T.S.B.. We thank members of the Trussell lab for helpful discussions. We are grateful for Michael Bateschell and Ruby Larisch for help with mouse colony management. Stargazer breeder mice were kindly provided by the Puthussery lab at the Casey Eye Institute. The authors declare no competing financial interests.

TABLE 2.1 Parameters for the AMPAR kinetic models

STATE OR K_{EQ}	BACKWARDS (S^{-1})	FORWARDS (S^{-1})
K*	20,000	$2x10^8$ (M^{-1})
O_1**	1,000	3,000
O_2	1,000	4,000
O_3	1,000	4,000
O_4	1,500	4,000
D_1	400	2,000
D_2	400	2,000
D_3	250	8,000
D_4	250	8,000
***TARP-LESS MODEL*:**		
D_1	250	8,000
D_2	250	8,000
D_3	250	8,000
D_4	250	8,000

* Forward binding rates for 1, 2, 3 or 4 bound are multiplied by 4, 3, 2, and 1 respectively. Unbinding rates follow the reverse pattern.

** Forward is rate into state; backwards is rate of exit.

Figure 2.1

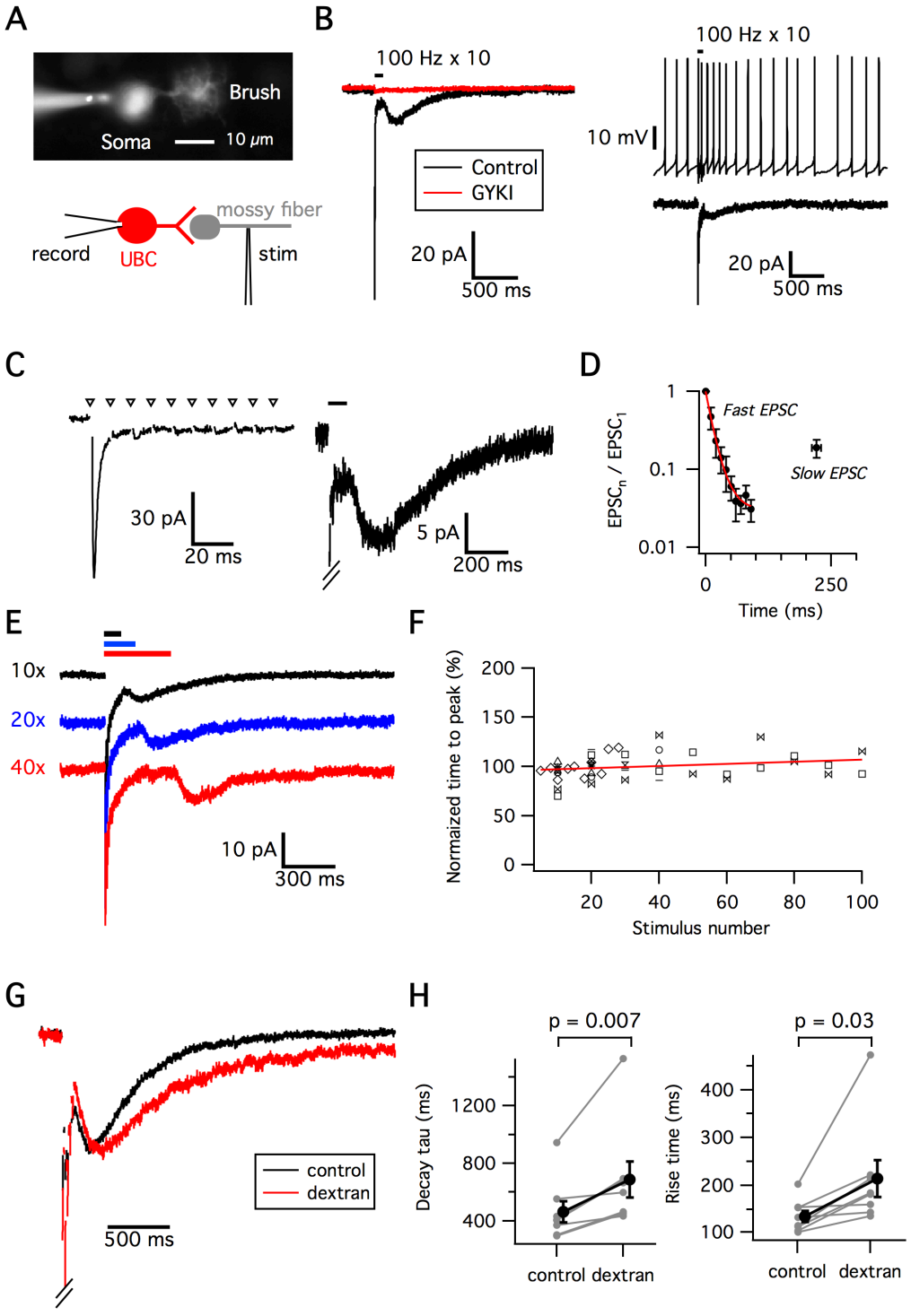

Figure 2.1 AMPARs mediate slow EPSC at mossy fiber – UBC synapse.

A, Recording diagram. Top, UBC was filled with Alexa 488 to visualize the location of the brush. Bottom, an electrode was placed nearby the brush to stimulate mossy fiber.

B, Left: Noncompetitive AMPAR antagonist GYKI 53655 (red) blocked both fast and slow EPSCs evoked by train stimulation. Black, control. Right: Slow EPSC (bottom) prolongs UBC firing (top).

C, Zoom-in of B. Left, fast EPSCs evoked during train stimulation (triangles) depress profoundly. Right, a slow EPSC emerged after train stimulation.

D, Short-term depression kinetics of the fast EPSCs can be fit by a double exponential decay (red). The peak of slow EPSC (triangle) emerged ~ 150 ms late.

E, The slow EPSC begins after cessation of stimuli.

F, Summary of the normalized time-to-peak from last stimulus of the slow EPSC vs number of stimuli from 9 cells. Each symbol represents a different cell. Linear regression fit (red) showed no significant correlation.

G, Application of 5% dextran solution slowed the rise and decay of slow EPSC. Traces are normalized to the peak slow EPSC.

H, Summary of dextran's effect.

Figure 2.2

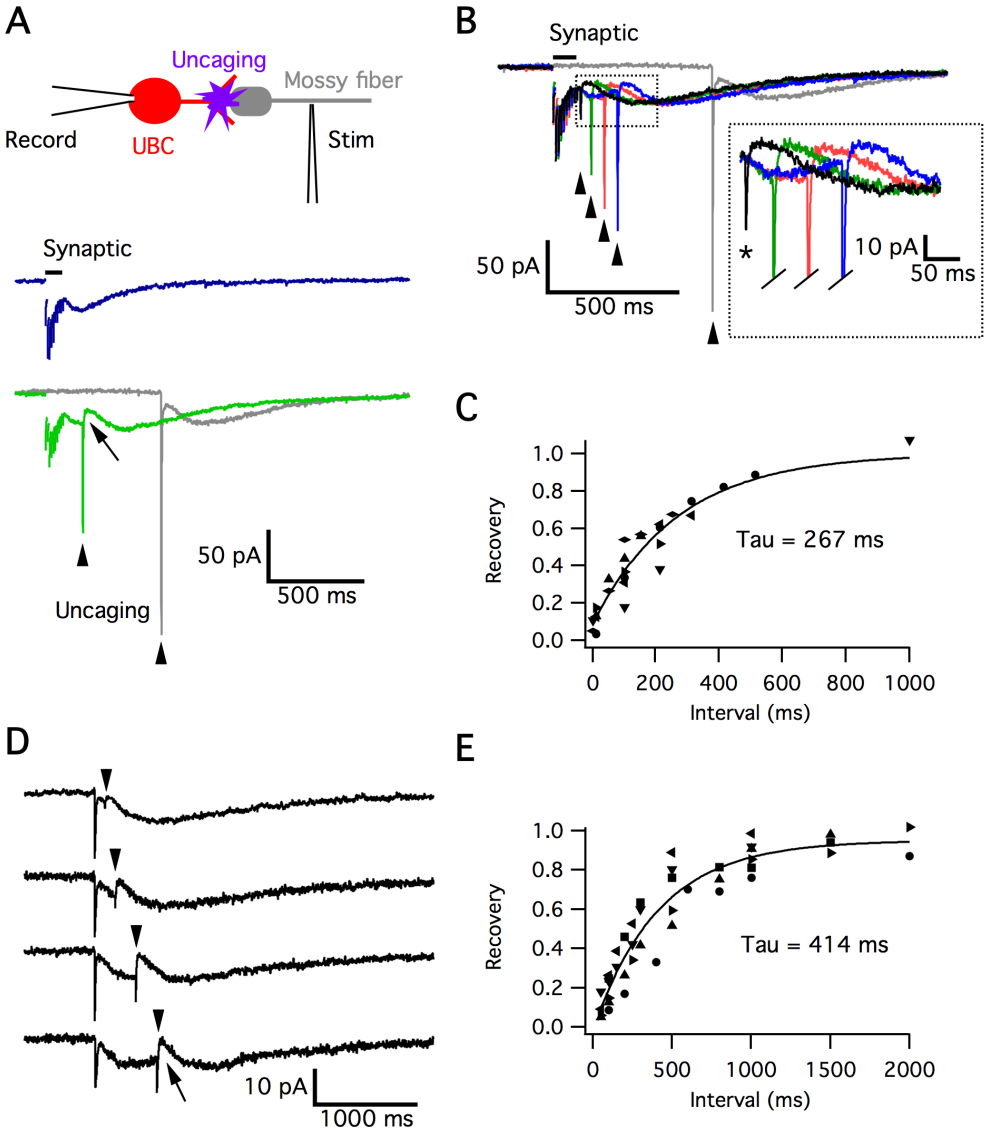

Figure 2.2 AMPARs are desensitized during slow EPSC.

A, Top: experimental configuration. UV-laser was targeted to the brush to uncage MNI-glutamate after synaptic stimulation. Bottom: black, synaptic responses; green, uEPSC after synaptic stimulation; gray, uEPSC without prior stimulation. Arrowheads mark the timing of uncaging. Arrow marks the undershoot current.

B, Uncaging at different times (arrowheads) during slow EPSC. Gray trace shows the control uEPSC. Inset: Expanded view showing diminished size of uncaging response (*) delivered 15 ms after final synaptic stimulation.

C, Summary of recovery time course shown in B. Each symbol represents a different cell. The recovery was fit by a single exponential (black line).

D, Paired-pulse uncaging also showed a desensitized second uEPSC. Note the undershoot current (arrow) in the second uEPSC.

E, Recovery time course for the second uEPSC in paired uncaging paradigm. Each symbol represents a different cell. Recovery was fit with a single exponential (black line).

Figure 2.3

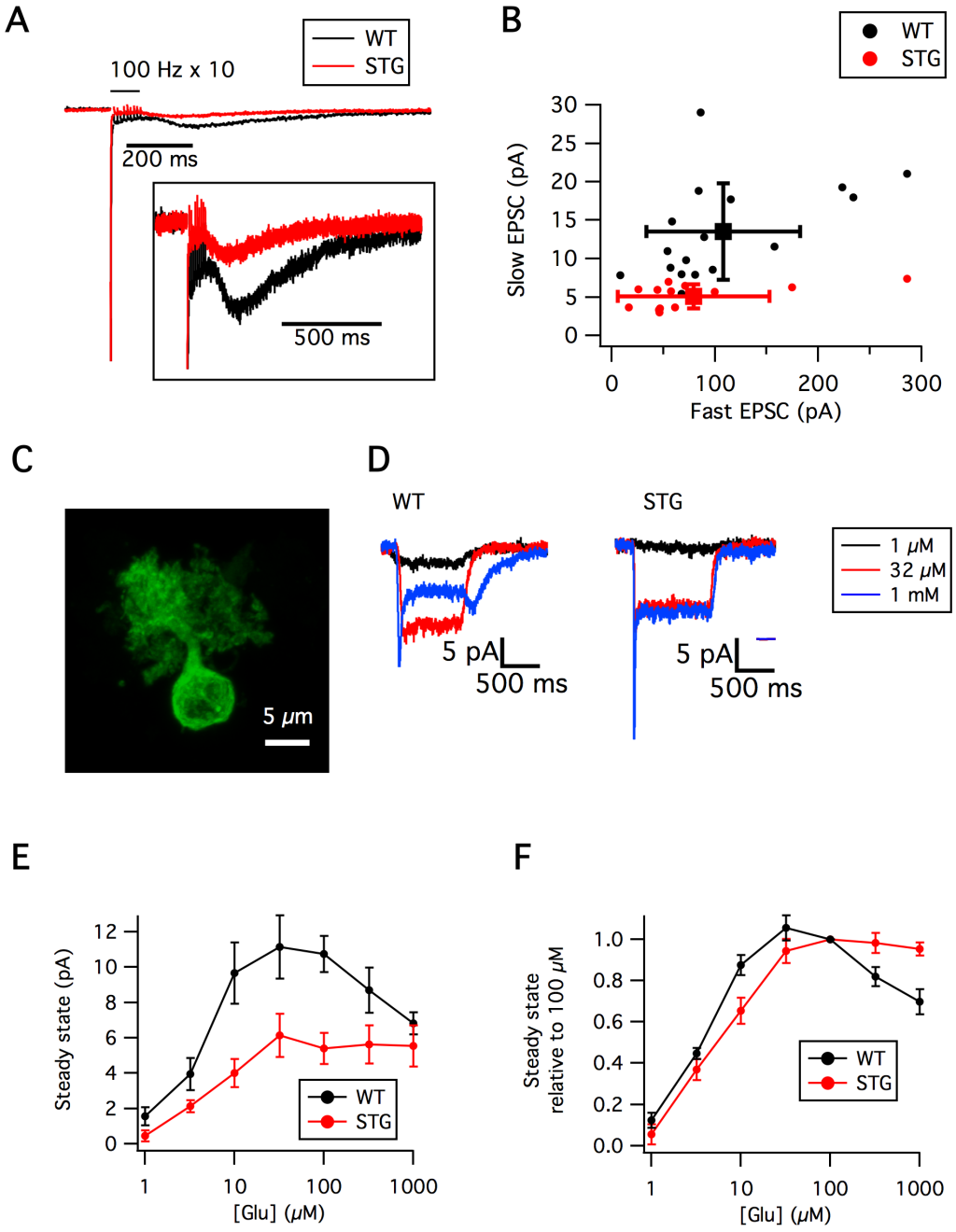

Figure 2.3 Stargazer UBCs showed a reduced slow EPSC and a monotonic dose response curve of steady-state AMPAR current.

A, Overlay of EPSCs from a wt (black) and a *stg* UBC (red). The peak of the fast EPSC is scaled to the same level. Inset: expanded view of the slow EPSC.

B, Plot of slow vs fast EPSC amplitudes from 17 wt and 13 *stg* UBCs. The peak amplitudes of slow but not fast EPSC in *stg* UBCs were significantly smaller compared to wt.

C, A GFP-labeled dissociated UBC with intact dendritic brush.

D, Exemplar AMPAR-mediated currents evoked by glutamate fast-applied to dissociated wt and *stg* UBCs.

E-F, Comparison of absolute (E) and normalized (F) amplitudes of steady-state AMPAR currents in wt and *stg* UBCs.

Figure 2.4

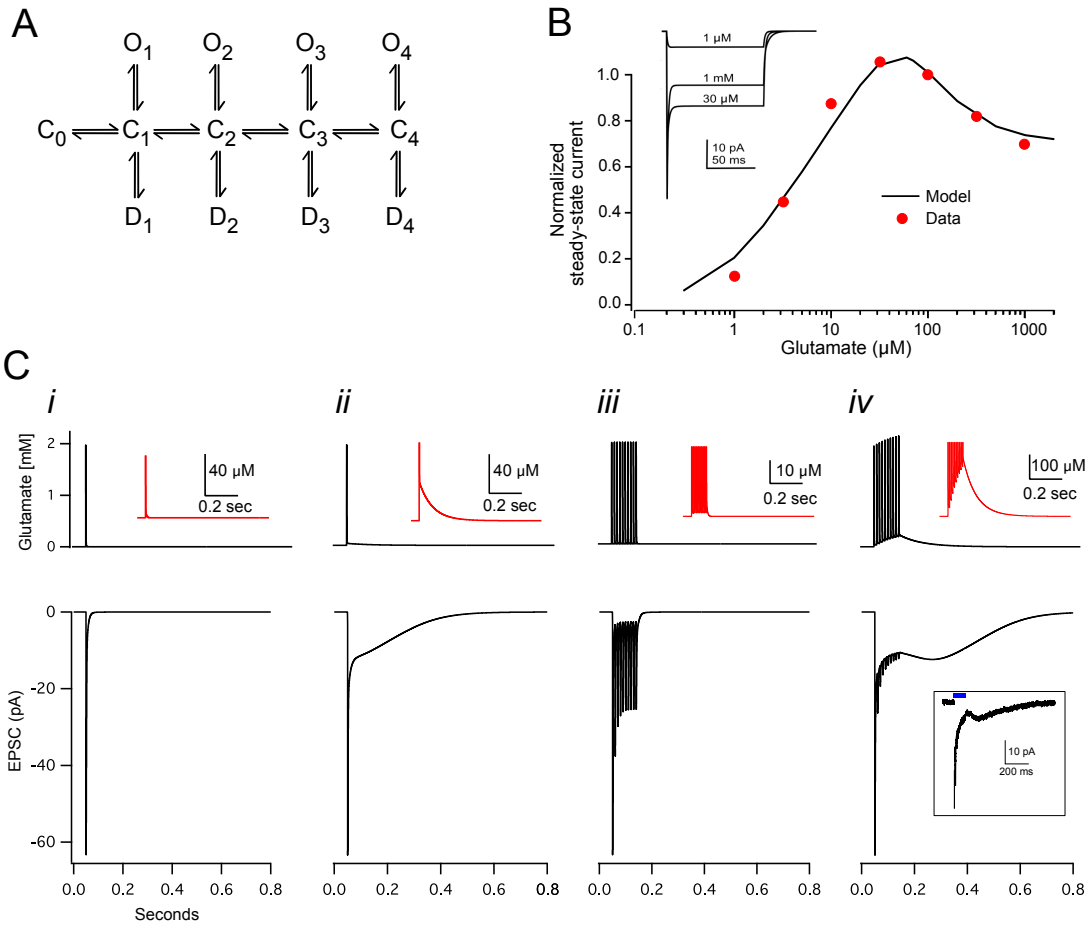

Figure 2.4 Kinetic model of AMPAR.

A, Kinetic scheme. *C:* closed states; *O*:open states*; D:* desensitized states. Subscripts indicate number of glutamates bound. Rates as in Table 2.1.

B, Simulation with model in A of square pulses of glutamate (inset) to the indicated concentrations. Red circles are data from wt UBCs in Fig 2.3E.

C, Upper row of panels i-iv shows simulated glutamate transients; red inset traces are expanded views to highlight slow decay phase of glutamate. Lower panels are the

responses of the kinetic model in A to the corresponding glutamate transients. Inset in lower panel of iv is an exemplary EPSC from a wt UBC for comparison to simulation.

Figure 2.5

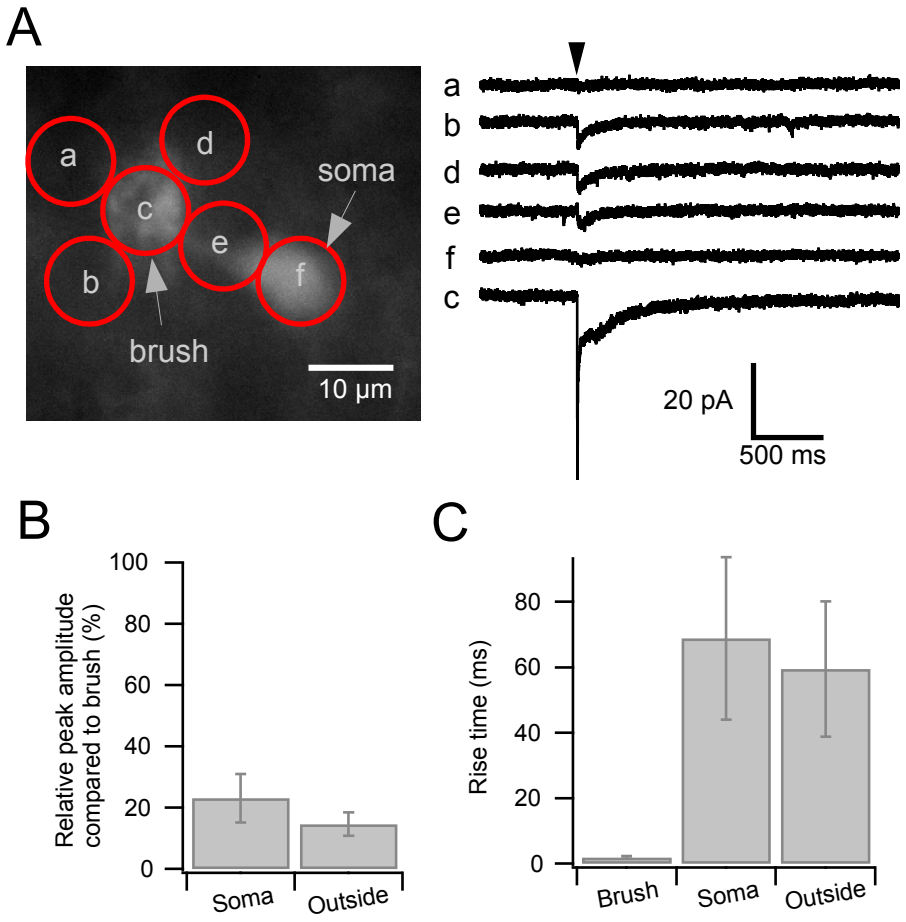

Figure 2.5 AMPARs are primarily located at the dendritic brush of UBCs.
A, Left: uncaging at different locations in and around an UBC. Right: responses evoked at corresponding locations in left figure. Note that the response is largest when uncaging at the brush (c). B, Comparison of the peak amplitudes when the uncaging beam was targeted at the soma or outside dendritic brush. Both were 80% smaller than that evoked at the brush. C, Comparison of the rise time of uncaging-evoked response at different locations. The rise times were significantly longer when uncaging at the soma or outside the dendritic brush compared to uncaging at the dendritic brush.

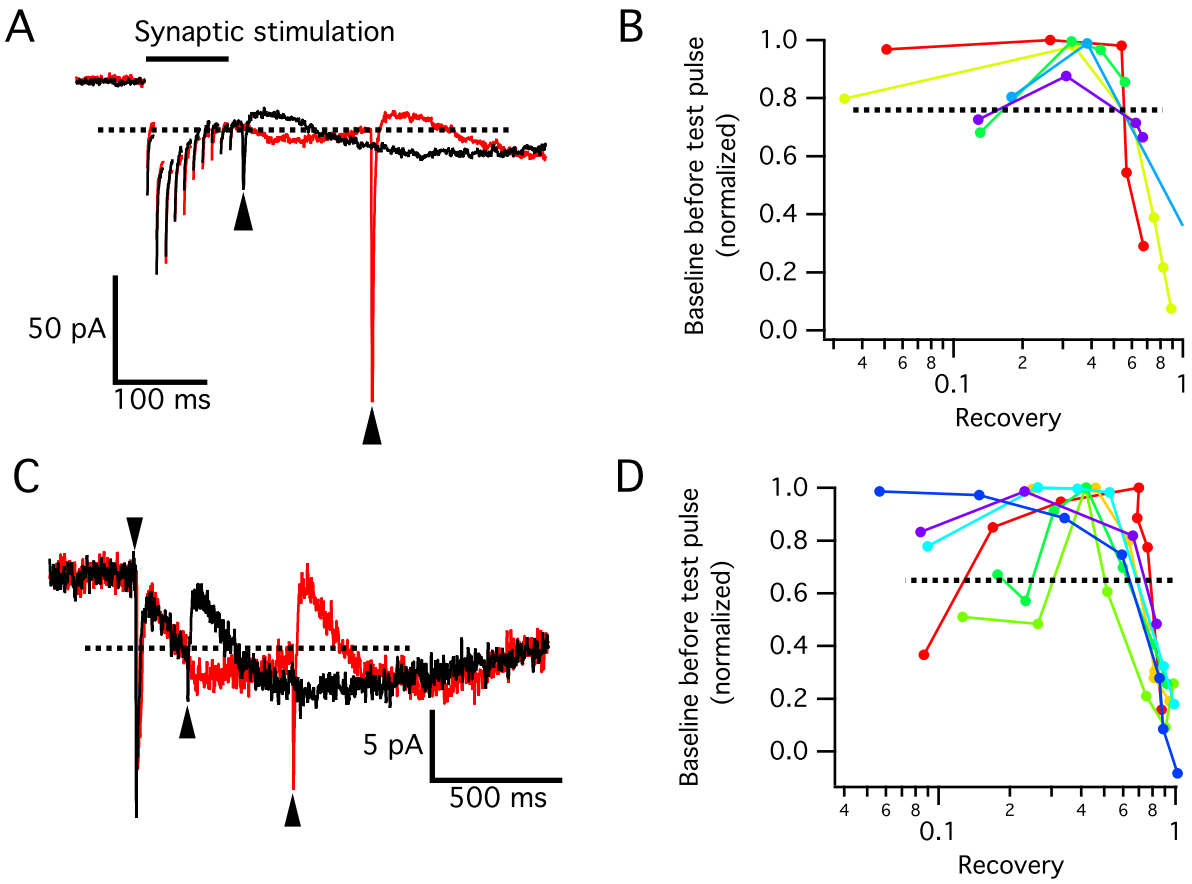

Figure 2.6 Different [glutamate] can generate the same equilibrium response
(A and C) Peak of uEPSC was smaller when evoked at the rise phase (red) than at the decay phase (gray) of the slow EPSC even though the steady-state current is the same (dashed lines). Arrowheads mark the timing of uncaging. Slow EPSC was evoked by synaptic stimulation in (A) and a 2-ms uncaging pulse in (C). (B and D) Plot of the steady-state current of the slow EPSC evoked just before the test uncaging pulse against the proportions of recovery. Slow EPSC was evoked by by synaptic stimulation in (B) and by uncaging in (D). Each color represents a different cell (B: n = 5; C: n = 6). The bell-shaped curves show that the same steady-state current correspond to two different recovery states, indicating that they might be produced by different [glutamate].

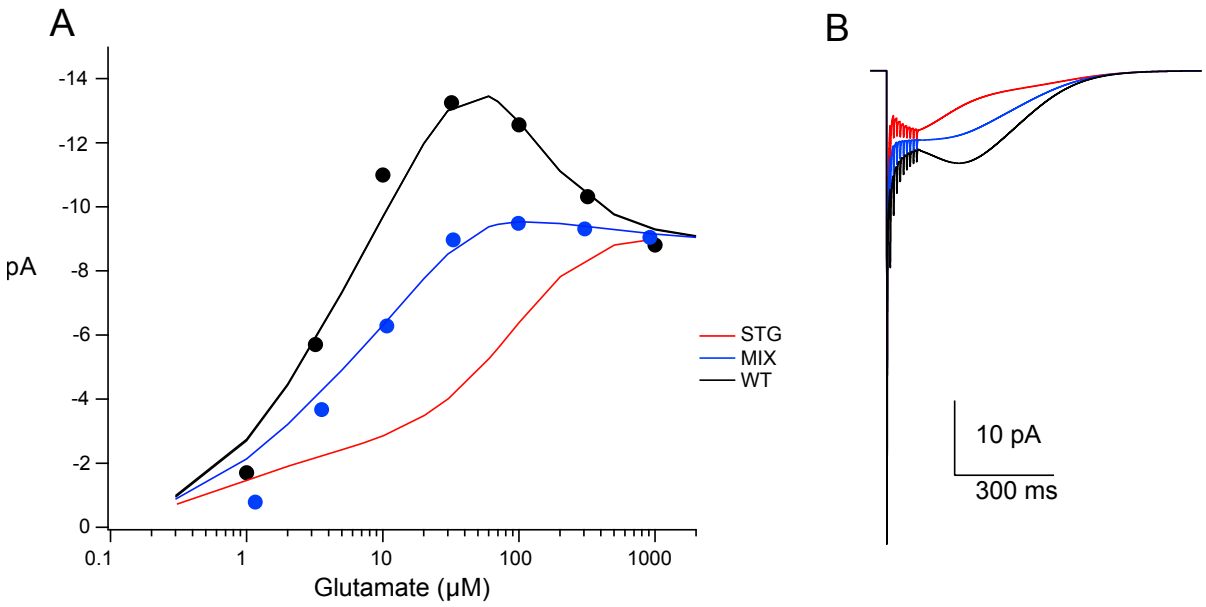

Figure 2.7 Modeling the AMPAR of *stg* mice.

A, Simulated steady-state dose-response relations for wildtype model (black line, model from Fig 2.4), TARP-less model (red line, Table 2.1), and a 50/50 mix of receptors, with total receptor number =100. Black dots are data from wildtype UBCs and blue dots from *stg* UBCs. B, Simulated EPSCs to the concentration transient of Fig 2.4Civ for the three conditions in A.

SUMMARY AND CONCLUSIONS

The work presented in this thesis elucidates how different mechanisms underlying synaptic depression shape synaptic transmission in two interneuron circuits, the cartwheel interneuron circuit in the DCN and the mossy fiber – UBC circuit in the cerebellum, respectively. Although the two interneuron networks differ in terms of transmitter content and the location of circuit, they both are parts of the mossy fiber – parallel fiber system of the cerebellum-like structures and thus play a role in predicting expected sensory or motor outcomes (Bell et al., 2008).

In Chapter 1, I examined how spontaneous spiking and short-term depression regulates the inhibitory network of cartwheel cells in the DCN. Since cartwheel cells are located in the molecular layer pathway and provide feedforward inhibition from multisensory inputs (Davis et al., 1996b; Shore, 2005; Koehler et al., 2011), they may be important to inhibit self-generated noise such as chewing or vocalization (Oertel and Young, 2004a; Bell et al., 2008). From paired recording in the brain slices, I found that cartwheel cells form powerful synapses onto fusiform cells, with unitary conductance around 40 nS. This is quite large as its cerebellum counterpart, the Purkinje cell – deep cerebellar nuclei synapse, has unitary conductance ~ 9 nS and is already considered a large conductance synapse (Person and Raman, 2012b). However, cartwheel cell synapses also depress profoundly during repetitive stimulation, with steady-state amplitude ~ 20 % of its original amplitude. Hence, when they fire spontaneously (Davis et al., 1996b; Brenowitz and Trussell, 2001; Kuo and Trussell, 2011), their inhibition onto fusiform cells is greatly reduced. Thus, spontaneous spiking in cartwheel cells can cause excitatory parallel fiber inputs relaying multisensory signals more easily to excite fusiform cells. On the other hand,

the feedforward inhibition provided by cartwheel cells can be enhanced once spontaneous spiking is silenced by neuromodulators such as noradrenaline (Kuo and Trussell, 2011).

However, feedforward inhibition may not come from one but multiple cartwheel cells. The summed inhibition may thus be powerful even under the conditions of spontaneous spiking and synaptic depression. The question then becomes whether cartwheel cells form a large enough convergent network to provide effective inhibition under synaptic depression. Previous studies using paired recordings of connected cartwheel-fusiform cells showed that they share a fraction of inhibitory inputs, indicating a fusiform cell is at least innervated by 3 cartwheel cells (Roberts and Trussell, 2010). Surprisingly, the two approaches aiming to estimate the total number of inputs in this thesis also suggests that the convergence ratio of cartwheel:fusiform cells is not significantly larger, ~ 3 - 4. By using channelrhodpsin excitation of potentially all converging cartwheel cell inputs during high rates of spontaneous spiking, I showed that such small size of a convergent circuit is sufficient to inhibit fusiform cell spiking. One possible reason for this small circuit to exert powerful inhibition is that the steady-state transmission does not depress much further but stays around ~20% of the original level even when the stimulus frequency is increased moderately. With computational modeling of vesicle recruitment during synaptic depression, I propose that a large low-Pr vesicle pool sustains such nearly frequency-independent steady-state transmission. Thus, a sum of 3 -4 depressed inputs is almost as powerful as a non-depressed single input. In conclusion, this study shows that interplay between spontaneous spiking, short-term synaptic depression and vesicle recruitment determines the size of an effective convergent circuit.

One key question raised in Chapter 1 is whether cartwheel cells converging onto the same fusiform cells can be activated by multisensory inputs at once. From dual cartwheel cell recordings in the brain slice it is suggested that neighboring cartwheel cells are innervated by different sets of parallel fibers (Roberts and Trussell, 2010). Thus to recruit all cartwheel cells it requires activation of a large set of parallel fibers, presumably from activation of multiple sensory modalities such as vestibular, somatosensory, and descending auditory inputs. Parallel fibers are axons of granule cells, and in cerebellum or other cerebellum-like structures, it is found that multisensory information already converge onto a single granule cell via activating different dendritic claws (Sawtell, 2010; Huang et al., 2013; Chabrol et al., 2015b). Whether multisensory information converges onto a single granule cell in DCN is still unknown and requires experiments such as retrograde labeling and selective activation of mossy fiber afferents. If multisensory signals do converge on a single granule cell, this indicates that even sparse cartwheel cell recruitment already requires activation of multiple sensory modalities. The other possible scenario to recruit multiple cartwheel cells is by activating multiple granule cells through UBCs, which receive only one extrinsic mossy fiber input but send at least 4 – 5 intrinsic mossy fiber inputs to granule cells. Thus, one sensory modality driving UBC to fire may actually recruit multiple cartwheel cells by activating several downstream granule cells. Future works such as characterizing the connectivity between UBC-granule cell or the sources of mossy fiber inputs to DCN UBCs are thus important.

In Chapter 2, I together with other colleagues studied the transmission at mossy fiber – UBC synapse. One characteristic of this synapse is a slow EPSC mediated by AMPARs emerging after conventional fast EPSC ends. Although it has been hypothesized to be

mediated by desensitized AMPARs as glutamate is slowly cleared from the synaptic cleft, no direct evidence has been observed. Our study provided solid new evidence supporting this hypothesis. By using MNI-glutamate uncaging, I directly showed that AMPARs are desensitized during slow EPSC at mossy fiber – UBC synapse. Furthermore, the transient outward current evoked by uncaging high concentrations of glutamate during slow EPSC suggests that the cleft [glutamate] is low according to the bell-shaped dose relations of the steady-state AMPARs described previously (Geoffroy et al., 1991; Raman and Trussell, 1992). We also confirmed that the steady-state AMPAR dose response relations from dissociated UBCs is bell shaped and suggested that the [glutamate] at peak of slow current is around 32 μM. Moreover, when we applied dextran to retard glutamate diffusion, an increase in holding current and a reduction in the steady-state current during synaptic stimulation was observed. This also supported that the wide extensive synaptic cleft between mossy fiber and UBC provides sufficient space to trap glutamate.

We also explored the possible molecular mechanism underlying the slow EPSC and the bell-shaped dose response relationship of steady-state AMPARs in UBCs. In expression systems, the bell-shaped dose response relations are present only when AMPARs are coexpressed with TARPγ2 subunit, stargazin (Morimoto-Tomita et al., 2009; Semenov et al., 2012). Accordingly, we found a significant, although not complete, reduction in the peak slow EPSC in stg UBCs. The steady-state dose response relations from dissociated stg UBCs was monotonic, however, low intensity-uncaging experiments in brain slices suggest that steady-state AMPARs in stg UBCs may still exhibit some bell-shaped dose relations. The unexpected presence of slow EPSC in stg UBCs could be due to that some unknown molecular mechanisms, presumably other types of TARP, may still enhance steady-state

AMPAR responses at low concentrations. Indeed, the TARP family contains several subtypes, and each can affect AMPAR gating differentially (Jackson and Nicoll, 2011). In cerebellum, multiple cell types such as granule cells and stellate cells express TARPγ7 in addition to stargazin (Coombs and Cull-Candy, 2009; Yamazaki et al., 2015). It may be possible that UBCs also express TARPγ7. Another possibility for the reduction in slow EPSC can be caused by lack of synaptic AMPARs due to the membrane trafficking role of stargazin (Chen et al., 2000), however, the lack of reduction in fast EPSC amplitude excludes this possibility. In short, the significant reduction of slow EPSC in the stg UBCs suggests that stargazin regulates at least partially the generation of this current. The presence of other TARPs could be assessed by using immunohistochemistry or molecular biology techniques such as knock-down in cultured UBCs (Bats et al., 2012).

Future works will be needed to determine the physiological roles for this slow AMPAR-mediated EPSC in UBCs. At circuit level, because UBC axons form intrinsic mossy fiber systems terminating onto granule cells, the prolonged firing induced by the slow EPSC (Rossi and Slater, 1993; Borges-Merjane and Trussell, 2015) may provide sustained depolarization in granule cells and broaden its time window for dendritic integration. Furthermore, since each dendritic claw of granule cell have been found to receive mossy fiber inputs from distinct sensory modalities (Sawtell, 2010; Huang et al., 2013; Chabrol et al., 2015b), the prolonged firing in UBCs may enhance the probability of multisensory integration in granule cells. However, this is dependent on the strength and short-term plasticity of the intrinsic mossy fiber-granule synapse, which have not been measured and may be different from synapses made by extrinsic mossy fibers (Chabrol et al., 2015b). Paired recordings between synaptically coupled UBC and granule cells, or selective

activation of intrinsic mossy fibers - granule cell synapse using channelrhodopsin driven by UBC-specific promoter is thus needed.

Another possible role for this giant synapse is to control the excitability of UBCs by trapping a certain level of glutamate in the cleft. In the cerebellum, UBCs are primarily located in the vestibulocerebellum and are innervated by primary and secondary vestibular inputs (Diño et al., 2000b). Because vestibular inputs are constantly active and their firing rates are linearly correlated with the speed of the head motion (Fernandez and Goldberg, 1971), it is possible that in vivo there is constant glutamate trapped in the synaptic cleft. Furthermore, this ambient [glutamate] may vary depending on the spontaneous firing rate of the vestibular input (or head speed). According to the dose response curve measured in this study, a few micromolar glutamate can activate steady-state AMPAR current in UBCs. It is thus possible that ambient glutamate caused by spontaneous mossy fiber activity can generate a tonic current that increases the excitability of the UBCs. Moreover, since AMPARs desensitize at low [glutamate] (Trussell and Fischbach, 1989; Colquhoun et al., 1992; Raman and Trussell, 1992), ambient glutamate may also depress the phasic fast EPSCs evoked during mossy fiber activity. Although we rarely observe spontaneous EPSCs in UBCs in brain slices, it is likely that the activity is lost during slicing procedure. It is therefore of interest to stimulate the synapse with spontaneous vestibular nerve activity recorded in vivo (McElvain et al., 2015) and observe its effect on UBC excitability and synaptic transmission.

Finally, UBCs express not only AMPARs but also metabotropic glutamate receptors (Nunzi et al., 2002; Borges-Merjane and Trussell, 2015). These metabotropic receptors also mediate synaptic response. A recent study in has found that UBCs can be categorized as ON

or OFF cells according their response to synaptic stimulation: ON cells show a fast-then slow inward current largely mediated by AMPARs; OFF cells show a slow outward current mediated by mGluR2 (Borges-Merjane and Trussell, 2015). Although AMPAR-mediated slow EPSC is present in both cell types, it is masked by the outward current generated by mGluR2 during synaptic stimulation in OFF cells. The experiments in this study blocked all metabotropic responses and therefore would not distinguish the ON or OFF cell type. However, under physiological conditions, metabotropic responses can play an important role in regulating UBC excitability. It is therefore important to investigate whether ON and OFF cell types receive mossy fiber originated from different sources. Retrograde tracing studies may answer this question.

REERENCES

Apostolides PF, Trussell LO (2013) Rapid, Activity-Independent Turnover of Vesicular Transmitter Content at a Mixed Glycine/GABA Synapse. J Neurosci 33:4768–4781.

Apostolides PF, Trussell LO (2014) Chemical synaptic transmission onto superficial stellate cells of the mouse dorsal cochlear nucleus. J Neurophysiol 111:1812–1822.

Barmack NH, Yakhnitsa V (2008) Functions of Interneurons in Mouse Cerebellum. J Neurosci 28:1140–1152.

Bats C, Soto D, Studniarczyk D, Farrant M, Cull-Candy SG (2012) Channel properties reveal differential expression of TARPed and TARPless AMPARs in stargazer neurons. Nat Neurosci 15:853–861.

Bell CC, Han V, Sawtell NB (2008) Cerebellum-Like Structures and Their Implications for Cerebellar Function. Annu Rev Neurosci 31:1–24.

Bender KJ, Ford CP, Trussell LO (2010) Dopaminergic modulation of axon initial segment calcium channels regulates action potential initiation. Neuron 68:500–511.

Bender KJ, Trussell LO (2009) Axon initial segment Ca2+ channels influence action potential generation and timing. Neuron 61:259–271.

Bender KJ, Uebele VN, Renger JJ, Trussell LO (2012) Control of firing patterns through modulation of axon initial segment T-type calcium channels. J Physiol 590:109–118.

Berrebi AS, Mugnaini E (1991) Distribution and targets of the cartwheel cell axon in the dorsal cochlear nucleus of the guinea pig. Anat Embryol (Berl) 183:427–454.

Berridge CW, Waterhouse BD (2003) The locus coeruleus–noradrenergic system: modulation of behavioral state and state-dependent cognitive processes. Brain Res Rev 42:33–84.

Betz WJ (1970a) Depression of transmitter release at the neuromuscular junction of the frog. J Physiol 206:629–644.

Betz WJ (1970b) Depression of transmitter release at the neuromuscular junction of the frog. J Physiol 206:629–644.

Bischofberger J, Engel D, Li L, Geiger JR, Jonas P (2006) Patch-clamp recording from mossy fiber terminals in hippocampal slices. Nat Protoc 1:2075–2081.

Borges-Merjane C, Trussell LO (2015) ON and OFF Unipolar Brush Cells Transform Multisensory Inputs to the Auditory System. Neuron 85:1029–1042.

Borst JGG (2010) The low synaptic release probability in vivo. Trends Neurosci 33:259–266.

Brenowitz S, Trussell LO (2001) Minimizing Synaptic Depression by Control of Release Probability. J Neurosci 21:1857–1867.

Brody DL, Yue DT (2000) Release-independent short-term synaptic depression in cultured hippocampal neurons. J Neurosci Off J Soc Neurosci 20:2480–2494.

Cao X-J, Oertel D (2010) Auditory Nerve Fibers Excite Targets Through Synapses That Vary in Convergence, Strength, and Short-Term Plasticity. J Neurophysiol 104:2308–2320.

Castillo JD, Katz B (1957) Interaction at End-Plate Receptors between Different Choline Derivatives. Proc R Soc Lond B Biol Sci 146:369–381.

Catterall WA, Few AP (2008) Calcium Channel Regulation and Presynaptic Plasticity. Neuron 59:882–901.

Chabrol FP, Arenz A, Wiechert MT, Margrie TW, DiGregorio DA (2015a) Synaptic diversity enables temporal coding of coincident multisensory inputs in single neurons. Nat Neurosci 18:718–727.

Chabrol FP, Arenz A, Wiechert MT, Margrie TW, DiGregorio DA (2015b) Synaptic diversity enables temporal coding of coincident multisensory inputs in single neurons. Nat Neurosci advance online publication Available at: http://www.nature.com/neuro/journal/vaop/ncurrent/full/nn.3974.html [Accessed April 2, 2015].

Chen C, Blitz DM, Regehr WG (2002) Contributions of Receptor Desensitization and Saturation to Plasticity at the Retinogeniculate Synapse. Neuron 33:779–788.

Chen L, Chetkovich DM, Petralia RS, Sweeney NT, Kawasaki Y, Wenthold RJ, Bredt DS, Nicoll RA (2000) Stargazin regulates synaptic targeting of AMPA receptors by two distinct mechanisms. Nature 408:936–943.

Clements JD, Lester RA, Tong G, Jahr CE, Westbrook GL (1992) The time course of glutamate in the synaptic cleft. Science 258:1498–1501.

Colquhoun D, Jonas P, Sakmann B (1992) Action of brief pulses of glutamate on AMPA/kainate receptors in patches from different neurones of rat hippocampal slices. J Physiol 458:261–287.

Cook DL, Schwindt PC, Grande LA, Spain WJ (2003) Synaptic depression in the localization of sound. Nature 421:66–70.

Coombs ID, Cull-Candy SG (2009) Transmembrane AMPA receptor regulatory proteins and AMPA receptor function in the cerebellum. Neuroscience 162:656–665.

Davis KA, Miller RL, Young ED (1996a) Effects of somatosensory and parallel-fiber stimulation on neurons in dorsal cochlear nucleus. J Neurophysiol 76:3012–3024.

Davis KA, Miller RL, Young ED (1996b) Effects of somatosensory and parallel-fiber stimulation on neurons in dorsal cochlear nucleus. J Neurophysiol 76:3012–3024.

Davis KA, Young ED (1997) Granule cell activation of complex-spiking neurons in dorsal cochlear nucleus. J Neurosci Off J Soc Neurosci 17:6798–6806.

Debanne D, Guérineau NC, Gähwiler BH, Thompson SM (1996) Paired-pulse facilitation and depression at unitary synapses in rat hippocampus: quantal fluctuation affects subsequent release. J Physiol 491:163–176.

Diamond JS, Jahr CE (1995) Asynchronous release of synaptic vesicles determines the time course of the AMPA receptor-mediated EPSC. Neuron 15:1097–1107.

DiGregorio DA, Rothman JS, Nielsen TA, Silver RA (2007) Desensitization properties of AMPA receptors at the cerebellar mossy fiber granule cell synapse. J Neurosci Off J Soc Neurosci 27:8344–8357.

Diño MR, Nunzi MG, Anelli R, Mugnaini E (2000a) Unipolar brush cells of the vestibulocerebellum: afferents and targets. Prog Brain Res 124:123–137.

Diño MR, Nunzi MG, Anelli R, Mugnaini E (2000b) Unipolar brush cells of the vestibulocerebellum: afferents and targets. In (Research B-P in B, ed), pp 123–137 Cerebellar modules: Molecules, morphology and function. Elsevier. Available at: http://www.sciencedirect.com/science/article/pii/S0079612300240132 [Accessed May 19, 2016].

Diño MR, Schuerger RJ, Liu Y-B, Slater NT, Mugnaini E (2000c) Unipolar brush cell: a potential feedforward excitatory interneuron of the cerebellum. Neuroscience 98:625–636.

Dittman JS, Regehr WG (1998) Calcium Dependence and Recovery Kinetics of Presynaptic Depression at the Climbing Fiber to Purkinje Cell Synapse. J Neurosci 18:6147–6162.

Do MTH, Bean BP (2003) Subthreshold sodium currents and pacemaking of subthalamic neurons: modulation by slow inactivation. Neuron 39:109–120.

Dobrunz LE, Stevens CF (1997) Heterogeneity of Release Probability, Facilitation, and Depletion at Central Synapses. Neuron 18:995–1008.

Dorp S van, Zeeuw CID (2014) Variable timing of synaptic transmission in cerebellar unipolar brush cells. Proc Natl Acad Sci 111:5403–5408.

Eccles JC, Katz B, Kuffler SW (1941) Nature of the "Endplate Potential" in Curarized Muscle. J Neurophysiol 4:362–387.

Elmqvist D, Quastel DM (1965) A quantitative study of end-plate potentials in isolated human muscle. J Physiol 178:505–529.

Feng T-P (1941) Studies on the neuromuscular junction XXVI. The changes of the end-plaste potential during and after prolonged stimulation. Chin J Physiol 16:341–372.

Fernandez C, Goldberg JM (1971) Physiology of peripheral neurons innervating semicircular canals of the squirrel monkey. II. Response to sinusoidal stimulation and dynamics of peripheral vestibular system. J Neurophysiol 34:661–675.

Ferragamo MJ, Golding NL, Oertel D (1998) Synaptic Inputs to Stellate Cells in the Ventral Cochlear Nucleus. J Neurophysiol 79:51–63.

Floris A, Diño M, Jacobowitz DM, Mugnaini E (1994) The unipolar brush cells of the rat cerebellar cortex and cochlear nucleus are calretinin-positive: a study by light and electron microscopic immunocytochemistry. Anat Embryol (Berl) 189:495–520.

Ford CP, Gantz SC, Phillips PEM, Williams JT (2010) Control of Extracellular Dopamine at Dendrite and Axon Terminals. J Neurosci 30:6975–6983.

Ford MC, Grothe B, Klug A (2009) Fenestration of the calyx of held occurs sequentially along the tonotopic axis, is influenced by afferent activity, and facilitates glutamate clearance. J Comp Neurol 514:92–106.

Forsythe ID, Tsujimoto T, Barnes-Davies M, Cuttle MF, Takahashi T (1998) Inactivation of Presynaptic Calcium Current Contributes to Synaptic Depression at a Fast Central Synapse. Neuron 20:797–807.

Geoffroy M, Lambolez B, Audinat E, Hamon B, Crepel F, Rossier J, Kado RT (1991) Reduction of desensitization of a glutamate ionotropic receptor by antagonists. Mol Pharmacol 39:587–591.

Golding NL, Oertel D (1997) Physiological Identification of the Targets of Cartwheel Cells in the Dorsal Cochlear Nucleus. J Neurophysiol 78:248–260.

Groh A, Kock CPJ de, Wimmer VC, Sakmann B, Kuner T (2008) Driver or Coincidence Detector: Modal Switch of a Corticothalamic Giant Synapse Controlled by Spontaneous Activity and Short-Term Depression. J Neurosci 28:9652–9663.

Harty TP, Manis PB (1998) Kinetic Analysis of Glycine Receptor Currents in Ventral Cochlear Nucleus. J Neurophysiol 79:1891–1901.

Hashimoto K, Fukaya M, Qiao X, Sakimura K, Watanabe M, Kano M (1999) Impairment of AMPA Receptor Function in Cerebellar Granule Cells of Ataxic Mutant Mouse Stargazer. J Neurosci 19:6027–6036.

Häusser M, Raman IM, Otis T, Smith SL, Nelson A, Lac S du, Loewenstein Y, Mahon S, Pennartz C, Cohen I, Yarom Y (2004) The Beat Goes On: Spontaneous Firing in Mammalian Neuronal Microcircuits. J Neurosci 24:9215–9219.

Hermann J, Pecka M, Gersdorff H von, Grothe B, Klug A (2007) Synaptic Transmission at the Calyx of Held Under In Vivo–Like Activity Levels. J Neurophysiol 98:807–820.

Hestrin S (1992) Activation and desensitization of glutamate-activated channels mediating fast excitatory synaptic currents in the visual cortex. Neuron 9:991–999.

Hestrin S (1993) Different glutamate receptor channels mediate fast excitatory synaptic currents in inhibitory and excitatory cortical neurons. Neuron 11:1083–1091.

Huang C-C, Sugino K, Shima Y, Guo C, Bai S, Mensh BD, Nelson SB, Hantman AW (2013) Convergence of pontine and proprioceptive streams onto multimodal cerebellar granule cells. eLife 2:e00400.

Jaarsma D, Dino MR, Ohishi H, Shigemoto R, Mugnaini E (1998) Metabotropic glutamate receptors are associated with non-synaptic appendages of unipolar brush cells in rat cerebellar cortex and cochlear nuclear complex. J Neurocytol 27:303–327.

Jackson AC, Nicoll RA (2011) The Expanding Social Network of Ionotropic Glutamate Receptors: TARPs and Other Transmembrane Auxiliary Subunits. Neuron 70:178–199.

Jonas P (2000) The Time Course of Signaling at Central Glutamatergic Synapses. Physiology 15:83–89.

Jonas P, Spruston N (1994) Mechanisms shaping glutamate-mediated excitatory postsynaptic currents in the CNS. Curr Opin Neurobiol 4:366–372.

Jones MV, Westbrook GL (1996) The impact of receptor desensitization on fast synaptic transmission. Trends Neurosci 19:96–101.

Kanold PO, Davis KA, Young ED (2011) Somatosensory context alters auditory responses in the cochlear nucleus. J Neurophysiol 105:1063–1070.

Katz B, Thesleff S (1957) A study of the “desensitization” produced by acetylcholine at the motor end-plate. J Physiol 138:63–80.

Kawaguchi S, Sakaba T (2015) Control of inhibitory synaptic outputs by low excitability of axon terminals revealed by direct recording. Neuron 85:1273–1288.

Kennedy A, Wayne G, Kaifosh P, Alviña K, Abbott LF, Sawtell NB (2014) A temporal basis for predicting the sensory consequences of motor commands in an electric fish. Nat Neurosci 17:416–422.

Kim Y, Trussell LO (2007) Ion channels generating complex spikes in cartwheel cells of the dorsal cochlear nucleus. J Neurophysiol 97:1705–1725.

Kim Y, Trussell LO (2009) Negative Shift in the Glycine Reversal Potential Mediated by a Ca2+- and pH-Dependent Mechanism in Interneurons. J Neurosci 29:11495–11510.

Kinney GA, Overstreet LS, Slater NT (1997) Prolonged Physiological Entrapment of Glutamate in the Synaptic Cleft of Cerebellar Unipolar Brush Cells. J Neurophysiol 78:1320–1333.

Kiskin NI, Krishtal OA, Tsyndrenko AYa null (1986) Excitatory amino acid receptors in hippocampal neurons: kainate fails to desensitize them. Neurosci Lett 63:225–230.

Koehler SD, Pradhan S, Manis PB, Shore SE (2011) Somatosensory inputs modify auditory spike timing in dorsal cochlear nucleus principal cells. Eur J Neurosci 33:409–420.

Kuba H, Koyano K, Ohmori H (2002) Synaptic depression improves coincidence detection in the nucleus laminaris in brainstem slices of the chick embryo. Eur J Neurosci 15:984–990.

Kuo SP, Lu H-W, Trussell LO (2012) Intrinsic and synaptic properties of vertical cells of the mouse dorsal cochlear nucleus. J Neurophysiol 108:1186–1198.

Kuo SP, Trussell LO (2011) Spontaneous spiking and synaptic depression underlie noradrenergic control of feed-forward inhibition. Neuron 71:306–318.

Kusano K, Landau EM (1975) Depression and recovery of transmission at the squid giant synapse. J Physiol 245:13–22.

Lee S-H, Dan Y (2012) Neuromodulation of Brain States. Neuron 76:209–222.

Letts VA (2005) Stargazer—A Mouse to Seize! Epilepsy Curr 5:161–165.

Letts VA, Felix R, Biddlecome GH, Arikkath J, Mahaffey CL, Valenzuela A, Bartlett FS, Mori Y, Campbell KP, Frankel WN (1998) The mouse stargazer gene encodes a neuronal Ca2+-channel γ subunit. Nat Genet 19:340–347.

Liley AW, North K a. K (1953) An Electrical Investigation of Effects of Repetitive Stimulation on Mammalian Neuromuscular Junction. J Neurophysiol 16:509–527.

Lu H-W, Trussell LO (2016) Spontaneous Activity Defines Effective Convergence Ratios in an Inhibitory Circuit. J Neurosci 36:3268–3280.

Lu T, Trussell LO (2000) Inhibitory Transmission Mediated by Asynchronous Transmitter Release. Neuron 26:683–694.

Ma W-LD, Brenowitz SD (2012) Single-neuron recordings from unanesthetized mouse dorsal cochlear nucleus. J Neurophysiol 107:824–835.

Magleby KL, Stevens CF (1972) A quantitative description of end-plate currents. J Physiol 223:173–197.

Mancilla JG, Manis PB (2009) Two Distinct Types of Inhibition Mediated by Cartwheel Cells in the Dorsal Cochlear Nucleus. J Neurophysiol 102:1287–1295.

May BJ (2000) Role of the dorsal cochlear nucleus in the sound localization behavior of cats. Hear Res 148:74–87.

McElvain LE, Faulstich M, Jeanne JM, Moore JD, du Lac S (2015) Implementation of Linear Sensory Signaling via Multiple Coordinated Mechanisms at Central Vestibular Nerve Synapses. Neuron 85:1132–1144.

Milstein AD, Nicoll RA (2008) Regulation of AMPA receptor gating and pharmacology by TARP auxiliary subunits. Trends Pharmacol Sci 29:333–339.

Min M-Y, Rusakov DA, Kullmann DM (1998) Activation of AMPA, Kainate, and Metabotropic Receptors at Hippocampal Mossy Fiber Synapses: Role of Glutamate Diffusion. Neuron 21:561–570.

Morimoto-Tomita M, Zhang W, Straub C, Cho C-H, Kim KS, Howe JR, Tomita S (2009) Autoinactivation of Neuronal AMPA Receptors via Glutamate-Regulated TARP Interaction. Neuron 61:101–112.

Morin F, Diño MR, Mugnaini E (2001) Postnatal differentiation of unipolar brush cells and mossy fiber-unipolar brush cell synapses in rat cerebellum. Neuroscience 104:1127–1139.

Moulder KL, Mennerick S (2005) Reluctant Vesicles Contribute to the Total Readily Releasable Pool in Glutamatergic Hippocampal Neurons. J Neurosci 25:3842–3850.

Mugnaini E, Sekerková G, Martina M (2011) The unipolar brush cell: a remarkable neuron finally receiving deserved attention. Brain Res Rev 66:220–245.

Müller M, Goutman JD, Kochubey O, Schneggenburger R (2010) Interaction between Facilitation and Depression at a Large CNS Synapse Reveals Mechanisms of Short-Term Plasticity. J Neurosci 30:2007–2016.

Murthy VN, Sejnowski TJ, Stevens CF (1997) Heterogeneous Release Properties of Visualized Individual Hippocampal Synapses. Neuron 18:599–612.

Neher E (2015) Merits and Limitations of Vesicle Pool Models in View of Heterogeneous Populations of Synaptic Vesicles. Neuron 87:1131–1142.

Neher E, Sakaba T (2001) Combining Deconvolution and Noise Analysis for the Estimation of Transmitter Release Rates at the Calyx of Held. J Neurosci 21:444–461.

Nielsen TA, DiGregorio DA, Silver RA (2004) Modulation of Glutamate Mobility Reveals the Mechanism Underlying Slow-Rising AMPAR EPSCs and the Diffusion Coefficient in the Synaptic Cleft. Neuron 42:757–771.

Noebels JL, Qiao X, Bronson RT, Spencer C, Davisson MT (1990) Stargazer: a new neurological mutant on chromosome 15 in the mouse with prolonged cortical seizures. Epilepsy Res 7:129–135.

Nunzi MG, Birnstiel S, Bhattacharyya BJ, Slater NT, Mugnaini E (2001) Unipolar brush cells form a glutamatergic projection system within the mouse cerebellar cortex. J Comp Neurol 434:329–341.

Nunzi M-G, Shigemoto R, Mugnaini E (2002) Differential expression of calretinin and metabotropic glutamate receptor mGluR1α defines subsets of unipolar brush cells in mouse cerebellum. J Comp Neurol 451:189–199.

Oertel D, Young ED (2004a) What's a cerebellar circuit doing in the auditory system? Trends Neurosci 27:104–110.

Oertel D, Young ED (2004b) What's a cerebellar circuit doing in the auditory system? Trends Neurosci 27:104–110.

Otis TS, Wu YC, Trussell LO (1996) Delayed clearance of transmitter and the role of glutamate transporters at synapses with multiple release sites. J Neurosci 16:1634–1644.

Owen SF, Tuncdemir SN, Bader PL, Tirko NN, Fishell G, Tsien RW (2013) Oxytocin enhances hippocampal spike transmission by modulating fast-spiking interneurons. Nature 500:458–462.

Parham K, Kim DO (1995) Spontaneous and sound-evoked discharge characteristics of complex-spiking neurons in the dorsal cochlear nucleus of the unanesthetized decerebrate cat. J Neurophysiol 73:550–561.

Partin KM, Patneau DK, Mayer ML (1994) Cyclothiazide differentially modulates desensitization of alpha-amino-3-hydroxy-5-methyl-4-isoxazolepropionic acid receptor splice variants. Mol Pharmacol 46:129–138.

Patneau DK, Vyklicky L, Mayer ML (1993) Hippocampal neurons exhibit cyclothiazide-sensitive rapidly desensitizing responses to kainate. J Neurosci Off J Soc Neurosci 13:3496–3509.

Person AL, Raman IM (2012a) Synchrony and neural coding in cerebellar circuits. Front Neural Circuits 6:97.

Person AL, Raman IM (2012b) Purkinje neuron synchrony elicits time-locked spiking in the cerebellar nuclei. Nature 481:502–505.

Portfors CV, Roberts PD (2007) Temporal and Frequency Characteristics of Cartwheel Cells in the Dorsal Cochlear Nucleus of the Awake Mouse. J Neurophysiol 98:744–756.

Prakriya M, Mennerick S (2000) Selective depression of low-release probability excitatory synapses by sodium channel blockers. Neuron 26:671–682.

Priel A, Kolleker A, Ayalon G, Gillor M, Osten P, Stern-Bach Y (2005) Stargazin Reduces Desensitization and Slows Deactivation of the AMPA-Type Glutamate Receptors. J Neurosci 25:2682–2686.

Qiao X, Hefti F, Knusel B, Noebels JL (1996) Selective failure of brain-derived neurotrophic factor mRNA expression in the cerebellum of stargazer, a mutant mouse with ataxia. J Neurosci 16:640–648.

Raman IM, Trussell LO (1992) The kinetics of the response to glutamate and kainate in neurons of the avian cochlear nucleus. Neuron 9:173–186.

Raman IM, Trussell LO (1995a) The mechanism of alpha-amino-3-hydroxy-5-methyl-4-isoxazolepropionate receptor desensitization after removal of glutamate. Biophys J 68:137–146.

Raman IM, Trussell LO (1995b) Concentration-jump analysis of voltage-dependent conductances activated by glutamate and kainate in neurons of the avian cochlear nucleus. Biophys J 69:1868–1879.

Regehr WG (2012) Short-Term Presynaptic Plasticity. Cold Spring Harb Perspect Biol 4 Available at: http://www.ncbi.nlm.nih.gov/pmc/articles/PMC3385958/ [Accessed June 16, 2015].

Reiss LAJ, Young ED (2005) Spectral edge sensitivity in neural circuits of the dorsal cochlear nucleus. J Neurosci Off J Soc Neurosci 25:3680–3691.

Rizzoli SO, Betz WJ (2005) Synaptic vesicle pools. Nat Rev Neurosci 6:57–69.

Roberts MT, Bender KJ, Trussell LO (2008) Fidelity of Complex Spike-Mediated Synaptic Transmission between Inhibitory Interneurons. J Neurosci 28:9440–9450.

Roberts MT, Trussell LO (2010) Molecular Layer Inhibitory Interneurons Provide Feedforward and Lateral Inhibition in the Dorsal Cochlear Nucleus. J Neurophysiol 104:2462–2473.

Rosenmund C, Stevens CF (1996) Definition of the readily releasable pool of vesicles at hippocampal synapses. Neuron 16:1197–1207.

Rossi DJ, Alford S, Mugnaini E, Slater NT (1995) Properties of transmission at a giant glutamatergic synapse in cerebellum: the mossy fiber-unipolar brush cell synapse. J Neurophysiol 74:24–42.

Rossi DJ, Slater NT (1993) The developmental onset of NMDA receptor-channel activity during neuronal migration. Neuropharmacology 32:1239–1248.

Rousseau CV, Dugué GP, Dumoulin A, Mugnaini E, Dieudonné S, Diana MA (2012) Mixed Inhibitory Synaptic Balance Correlates with Glutamatergic Synaptic Phenotype in Cerebellar Unipolar Brush Cells. J Neurosci 32:4632–4644.

Rozov A, Jerecic J, Sakmann B, Burnashev N (2001) AMPA Receptor Channels with Long-Lasting Desensitization in Bipolar Interneurons Contribute to Synaptic Depression in a Novel Feedback Circuit in Layer 2/3 of Rat Neocortex. J Neurosci 21:8062–8071.

Rusakov DA, Kullmann DM (1998) Geometric and viscous components of the tortuosity of the extracellular space in the brain. Proc Natl Acad Sci 95:8975–8980.

Rusakov DA, Savtchenko LP, Zheng K, Henley JM (2011) Shaping the synaptic signal: molecular mobility inside and outside the cleft. Trends Neurosci 34:359–369.

Ryugo DK, Haenggeli C-A, Doucet JR (2003) Multimodal inputs to the granule cell domain of the cochlear nucleus. Exp Brain Res 153:477–485.

Sakaba T, Neher E (2001a) Quantitative Relationship between Transmitter Release and Calcium Current at the Calyx of Held Synapse. J Neurosci 21:462–476.

Sakaba T, Neher E (2001b) Calmodulin Mediates Rapid Recruitment of Fast-Releasing Synaptic Vesicles at a Calyx-Type Synapse. Neuron 32:1119–1131.

Salloum RH, Chen G, Velet L, Manzoor NF, Elkin R, Kidd GJ, Coughlin J, Yurosko C, Bou-Anak S, Azadi S, Gohlsch S, Schneider H, Kaltenbach JA (2014) Mapping and morphometric analysis of synapses and spines on fusiform cells in the dorsal cochlear nucleus. Front Syst Neurosci 8:167.

Saviane C, Silver RA (2006) Fast vesicle reloading and a large pool sustain high bandwidth transmission at a central synapse. Nature 439:983–987.

Sawtell NB (2010) Multimodal Integration in Granule Cells as a Basis for Associative Plasticity and Sensory Prediction in a Cerebellum-like Circuit. Neuron 66:573–584.

Schneggenburger R, Meyer AC, Neher E (1999) Released Fraction and Total Size of a Pool of Immediately Available Transmitter Quanta at a Calyx Synapse. Neuron 23:399–409.

Semenov A, Möykkynen T, Coleman SK, Korpi ER, Keinänen K (2012) Autoinactivation of the Stargazin–AMPA Receptor Complex: Subunit-Dependency and Independence from Physical Dissociation. PLOS ONE 7:e49282.

Shepherd GMG (2012) Circuit Mapping by Ultraviolet Uncaging of Glutamate. Cold Spring Harb Protoc 2012:pdb.prot070664.

Shore SE (2005) Multisensory integration in the dorsal cochlear nucleus: unit responses to acoustic and trigeminal ganglion stimulation. Eur J Neurosci 21:3334–3348.

Silver RA, Colquhoun D, Cull-Candy SG, Edmonds B (1996) Deactivation and desensitization of non-NMDA receptors in patches and the time course of EPSCs in rat cerebellar granule cells. J Physiol 493:167–173.

Suter BA, O'Connor T, Iyer V, Petreanu L, Hooks BM, Kiritani T, Svoboda K, Shepherd GMG (2010) Ephus: multipurpose data acquisition software for neuroscience experiments. Front Neural Circuits 4:100.

Tang CM, Dichter M, Morad M (1989) Quisqualate activates a rapidly inactivating high conductance ionic channel in hippocampal neurons. Science 243:1474–1477.

Telgkamp P, Raman IM (2002) Depression of Inhibitory Synaptic Transmission between Purkinje Cells and Neurons of the Cerebellar Nuclei. J Neurosci 22:8447–8457.

Thanawala MS, Regehr WG (2013) Presynaptic calcium influx controls neurotransmitter release in part by regulating the effective size of the readily releasable pool. J Neurosci 33:4625–4633.

Thesleff S (1955) The Effects of Acetyleholine, Decamethonium and Suneeinylcholine on Neuromuscular Transmission in the Rat. Acta Physiol Scand 34:386–392.

Thompson SM, Gahwiler BH (1989) Activity-dependent disinhibition. I. Repetitive stimulation reduces IPSP driving force and conductance in the hippocampus in vitro. J Neurophysiol 61:501–511.

Tomita S (2010) Regulation of Ionotropic Glutamate Receptors by Their Auxiliary Subunits. Physiology 25:41–49.

Tomita S, Adesnik H, Sekiguchi M, Zhang W, Wada K, Howe JR, Nicoll RA, Bredt DS (2005) Stargazin modulates AMPA receptor gating and trafficking by distinct domains. Nature 435:1052–1058.

Trommershäuser J, Schneggenburger R, Zippelius A, Neher E (2003) Heterogeneous Presynaptic Release Probabilities: Functional Relevance for Short-Term Plasticity. Biophys J 84:1563–1579.

Trussell LO, Fischbach GD (1989) Glutamate receptor desensitization and its role in synaptic transmission. Neuron 3:209–218.

Trussell LO, Thio LL, Zorumski CF, Fischbach GD (1988) Rapid desensitization of glutamate receptors in vertebrate central neurons. Proc Natl Acad Sci U S A 85:4562–4566.

Trussell LO, Zhang S, Ramant IM (1993) Desensitization of AMPA receptors upon multiquantal neurotransmitter release. Neuron 10:1185–1196.

Turetsky D, Garringer E, Patneau DK (2005) Stargazin Modulates Native AMPA Receptor Functional Properties by Two Distinct Mechanisms. J Neurosci 25:7438–7448.

von Gersdorff H, Borst JGG (2002) Short-term plasticity at the calyx of held. Nat Rev Neurosci 3:53–64.

Wang L-Y, Kaczmarek LK (1998) High-frequency firing helps replenish the readily releasable pool of synaptic vesicles. Nature 394:384–388.

Watanabe D, Inokawa H, Hashimoto K, Suzuki N, Kano M, Shigemoto R, Hirano T, Toyama K, Kaneko S, Yokoi M, Moriyoshi K, Suzuki M, Kobayashi K, Nagatsu T, Kreitman RJ, Pastan I, Nakanishi S (1998) Ablation of Cerebellar Golgi Cells Disrupts Synaptic Integration Involving GABA Inhibition and NMDA Receptor Activation in Motor Coordination. Cell 95:17–27.

Weis S, Schneggenburger R, Neher E (1999) Properties of a model of Ca(++)-dependent vesicle pool dynamics and short term synaptic depression. Biophys J 77:2418–2429.

Wouterlood FG, Mugnaini E (1984) Cartwheel neurons of the dorsal cochlear nucleus: A Golgi-electron microscopic study in rat. J Comp Neurol 227:136–157.

Wu LG, Borst JG (1999) The reduced release probability of releasable vesicles during recovery from short-term synaptic depression. Neuron 23:821–832.

Xu J, Wu L-G (2005) The Decrease in the Presynaptic Calcium Current Is a Major Cause of Short-Term Depression at a Calyx-Type Synapse. Neuron 46:633–645.

Xu-Friedman MA, Harris KM, Regehr WG (2001) Three-Dimensional Comparison of Ultrastructural Characteristics at Depressing and Facilitating Synapses onto Cerebellar Purkinje Cells. J Neurosci 21:6666–6672.

Xu-Friedman MA, Regehr WG (2003a) Ultrastructural Contributions to Desensitization at Cerebellar Mossy Fiber to Granule Cell Synapses. J Neurosci 23:2182–2192.

Xu-Friedman MA, Regehr WG (2003b) Ultrastructural Contributions to Desensitization at Cerebellar Mossy Fiber to Granule Cell Synapses. J Neurosci 23:2182–2192.

Xu-Friedman MA, Regehr WG (2004) Structural Contributions to Short-Term Synaptic Plasticity. Physiol Rev 84:69–85.

Xu-Friedman MA, Regehr WG (2005) Dynamic-clamp analysis of the effects of convergence on spike timing. II. Few synaptic inputs. J Neurophysiol 94:2526–2534.

Yamada KA, Tang CM (1993) Benzothiadiazides inhibit rapid glutamate receptor desensitization and enhance glutamatergic synaptic currents. J Neurosci 13:3904–3915.

Yamazaki M, Fukaya M, Hashimoto K, Yamasaki M, Tsujita M, Itakura M, Abe M, Natsume R, Takahashi M, Kano M, Sakimura K, Watanabe M (2010) TARPs γ-2 and γ-7 are essential for AMPA receptor expression in the cerebellum. Eur J Neurosci 31:2204–2220.

Yamazaki M, Pichon CEL, Jackson AC, Cerpas M, Sakimura K, Scearce-Levie K, Nicoll RA (2015) Relative contribution of TARPs γ-2 and γ-7 to cerebellar excitatory synaptic transmission and motor behavior. Proc Natl Acad Sci 112:E371–E379.

Yang H, Xu-Friedman MA (2015) Skipped-Stimulus Approach Reveals That Short-Term Plasticity Dominates Synaptic Strength during Ongoing Activity. J Neurosci 35:8297–8307.

Young ED, Nelken I, Conley RA (1995) Somatosensory effects on neurons in dorsal cochlear nucleus. J Neurophysiol 73:743–765.

Zucker RS (1989) Short-Term Synaptic Plasticity. Annu Rev Neurosci 12:13–31.

Zucker RS, Regehr WG (2002) Short-Term Synaptic Plasticity. Annu Rev Physiol 64:355–405.